Motion Compensated Drilling From a Floating Vessel

Performance-based Motion Compensation selection for Floating Large Diameter Drilling

MSc Offshore & Dredging Engineering

D.P.F. de Koning

Delft University of Technology

TU Delft

Boskalis

Motion Compensated Drilling From a Floating Vessel

Performance-based Motion Compensation selection for Floating Large Diameter Drilling

by

D.P.F. de Koning

to obtain the degree of Master of Science
at the Delft University of Technology,
to be defended publicly on Tuesday January 30, 2024 at 15:00.

Student number:	4706153	
Project duration:	April 1, 2023 – January 30, 2024	
Thesis committee:	Prof. dr. A. V. Metrikine,	TU Delft, Chair
	Dr. A. Tsetas,	TU Delft, supervisor
	Ir. I. K. van Giffen,	Boskalis, supervisor
	Ir. R. J. van der Wal,	Boskalis, supervisor

This thesis is confidential and cannot be made public until January 30, 2026.

Cover:	Drill Derrick - Ocean Vantage by Emily Dye, Boskalis
Style:	TU Delft Report Style, with modifications by Daan Zwaneveld

An electronic version of this thesis is available at `http://repository.tudelft.nl/`.

TU Delft Boskalis

Preface

The journey of writing this master thesis has been a truly valuable experience. I have gained many insights that have helped me become a better engineer. First, I want to thank all the people who supported me during the process of writing my master thesis. I want to thank my Boskalis supervisors, Ir. Ike van Giffen and Ir. Remmelt van der Wal, for their technical guidance and support. The many meetings left me almost always with more knowledge, confidence, and new insights. I want to thank them for often taking the time to sit down and discuss problems with me or show me how to perform helpful analyses in the software used. Additionally, I want to thank my TU Delft graduation committee. First, my daily supervisor, Dr. Athanasios Tsetas, who provided me with project guidance and often introduced me to new theories that I could use to further enhance the analysis of specific system characteristics. I also want to thank the Chair of my graduation, Prof. Dr. Andrei Metrikine. It was very helpful to experience his extremely critical and fair attitude towards my research. It really helped me look critically at my own work and become more precise in my reasoning. I also want to thank everyone at Boskalis who has helped me in any way possible over the last couple of months. I really felt welcome here, and it was amazing to work with such talented people who were so willing to help me at any time.

During my time as a student, I found that support is created not only by people helping with studies, but also by the friends who surround me. Dennis, Moniek, Stef, and Cenedra, I want to thank you all for the time we have spent over the last 6 years. The countless times we studied for our exams, had dinner together or went out for drinks, I cherish these memories. You helped make my student time one of the best periods of my life, and I am confident that we will be friends for decades to come. This is also true for all my roommates with whom I have lived at Kloosterkade. We created some memorable moments together, and you all helped me relax and focus over the last couple of years.

Finally, I want to thank my family for always supporting me, even during difficult times. The relentless support my parents gave me means the world to me and I am proud to have finished my studies at TU Delft with their backing. Also, a very special thank you to my girlfriend Roosmarijn. You have supported me greatly during the writing of my thesis. It was very helpful to vent my emotions to you, and you have given me some solid advice in the process.

Finishing my thesis marks the end of my student career, but opens the door to new adventures in my life. I look back on an amazing time as a student, but I am confident that the future holds even more exciting things. Time flies, but sometimes it is essential to take a moment to reflect on how amazing life is!

Daan de Koning
Delft, January 2024

Abstract

To accelerate the floating wind industry, a cost-effective solution must be found for drilling anchor piles in cases where the soil conditions do not favour any other type of design. The water depths often encountered in floating wind projects are too deep for jack-up vessels. For this operation, an alternative drilling method must be used. This drilling method used to construct such boreholes is the reversed circulation drilling (RCD) method. Floating application of this method has only been done up until now in mild wave conditions. To increase economic viability and reduce operational costs, it is necessary to increase the workability of this operation under more challenging environmental conditions. A motion compensation device is a vital aspect in this.
A systematic approach is used to determine which type of motion compensation device is best suited for this operation. Numerical models are set up in the commercial software OrcaFlex, where a wide range of different types of motion compensation are tested. These motion compensation systems vary in the amount of degrees of freedom compensated and in the actuation method. The actuation methods are passively actuated gas springs and position-based motion control using hydraulic actuators.

First, it is identified what combination of degrees of freedom and the actuation method is best suitable for this application. This is determined by performing a regular wave analysis and comparing the performance of the proposed motion compensation systems. Performance is indicated by the ability of the motion compensation system to control the weight on bit, reduce the maximum stress, and increase fatigue life by reducing the accumulated fatigue damage in the drill string. From this analysis, it is concluded that a passive-actuated concept that compensates for the heave, roll, and pitch of the vessel is the most effective scheme. Passive motion compensation allows for large vessel motions while keeping relatively constant forcing, compensation for roll and pitch reduces bending moments in the drill string, and reduce stress levels and fatigue damage accumulation.
In the second phase, the goal is to design and optimise two different systems capable of compensating for the heave, roll, and pitch motion of the vessel. The first, relatively simple, type consists of a vertical gas spring and a universal joint where the drill rig can rotate freely. The other type is a passive variant of the Barge Master platform motion compensation system. This second concept is designed using a multi-objective optimisation algorithm, the NSGA-II algorithm. The difference between these two systems is that the platform concept has rotational stiffness, while the simple type is free in this degree of freedom.

It is finally concluded that both concepts are viable solutions and that both systems represent a motion compensation system that compensates for the heave, roll, and pitch motion of the vessel. The performance regarding the indicators is very similar, therefore, choosing one of the concepts would come down to the other practical advantages and disadvantages of the concepts.

Contents

List of Figures

List of Tables

Nomenclature

Abbreviations

Abbreviation	Definition
BHA	Bottom hole assembly
CoG	Centre of Gravity
CSV	Construction Support Vessel
DoF	Degree of Freedom
DP	Dynamic Positioning
FEM	Finite element method
JONSWAP	Joint North Sea Wave Observation Project
KPI	Key Performance Indicator
PM	Pierson-Moskowitz
PID	Proportional, Integral, Derivative
PSD	Power Spectral Density
RAO	Response Operator Amplitude
RCD	Reversed circulation drilling
SD	Standard Deviation
SCF	Stress Concentration Factor
TOB	Torque-on-bit
VIV	Vortex Induced Vibratinos
WoB	Weight-on-bit
QTF	Quadratic Transfer Function

Symbols

Symbol	Definition	Unit
A	Amplitude	[m]
A	Surface area	[m^2]
a	Acceleration	[m/s^2]
$\overline{B}$	Damping matrix	[Ns/m]
b	Damping	[Ns/m]
$\overline{C}$	Stiffness matrix	[N/m]
C_d	Drag coefficient	[-]
C_m	Mass coefficient	[-]
D	Diameter	[m]
D	Fatigue damage	[-]
d	Water depth	[m]
E	Young's Modulus	[Pa]
$\overline{F}$	Force matrix	[N]
F	Force	[N]
F	degrees of freedom	[-]
f	degrees of freedom of a joint	[-]
f	Frequency	[Hz]
g	Gravititional acceleration	[m/s^2]
g	Number of joints	[-]
H	Wave height	[m]
H_s	Significant wave height	[m]
I	Area moment of inertia	[m^4]
k	Spring stiffness	[N/m]
k_t	Stress concentration factor	[-]
L	Length	[m]
M	Moment	[Nm]
$\overline{M}$	Mass matrix	[kg]
m	Mass	[kg]
m_0	Zeroth spectral moment	[-]
n	Number of stress cycles	[-]
N	Stress cycles for failure	[-]
N	Number of components	[-]
n	Polytropic gas constant	[-]
p	Position	[m]
p	Pressure	[Pa]
Q	Q factor	[-]
q	External load	[N]
Re	Reynolds number	[-]
r	Radius	[m]
S	Fatigue stress	[Pa]
St	Strouhal number	[-]
t	Time	[s]
T	Tension	[N]
T	Period	[s]
T_p	Peak period	[s]
U	Constant fluid velocity	[m/s]
u	Fluid velocity	[m/s]
u	Axial beam displacement	[m]
V	Volume	[m^3]
v	Velocity	[m/s]
w	Lateral beam displacement	[m]

Symbol	Definition	Unit
α	Incoming wave angle	[°]
β	Damping ratio	[-]
Δt	Time step	[s]
ϵ	Error	[-]
ϵ	phase	[rad]
η	efficiency	[-]
γ	JONSWAP shape factor	[-]
ν	Kinematic viscosity	[m^2/s]
ω	Rotation speed, frequency	[rad/s]
ϕ	Vessel roll	[rad] or [°]
ψ	Vessel Yaw	[rad] or [°]
ρ	Density	[kg/m^3]
σ	Stress	[Pa]
θ	Vessel Pitch	[rad] or [°]
ξ	Damping ratio	[-]
ζ	Wave amplitude	[m]

1. Introduction

To reduce carbon emissions, it is necessary to generate energy via renewable energy sources, for example, wind energy. According to Cuesta et al. (2011)[6], offshore wind farm construction is favourable because it reduces land use, noise disturbance, and visual pollution, while also increasing energy yield due to higher wind speed. However, suitable locations for relatively cheap bottom fixed wind turbines are running out. The current areas being developed have larger water depths that do not suit bottom fixed wind anymore, as bottom fixed wind energy is currently limited to approximately 50 metres, and at larger depths become uneconomic (Wu et al., 2019)[35]. Therefore, floating wind turbines are being developed and tested to allow the exploitation of these deeper water areas.

The use of drag anchors for mooring floating wind turbines may not always be feasible due to variations in soil conditions in different locations. Where the soil is too hard, other solutions need to be used, such as drilled and grouted piles, which require large diameter holes to be drilled. This type of drilling has only been done from jack-up vessels up until now, however the water depths for floating wind are in between 50m-250m, which is too deep for current wind installation jack-up vessels, these vessels are limited to around 70m (NG-20000X Self-propelled Jack-up | NOV)[29]. Therefore, it aims at performing this operation from a floating vessel. It is also crucial to develop cost-effective drilling operations which result in the vessel of choice, this is a relatively small offshore construction support vessel. These vessels are widely available, but because of their size, exhibit larger excitations. This research aims to increase the feasibility and efficiency of drilling from such a vessel by testing different motion compensations for this operation.

The research question for this thesis is as follows:

What is the most effective compensation methodology for large-diameter drilling from an offshore construction vessel in relatively shallow waters?

1.1. Research Objective

Multiple studies have been done on the design of a heave compensator for floating drilling. The objective is to increase the efficiency of the drilling process by reducing the residual motion of the top of the drill string as much as possible. However, the objective of this study aligns with previous research, albeit with variations in drilling technique, shallower water conditions, and increased ship movement. These distinct factors may yield a different motion compensation system that is considered optimal. The goal of this thesis is as the following:

The research objective is to propose a motion compensation setup that is most effective for drilling large diameter holes in relatively shallow waters using a construction support vessel.

1.2. Research Structure

The research is structured into two parts, the first part is the identification of the compensation type. Here, it will be explored what global properties the motion compensation should have. It will have the following subquestions:

- How many degrees of freedom (DoF) need to be compensated?
- Is this compensation actively or passively controlled?

The final result of this part will be a description of a motion compensation system that answers these two questions. This result will then be used for the second part of the research. The realisation of the motion compensation system. Here, the system will be roughly designed and optimised. In addition, a more realistic analysis will be done. This part has the following subquestions:

- How does the best performing type of combination look like in real life?
- What are the most optimal parameters for this system?
- What is the final performance of this system?

The final result will be a recommendation of a motion compensation system that works best for this specific application. There will be a description of what the system will look like globally in real life on the vessel and what performance can be expected.

2. Background information

Floating drilling has been an intensively studied field in offshore operations since the 1950s, when offshore drilling for oil and gas was transitioning from shallow waters to deeper waters. Today, offshore drilling is a mature technology that is vital to the world economy. Over time, offshore drilling purposes have diverged and now include, for example, geotechnical or foundation drilling. One of the most important aspects of accelerated offshore drilling was the introduction of heave compensation. This heave compensation has been shown to be essential for increasing the cost effectiveness of offshore drilling by increasing the workability [34]. For the drilling of large-diameter holes for floating wind anchor piles, a different drilling method is used compared to oil and gas or geotechnical drilling, which has not been widely used in floating applications.

In this chapter, background information regarding the most important aspects of this research is briefly explained. First, a short overview of the most relevant hydrodynamic forces that act on the system is given, followed by a section on drilling mechanics, where the basic principles of the drilling operation are elaborated. In the final section, the basics for motion compensation are discussed, the basics lay the foundation for the compensation models used in this research.

2.1. Hydrodynamics

For floating offshore structures, it is important to assess the motions caused by environmental conditions. The motions of a vessel can be described in six different directions. Three translations and three rotations. These motions are shown in figure 2.1. The motions are mainly caused by the forces that are exerted on the structure by the waves. The equation of motion of the structure is then the following.

$$\ddot{X}\left[\overline{M}+\overline{A}\right]+\dot{X}\left[\overline{B}\right]+X\left[C\right]=\overline{F_{ext}} \tag{2.1}$$

All the values are 6x6 matrices except X, $\dot{X}$, $\ddot{X}$, which are the position, velocity, and acceleration vectors, respectively. $\overline{M}$ is the mass matrix that contains the mass and the moment of inertia, $\overline{A}$ is the added mass matrix, $\overline{B}$ is the hydrodynamic damping matrix, and $\overline{C}$ is the hydrodynamic stiffness matrix. If the incoming waves are considered to be regular, then the ship motions are regular as well. Ship motions can also be calculated using a response amplitude operator (RAO). This factor describes the amplitude and phase of the motion. This factor varies for different frequencies and is dependent on the shape of the hull, the mass of the ship, and the loading conditions. These RAOs are calculated using a panel method, this is based on potential flow theory and assumes that the hull consists of sources. These sources are potential flow elements. These elements generate flow from a point that counteracts the wave potential. This is a numerical approximation that is performed using special diffraction software.

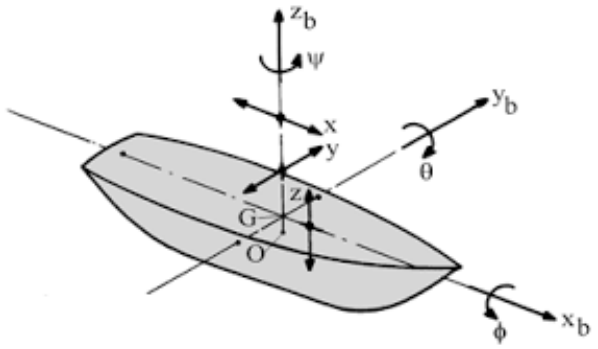

Figure 2.1: The six motions of a ship. [20]

Symbol	x	y	z	ϕ	θ	ψ
Name	Surge	Sway	Heave	Roll	Pitch	Yaw

Table 2.1: Degrees of freedom of the ship, their symbols and names.

The motion of the vessel, which has periods similar to waves, is classified as first-order motions. It is also important to consider second-order, long periodic motions. These motions are mainly influenced by second-order wave forces. Other sources of low-frequency ship excitation, such as current and wind, can also contribute to these motions by generating an almost static force. The frequency of these motions is lower than that of the first-order motions, and they have larger amplitudes. The behavior of this second-order motion is crucial for the stationkeeping system, which uses anchoring or dynamic positioning systems to maintain the desired position. The calculation of the second-order wave forces can be done using the following formula. This function is called the Quadratic Transfer Function (QTF)

$$\begin{aligned}\mathbf{F}^{(2)} = &\sum_{i=1}^{N}\sum_{j=1}^{N} \zeta_i\zeta_j P_{ij}^{-} \cos((\omega_i-\omega_j)t+(\epsilon_i-\epsilon_j)) \\ &+\sum_{i=1}^{N}\sum_{i=j}^{N} \zeta_i\zeta_j Q_{ij}^{-} \sin((\omega_i-\omega_j)t+(\epsilon_i-\epsilon_j)) \\ &+\sum_{i=1}^{N}\sum_{i=j}^{N} \zeta_i\zeta_j P_{ij}^{+} \sin((\omega_i+\omega_j)t+(\epsilon_i+\epsilon_j)) \\ &+\sum_{i=1}^{N}\sum_{i=j}^{N} \zeta_i\zeta_j Q_{ij}^{+} \sin((\omega_i+\omega_j)t+(\epsilon_i+\epsilon_j))\end{aligned} \tag{2.2}$$

There are sum-frequency and difference frequency terms in this formula. The sum frequency parts are important to assess for stiffly moored structures, while the difference frequency parts are important for softly moored or free-floating structures.

These second-order motions occur only in the XY plane and are always compensated for using an anchor mooring or dynamic positioning (DP) system. The first type of mooring uses drag anchors and mooring lines to physically anchor the vessel to the seabed. The second option uses actively controlled thrusters. Anchored mooring usually takes more time to set up and could require the need for anchor handling tugs. The responses of such systems depend on the stiffness of the mooring system, this is dictated by the mass and tension of the mooring line and the mass of the ship. The DP system is quick and more accurate but requires an external energy input. For DP systems the performance varies with every system, it depends on aspects like thruster layout and control scheme.

Another important source of excitation for floating drilling is the hydrodynamic forcing on the drill string. The drill string is considered to be a slender structure, the width or diameter is very small compared

to the length. For these kind of structure, the hydrodynamic force can be easily calculated using the Morison force. This force is given in the following [28].

$$F(t) = C_M \rho \frac{\pi}{4} D^2 \dot{u}(t) + C_D \frac{1}{2} \rho D u(t) \left| u(t) \right| \tag{2.3}$$

Here C_m is the added mass coefficient, ρ the fluid density, D the cylinder diameter, $\dot{u}(t)$ the fluid acceleration, C_d the drag coefficient and $u(t)$ the fluid velocity. The first part on the right side of the equation is dependent on the fluid acceleration, while the second part is dependent on the fluid velocity. Fluid velocity and acceleration can be calculated using wave theory. The wave theory describes the orbital path of the water particle in waves, thus the velocity and acceleration can be derived, the shape of the orbital path varies with every wave theory. For the velocity, the current velocity can be simply added to the orbital velocity. An important aspect of this equation is that the velocity and acceleration for wave particles are 90° out of phase, this means that the maximum Morison force that occurs is not the maximum velocity and maximum acceleration combined, but somewhere in between.

As mentioned above, the main excitation source is caused by ocean waves. Ocean waves can be described by many different wave theories. Wave theory has to be chosen to suit the relative water depth and wavelength. More about this in chapter 3. Furthermore, waves can exhibit regular or irregular behavior. Regular waves are characterized by their precise amplitude and period, representing idealized wave patterns. On the other hand, irregular waves are employed to describe the more realistic wave conditions encountered in actual oceanic environments. Irregular waves consist of many different regular waves added to represent surface elevation. A real sea state is described by a wave spectrum, this wave spectrum describes the energy that is present in the waves at that specific amplitude. The energy is proportional to the wave height. This is all shown in figure 2.2. Wave spectra are categorise using statistical values such as significant wave height and peak period. The exact shape of the wave spectrum is derived from scientifically proposed wave spectra such as JONSWAP or Pierson-Moskowitz spectra.

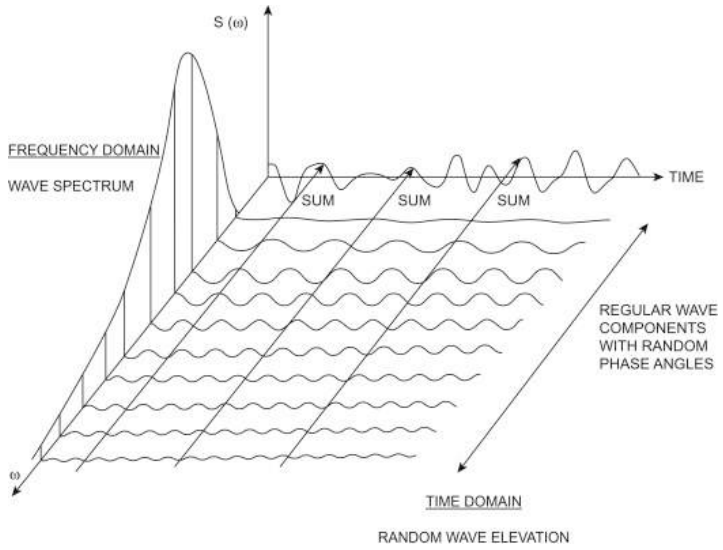

Figure 2.2: Example of a composition of irregular waves and wave spectrum [10].

2.2. Drilling mechanics

Offshore drilling is a vital aspect in offshore engineering, it enables the exploitation of offshore oil and gas reserves around the world currently necessary for energy production and the chemical industry. But offshore drilling is now becoming more important for renewable energy sources as well, many offshore wind farms that are being constructed today are dependent on offshore large diameter drilling technology. Although drilling for these wind farms is mostly done using jack-ups, the next step is to make this drilling method suitable for floating vessels as well.

2.2.1. Reversed Circulation Drilling

The drilling method considered in this thesis is different in some aspects from the widely used and discussed drilling method in the oil and gas industry. One aspect that is the same is the fact that most of the drilling is done via roller-cone drilling. Here, a roller rolls over the rock, the rock is then crushed under the weight that is on the drill bit and the small contact patch between the rock and the roller. There are three different types of rollers available that are used based on the strength of the rock. The grit produced by the drilling process is transported from the hole to the surface. The grit is removed from the borehole by using the airlift effect. Compressed air is pushed into two small pipes attached to the drill pipe. This air enters the drill pipe below the water level and above the drill bit. If air expands in the drill pipe, the overall density increases. The hydrostatic pressure that surrounds the drill string pushes the inside mixture of air and crushed rock to the surface where it is dumped. This method is also called reversed circulation drilling (RCD) or airlift drilling[1]. It is different from oil and gas drilling, where the rock is transported outside the drill pipe but inside the riser. For the RCD drilling method, the drill pipe rotates in open water, while for oil and gas drilling, the drill pipe rotates within the riser.

Figure 2.3: The three different roller cutters [5].

2.2.2. Drill String mechanics

Offshore drilling is a very costly and time-consuming operation. Drilling rates are usually relatively low and the process can take several days. In addition, there is a high risk of a damaged or even lost bottom hole assembly, resulting in a large downtime, and losing such a part is very costly. Therefore, it is important to consider the mechanical behaviour of the drill string to estimate when failure could occur[24].
Drill strings vibrate in many complex patterns, and these vibrations can be assessed as coupled and uncoupled[11]. The uncoupled vibrations are lateral (bending), axial, and torsional vibration. The most important coupled vibrations are lateral-axial, lateral-torsional, and finally axial-torsional. Fully coupled models do exist as well where all vibrations are coupled together. Uncoupled vibrations are easily calculated and are fairly accurate, coupled vibrations are more complex and require numerical software to solve.

In uncoupled axial modelling, the linear partial differential equation is used for the longitudinal oscillation of a beam. This equation is given below. In order to get an accurate estimate of the response via modal analysis, only the first six modes should be considered, higher-order modes contributing little to significant accuracy.

$$\rho A \frac{\partial^2 u(x,t)}{\partial t^2} = EA \frac{\partial^2 u(x,t)}{\partial x^2} + q \tag{2.4}$$

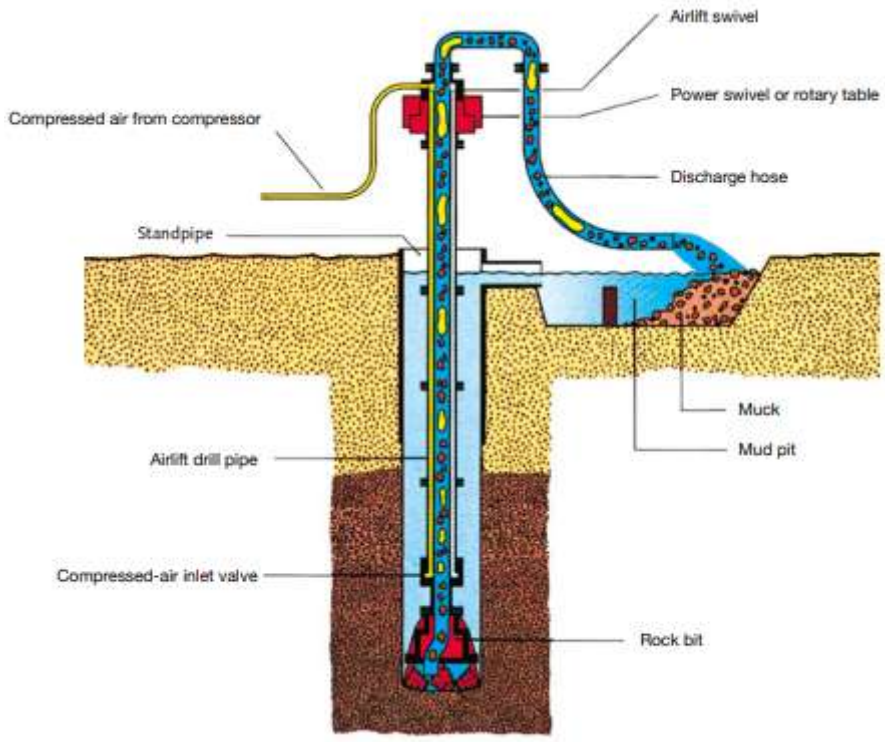

Figure 2.4: Schematic drawing of the working principle of the Reversed Circulation Drilling method [1].

For uncoupled lateral vibration modelling, the most widely used theory is the Euler-Bernoulli beam theory, this is due to the high slenderness ratio. Euler-Timoshenko theory is recommended for shear-dominated shorter beams. The modelling is mostly done in two manners, single-plane and three-dimensional. Single-plane methods make use of polar coordinates, while three-dimensional methods keep the x- and y-planes separate. If tension is present in the beam, then the equation of motion gets an extra term. The equation is then as follows:

$$\rho A \frac{\partial^2 w(x,t)}{\partial t^2} + EI \frac{\partial^4 w(x,t)}{\partial x^4} - T(x,t) \frac{\partial^2 w(x,t)}{\partial x^2} = q \tag{2.5}$$

Finally, the uncoupled torsional vibrations are thus important to model vibration modes such as stick-slip. The most common way of modelling is a torsional pendulum, where the BHA represents the suspended mass and the drill pipe is the spring, the drill pipe is considered to be intertialess in this case. This equation of motion is given as:

$$I \frac{d^2\theta}{dt^2} = -k_{rotational}\theta \tag{2.6}$$

Boundary conditions dictate the behaviour of the drill string at specific points in space. Some examples of the most used boundary conditions for axial vibrations in literature are:

- Fixed at the top, fixed at the bottom
- Fixed at the top, free at the bottom
- Mass-spring-damper at the top and sinusoidal bit displacement at the bottom

The mass-spring-damper at the top is used to model the behaviour of the drill rig used. The sinusoidal bit displacement at the bottom is used to model the rolling profile of the bit. This bit displacement depends on the geometry of the bit. The motion is assumed to be sinusoidal, the frequency depends on the number of rollers on the drill bit. A drill bit with three rollers is then modelled to have an end displacement with a frequency of three times the rotating frequency. This combination is assumed to be the most accurate set of boundary conditions.

For lateral boundary conditions, the following boundary conditions combinations are mainly used in research:

- Simply supported top and bottom
- Free-free
- Fixed-fixed
- Deflected springs at each end
- Mass loaded ends
- Simply supported at stabilizers
- Fixed at the top (rotary table) and free at the bottom

Finally for torsion the options are more limited, but they include an upper-end constant rotating speed, another option is to setup a control system to control the rotary speed and torque to maintain a specific rotation speed at the bottom. Rotation is also often not considered for simplicity.

Marine drill strings are loaded with many different cyclic loads such as waves, ship motions, their own rotation, or bit-rock forces. All these cyclic loads will cause cumulative damage to the drill string and will end up in failure if not accurately assessed. Fatigue failure is the main cause of failure in 65% of the failure cases observed during drilling, and these failures are, as already mentioned, very costly[27].

Cumulative fatigue damage is described with Miner's linear rule. This simple rule calculates the damage caused by a specific stress amplitude. This must be multiplied by the corresponding number of cycles. If the damage is equal to one, it is assumed that fatigue failure has occurred.

$$D = \sum \frac{n_i}{N_i} \tag{2.7}$$

Here, n_i is the number of measured cycles at a specific stress amplitude and N_i is the number of cycles for failure for that specific stress amplitude. N_i can be found in S-N curves, these S-N curves describe the number of cycles a material can endure for a specific stress amplitude. These S-N curves are derived from experiments. And vary only with the material.

2.3. Motion compensation

Heave compensation is a necessity for floating offshore drilling. Heave compensation is the most basic form of motion compensation in the offshore industry. The goal of a motion compensation system is to decouple the motion of a specific point or object from the ship's motion, in other words, to keep it stationary at a specific point in the world. Motion compensation is mostly done in two ways, passively and actively. The differences between the two types are given in section 2.3. A combination of both active and passive combination is also widely used and is called hybrid compensation, however, in this thesis, this will be considered as an active system. Motion compensation comes in many different forms in the offshore industry. The number of degrees of freedom that are compensated for varies from system to system. The most common systems are heave compensation systems that only compensate for the vertical motion of the ship. They were first introduced in the 1960s in order to improve drilling workability for oil and gas exploration [34]. Another common compensator system decouples the motions of a vessel that cannot be controlled by anchoring or dynamic positioning. The remaining motions that this type reduces are heave, roll, and pitch. Finally, a full motion compensation system that is currently used in the industry is discussed. This system is based on a Stewart platform and uses six cylinders to control its attitude. Some examples of these devices are given in figure 2.5

	Passive	**Active Motion Control**
Actuation	Hydraulic gas spring systems	Hydraulic or electric actuators
Control	No control scheme	Many different control schemes used
Frequency	Designed for a specific frequency band	Flexible for a wide variety of frequencies
Energy input	No energy input	External energy input necessary
Complexity	Low complexity	More complex

Table 2.2: Major differences between passive and active motion compensation.

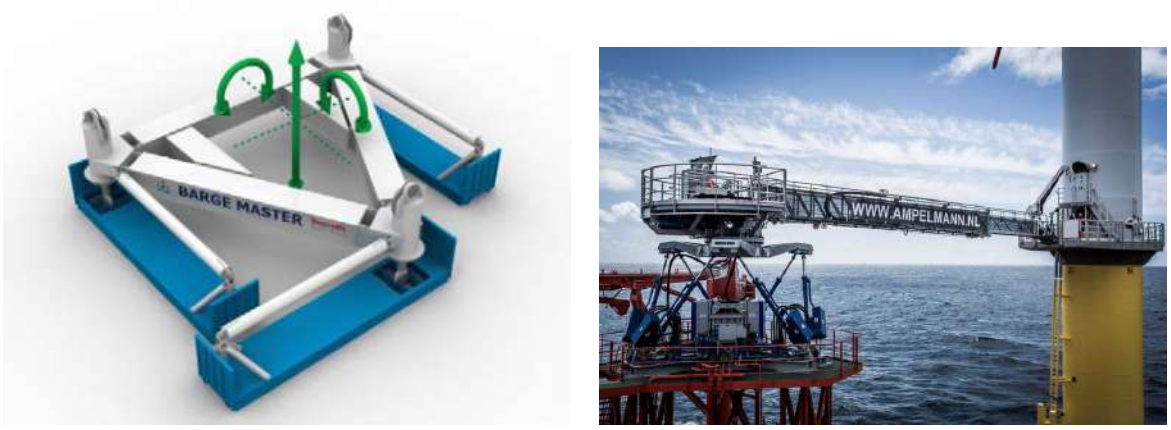

(a) The Barge Master motion compensation system [19].

(b) The Ampelmann crew transfer system using a Stewart platform [3].

Figure 2.5: Two examples of multiple degree of freedom motion compensation systems

2.3.1. Passive Motion Compensation

Passive motion compensation does not require an input of external energy. Motion is controlled by springs and dampers. In the offshore environment, the springs used are gas springs with an accumulator. The main cylinders are filled with a hydraulic fluid that transfers the load to the accumulator, which is filled with a gas, mostly nitrogen. The compressibility of the gas in the accumulator is responsible for the stiffness. This stiffness is described by rewriting the polytropic process relation given in the following:

$$p_0 V_0^n = p_1 V_1^n \tag{2.8}$$

Rewriting this when p_0 and V_0 are the initial pressure and volume and the piston moves to change the volume to V_1 and to an unknown pressure p_1. Finally, n is the polytropic constant. This results in a nonlinear spring stiffness where the force is described by:

$$F_1 = AP_0 \left(\frac{V_0}{V_0 - Ax} \right)^n \tag{2.9}$$

Where F the force is$A$ is the area of the piston and x is the position of the cylinder with respect to the initial situation. This can be linearised and transformed into a stiffness as Woodacre did[33]. Where the force becomes:

$$F = \frac{nP_0 A^2}{V_0} x \tag{2.10}$$

Where the stiffness then becomes:

$$k = \frac{nP_0 A^2}{V_0} \tag{2.11}$$

It can be seen that when the initial volume V_0 increases to infinity, the stiffness becomes zero, meaning that for every position the gas spring has a constant force. This is in theory also the perfect passive compensator, ignoring damping. Damping for passive systems is very system-specific, and some elements that contribute to gas spring damping are: viscous flow losses, cylinder seal friction, and cylinder seal stick-slip. These effects also cause the damping characteristic of a gas spring to be non-linear.

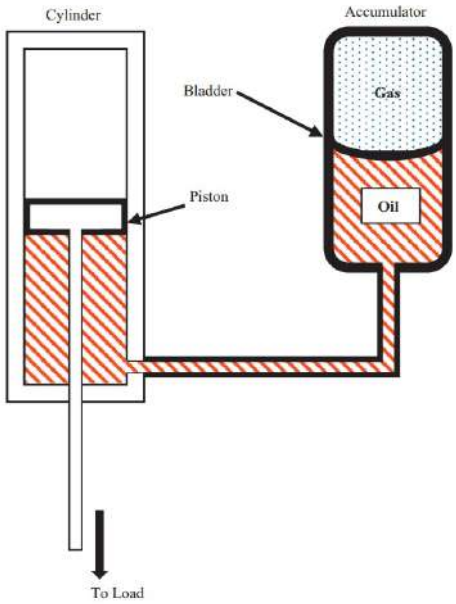

Figure 2.6: Example of a passive compensation system

2.3.2. Active Motion Compensation

Active systems try to actively control the position of a load by extending or retracting the cylinders according to the heave of the ship. These systems require, in contrast to passive systems, energy input. In such systems, ship heave is measured and transmitted to a controller, which sends a control signal to move an actuator to oppose the vertical motion of the mounting point. The first active heave compensator was introduced by Sutherland (1970)[31]. Overall little work on active heave compensation was published up until the 1990s, when real-time computer control became mature enough for this application. A paper by Korde (1997)[22], where he proposed a linearised model of an active heave compensation system for a drill string, showed that it is possible to fully decouple the heave motion or, in other words, perfect efficiency. More on that paper is given in the section Active heave compensation. However Do & Pan (2008)[9] showed that it is impossible to fully decouple the load, the model of Do & Pan was non-linear, suggesting that linearisation is too simple to model the entire system. For pure active systems, power consumption must be considered, the system always requires maximum power to be available to work properly, and for pure active systems, power is also necessary even when the load is static. So, if power consumption or delivery is a problem, a solution could be a hybrid compensation device. This uses aspects of both passive and active systems.

Hybrid systems are a combination of passive and active systems. These systems have passive and active cylinders. An example of such a system is given in figure 2.6. The static load is carried by the two passive cylinders, and the smaller active cylinder in the middle can exert an additional adjustment force to overcome the shortcomings of the passive system. This active cylinder generally applies forces much smaller than that of cylinders from a pure active system. Therefore, it can be much smaller, resulting in less flow, lower pressure, and thus less power consumption. Most systems are hybrid systems due to their superior energy efficiency.
Control is an essential part of an active or hybrid heave compensation system. Much of the work available in the academic literature only presents a design with occasional simulation results. Different types of controller are used in the above-mentioned papers. The first active heave controller proposed by Southerland in 1970 used a simple proportional controller. From the end of the 1990s onwards more complex control schemes were proposed due to the increase in computer capabilities. Linear controllers like P-PI, PD, and PID are used often, and more complex nonlinear controllers like a Linear Quadratic Regulator (LQR) or control with Lyapunov's Direct method are mentioned in the literature as well. Heave prediction algorithms are used as well, these algorithms try to estimate the future heave profile of the vessel. From this prediction, a more accurate heave compensation is possible. However,

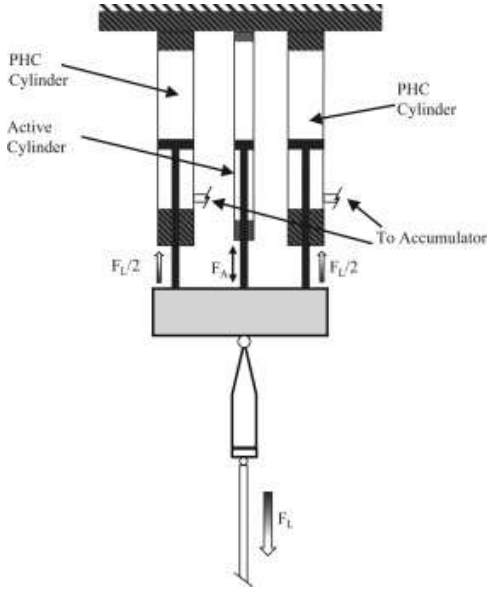

Figure 2.7: Example of a hybrid heave compensation system[33]

a reliable prediction of the heave is very hard due to the random nature of the ocean waves.

Compensation efficiency is an important characteristic of active heave compensation. On a position-based active heave compensator,tab the efficiency is usually determined as:

$$\eta_{compensation} = 1 - \frac{\text{Residual heave}}{\text{Ship heave}} \times 100\% \tag{2.12}$$

Efficiency varies a lot from system to system and manufacturers of active motion compensation systems do not share their exact efficiencies. Most efficiencies that can be found are derived in literature using computational or scale models. These efficiencies range from 100% [22] to 88% [19]. And can be dependent on frequency.

3. Concept Identification: Methodology

This chapter outlines the research methodology. Initially, the research approach is discussed, followed by a section on the types of assets used in the drilling process. Subsequently, the modelling method is described, including the basic equations used by the software, as well as the time step, and segment length used in all simulations. Each aspect of the model is then discussed in detail, with the assumptions made and the most important parameters of the object outlined. Finally, the Key Performance Indicators (KPIs) are discussed. These parameters measure the performance of each concept and are briefly explained in terms of what they physically represent and how they are calculated.

3.1. Research approach

The goal of this research is to find the most effective type of motion compensation for floating drilling using the RCD method. A ship can, as mentioned in chapter 2 have movements in six different directions (see figure 2.1), and what motions can be compensated by a motion compensation system can be chosen. A compensation type consists of a specific combination of compensated motion directions. To find this type, 8 different concepts are derived. These concepts consist of different numbers and combinations of degrees of freedom that are compensated. Each number and combination has two types, a passive and an active type. The number and combinations of degrees of freedom to be compensated for are chosen in such a way that there are no random combinations. An overview of the concepts is given in table 3.1 below.

Concept #	Name	Active/Passive	# DoFs	Compensated motions
1	1DoF Passive	Passive	1	Z
2	1DoF Active	Active	1	Z
3	3DoF Translation Passive	Passive	3	X, Y, Z
4	3DoF Translation Active	Active	3	X, Y, Z
5	3DoF Rotation Passive	Passive	3	Z, Roll, Pitch
6	3DoF Rotation Active	Active	3	Z, Roll, Pitch
7	6DoF Passive	Passive	6	X, Y, Z, Roll, Pitch, Yaw
8	6DoF Active	Active	6	X, Y, Z, Roll, Pitch, Yaw

Table 3.1: The 8 considered concepts that are tested in this research.

The most simple type of compensation is heave compensation only and is the minimum amount of compensation necessary for offshore drilling, as mentioned by Woodall-Mason and Tilbe (1976)[34]. Then the 3DoF Translation concepts add the X and Y motions to heave compensation. The 3DoF Rotation compensation concepts add two ship rotations compensation to the heave compensation, these three motions are considered impossible to compensate for with anchoring or DP systems, which compensate for all motions in the X,Y-plane (X,Y, and Yaw), this concept is also based on the existing Barge Master platform [19]. And finally, a full 6DoF compensation system that compensates for all possible motions a ship can experience. An example of such a compensation system is the Ampelmann crew transfer system [3].

The scenario that is evaluated is during the drilling operation, where the drill bit is already 15 metres below the seabed, which would represent a maximum depth that needs to be drilled for an anchor pile.

3.2. Asset overview

To make this operation more versatile and economically feasible, a construction support vessel (CSV) was chosen. These vessels are abundant and relatively small and cheap compared to dedicated drill ships or larger crane vessels. Boskalis has a fleet of several different types of construction support vessel. The final choice of vessel is not yet determined, thus, for this research, the smallest CSV is chosen. This vessel is the BOKA Falcon, global data on the vessel can be found in appendix A. The vessel features a dynamic positioning system that will be used during the drilling process.

Figure 3.1: The BOKA Falcon vessel considered for this research.

The drilling method used is the RCD method, this is described in chapter 2. The drilling method uses a larger diameter drill pipe leading to a stiffer drill string. In appendix B is a drawing of a drill pipe with all its dimensions. The drill string material is S690 steel, which is a good high-strength weldable steel that is often used offshore. The drill string at the bottom is called the bottom hole assembly (BHA) and consists of parts different from the regular drill string. Here, the majority of the weight is located and the downhole equipment is stabilised to minimise the risk of crooked boreholes. This stabilisation is done using stabilisers, these stabilisers have in the modelling specific boundary conditions, but more on that in section 3.3.4. An example of a BHA is shown in figure 3.2.

Figure 3.2: Example of a bottom hole assembly for the RCD method [5].

The system consists thus of a vessel, a motion compensation device, a drill rig, a drill string, and finally a bottom hole assembly that is placed on the bottom. A schematic overview of this system is given in figure 3.3.

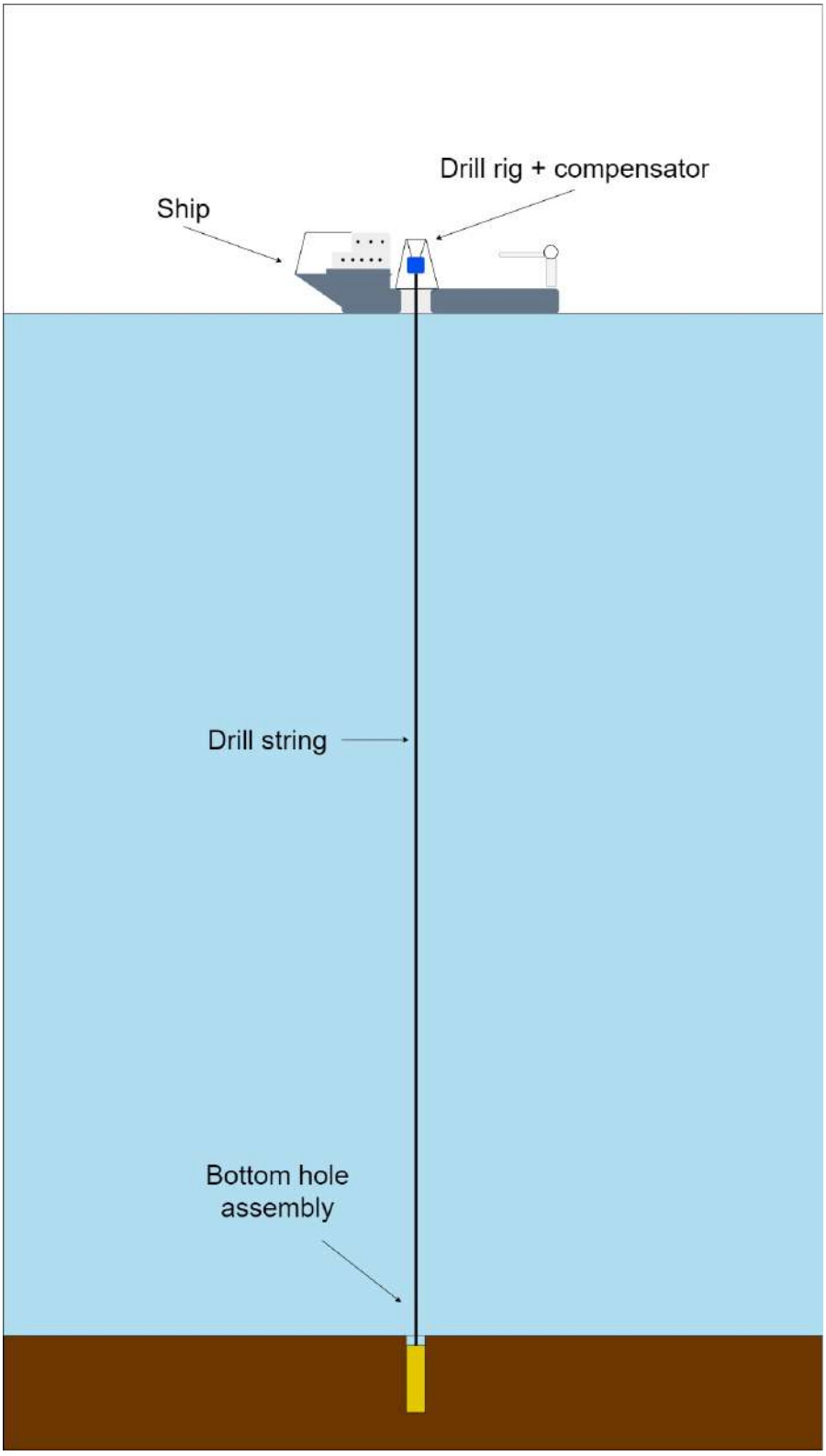

Figure 3.3: Schematic overview of the system considered.

3.3. Modeling

In this section the principles of the models of specific subsystems are described, there are many different aspects in the total system. Each aspect requires different assumptions and simplifications. First, the modelling method is briefly explained, along with its basic calculation methodology, and validation and accuracy with respect to the analytical theory. This is followed by an explanation of the model of subsystems and their most important characteristics. This is explained for the vessel model, drill string model, and the motion compensation systems.

3.3.1. Modeling Method

OrcaFlex is the software of choice for modelling the system. Although it is less accurate than a structural-specific finite element method (FEM), it is very good at combining everything hydrodynamics with slender structures. It is a time domain analysis software that solves the equations of motion in the time domain:

$$M(p,a) + C(p,v) + K(p) = F(p,v,t) \tag{3.1}$$

In this equation, $M(p,a)$ is the inertial force, $C(p,v)$ the damping force, $K(p)$ the stiffness force and $F(p,v,t)$ the external forcing. Furthermore, p is the position, v the velocity, and a the acceleration. Finally, t is the simulation time. This can be solved using one of two available integration schemes, explicit and implicit, in this research only explicit is used. The local equation of motion for each line element is solved with a Euler integration.

$$v_{t+dt} = v_t + dta_t \tag{3.2}$$

$$p_{t+dt} = p_t + dtv_{t+dt} \tag{3.3}$$

The files are constructed by making six base files, three for active compensation and three for passive compensation. There are three different base files because of the water depth. The increase in degree-of-freedom can be easily selected by turning on or off specific settings in the base model. These settings are changed to create base files for every compensation concept and water depth. Then, by means of the file manipulation script, the environmental parameters are changed, these will be highlighted in the next subsection section 3.3.2. These files are then batch-calculated in OrcaFlex, and the simulation files are saved. The results are then extracted from the OrcaFlex files using the Python interface.

Time step & line element length

For the simulations, a standard time step of $\Delta t = 0.1s$ is used and a segment length $\Delta x = 1m$. It must be checked whether these are valid time steps. A small analysis is performed on a concept with more problematic behaviour, small wave periods, and shallow water, the scenario considered is the 50 metre water depth 1DoF Active system with a wave period of 6s. One analysis focuses on the time step and the other on the segment length.

For the initial analysis, the time step is changed, with values ranging from 0.01 to 2 seconds. The relative error of the WoB amplitude is then plotted against the time step. To calculate the relative error, the value with the smallest time step is taken as the ideal result. This is not necessarily accurate, as no numerical result is completely error-free, but it is the most precise value in the data set, so it is reasonable to compare the other results with it. The relative error is calculated as:

$$\epsilon_{rel} = \frac{v - v_{approx}}{v} \tag{3.4}$$

It is evident from figure 3.4 that the relative error increases as the time step size increases, as anticipated. A relative error of 0.02 is observed for $\Delta t = 0.1m$, which is satisfactory, thus making the time step of 0.1s suitable for all the analyses.
The segment length of the drill string ranged from 0.05m to 5m. The bottom hole assembly was kept at 1m, as this part is relatively stationary. The relative error was calculated using the WoB amplitude for the smallest segment length as a reference value.

The error in the chosen segment length is approximately 0.002, which is precise enough for the purpose of this study while still having reasonable computation times. Consequently, the time step and segment length chosen here are suitable for the analysis conducted in this research.

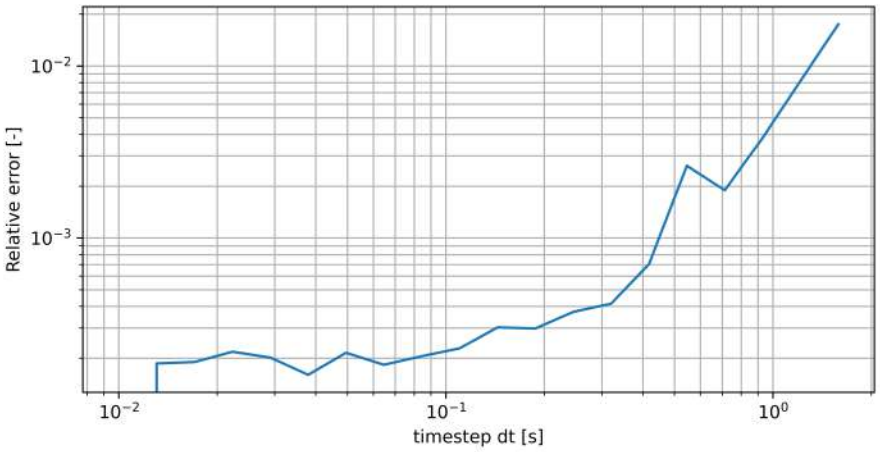

Figure 3.4: Relative error evolution for different time steps

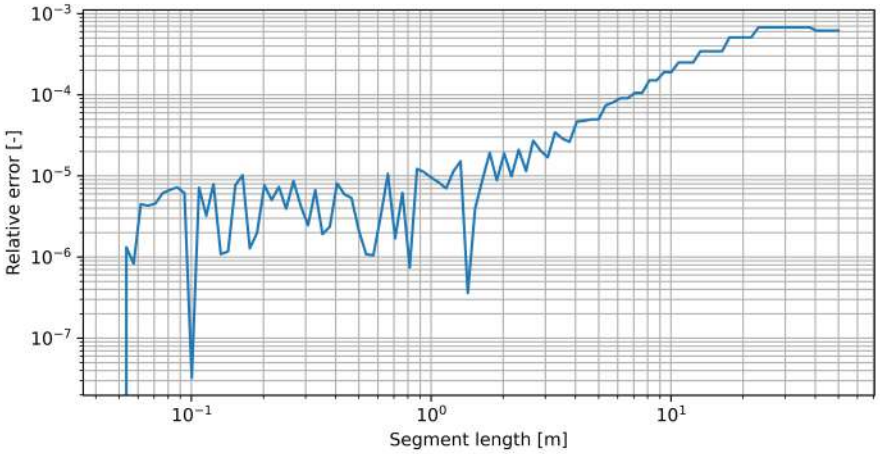

Figure 3.5: Relative error evolution for different segment lengths.

3.3.2. Environmental Conditions Selection

The aim is to provide a solution that can work in many different scenarios, from calm seas in shallow waters to rough seas in deep water. Therefore, the objective of the compensation system is to work in seas with a significant wave height of 2.5 metres ($H_s = 2.5m$). For the water depth, three depths are chosen that cover the entire range in which this operation would be performed. The assumed water depths are 50, 100 and 200 metres. Frequency is an important aspect of the excitation force, and if such a frequency is near the natural frequency, and damping is relatively low, excitations can become very large and destructive. More on the identification of natural frequencies in section 3.5. Therefore, the system needs to be tested with all periods that represent the frequency bandwidth of the wave. These are determined to be periods between 6 and 16 seconds. For simplicity in the analysis, regular waves are used. The periods of these regular waves between 6 and 16 seconds with steps of 1 second. When using regular waves, one should pay close attention to what wave theory should be used. The selection of wave theory depends on the dimensionless wave height and dimensionless water depth. This is visualised in figure 3.6. The dots in the graph represent the outer values for each dimensionless constant, the other values are in between these two points on the dotted line. The red line represents a water depth of 50 meters, the green line 100 metres, and the blue line 200 meters. It can be seen

that the entire range falls into the Stokes theory region. Thus, this is also the wave theory selected in OrcaFlex. The vessel is assumed to maintain a stationary position and its heading optimal at zero degrees with the waves. However, to compensate for the fact that DP cannot keep the vessel heading perfect and to trigger all motions, the incoming wave angle is set to 165°, which means that the waves impact the vessel at an angle of -15° with respect to the bow.

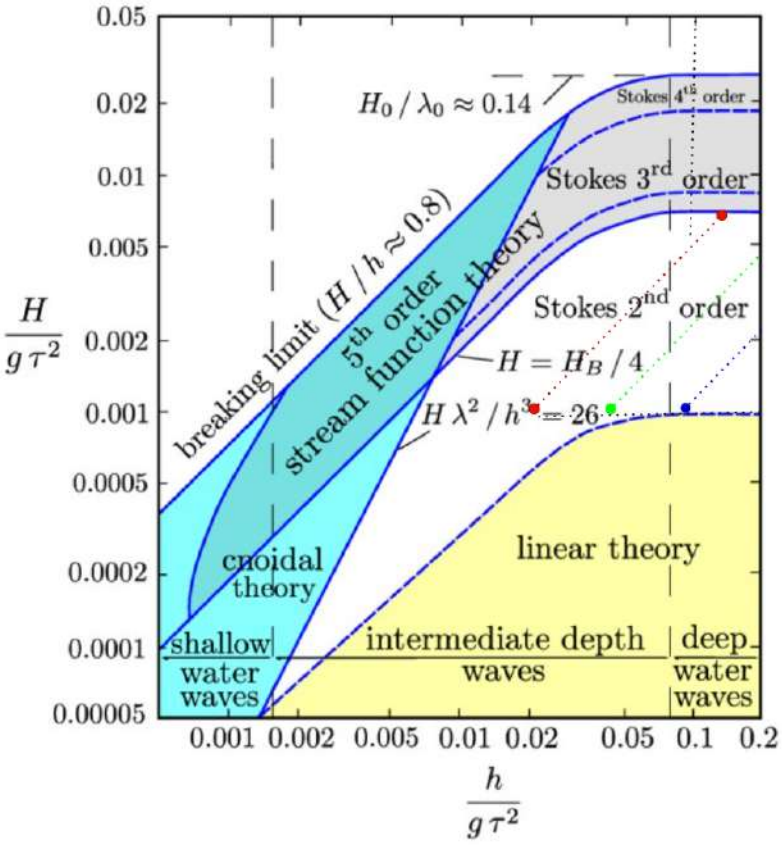

Figure 3.6: Wave theory selection based on dimensionless wave height and water depth with dots representing used wave conditions[26]

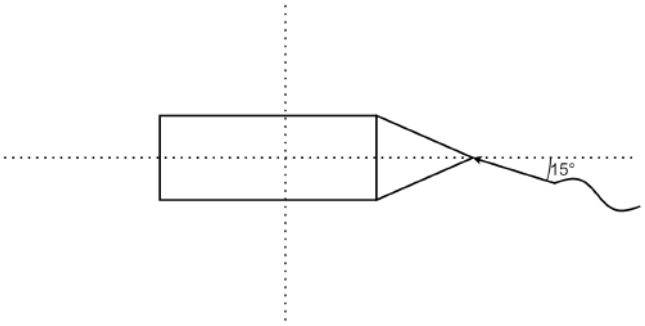

Figure 3.7: Angle of the considered incoming waves with respect to the vessel.

Environmental condition	Value	Unit
Wave height	2.5	m
Wave period	6 - 16	s
Wave incident angle	165	°
Wave type	Stokes	-
Water depth	50, 100 , 200	m

Table 3.2: Environmental conditions used in the modelling.

3.3.3. BOKA Falcon model

The BOKA Falcon is in OrcaFlex modelled as a vessel object. Its characteristics are known, and displacement RAOs are already available within Boskalis. These displacement RAOs are derived via the OrcaWave diffraction software using a mesh that represents the ship's hull. The RAOs are shown in appendix C. The motion in OrcaFlex is now easily calculated using the following equation:

$$x = Ra\cos\left(\omega t - \epsilon\right) \tag{3.5}$$

With x the position of the ship in m, R the RAO factor, a the wave amplitude, ω the wave frequency in rad/s, t the time in s and ϵ the phase shift in rad. Drilling is considered to be done from a point above the center of gravity (CoG) of the vessel. This reduces the heave motion caused by a rolling or yawing motion because there is no lever arm to create such heave motion. This is because r_x and r_y are zero in equation (3.6). Which are large contributors to the heave motion combined with the roll and pitch.

When using displacement RAOs in OrcaFlex, the vessel motion is not influenced by any other force. In other words, the motion of the vessel is only influenced by the waves, and thus the drilling process is assumed to have no influence on the motion of the vessel. The vessel and the drill rig are fully decoupled.

$$\begin{bmatrix} x_p \\ y_p \\ z_p \end{bmatrix} = \begin{bmatrix} x_s \\ y_s \\ z_s \end{bmatrix} + \begin{bmatrix} \phi_s \\ \theta_s \\ \psi_s \end{bmatrix} \times \begin{bmatrix} r_x \\ r_y \\ r_z \end{bmatrix} \tag{3.6}$$

In this equation, x is the x-position in m, y is the y-position in m, z is the z-position in m, ϕ is the roll angle in rad, θ is the pitch angle in rad, ψ is the yaw angle in rad, r_x is the distance in x-direction between the vessel CoG and the considered point on the vessel, r_y is the distance in x-direction between the vessel CoG and the considered point on the vessel, and r_z is the distance in x-direction between the vessel CoG and the considered point on the vessel.
The moonpool of the vessel in OrcaFlex is modelled as four objects that represent the walls of the moonpool. This makes sure that any possible contact between the drill string and the moonpool walls will be modelled and identified. The water in the moonpool is described by a so-called trapped water object in OrcaFlex. The fluid moves along with the object, so the sheltering effect is taken into account.

Another important aspect to consider, as mentioned before, is the low-frequency displacement. These motions are, in reality, compensated for by the dynamic positioning (DP) system on board the BOKA Falcon. Nevertheless, it cannot be presumed that the DP system is functioning perfectly, in other words, there will always be some sort of low-frequency motion pattern. Therefore, one scenario in the modelling will include such an excursion. But since these excursions are highly dependent on environmental conditions and DP settings, they motion behaviour is considered to be random, it is thus very hard to accurately model the second order motion of a DP vessel. These simulations exist, but require high computation times to obtain useful data. The scenario in which a second-order motion is considered is thus simplified. Because the exact motion of this effect is unknown, a fixed displacement is assumed to represent an extreme excursion that can occur during DP operations. The vessel is fixed at that point and experiences the same first-order motions as in the scenario excluding DP excursions. From internal sources at Boskalis, some data on DP operation of the BOKA Falcon vessel with the corresponding environmental conditions were gathered. Then it was decided to assume a severe case, where the static offset is assumed to be 1.5m from the centre of the borehole. The exact location is on the circle with a radius of 1.5m along the same direction as the incoming waves. It is visualised in figure 3.8.

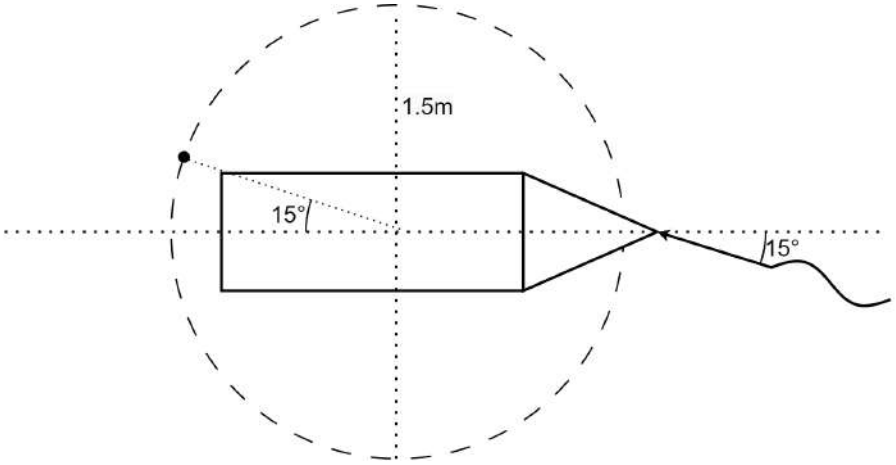

Figure 3.8: The used DP excursion point in the model, this drawing is not to scale.

3.3.4. Drill String model

The drill string is one of the most important aspects of the system. Most of the time, it is the limiting factor while drilling, and although this part is relatively inexpensive compared to other assets like the bottom hole assembly or motion compensation system, failure of this part can lead to high downtime and costly equipment damage. The drill string used in the RCD method is a relatively large diameter drill pipe. The exact dimensions can be found in appendix B. The drill string in OrcaFlex is modelled as a line element. A line element in OrcaFlex is a structural element, the behaviour of the element is calculated via a finite element method line theory. This line theory divides slender structures into many line segments. Each segment has a node at its end. On the nodes, material properties such as weight, buoyancy, and drag are lumped together. The nodes are connected to each other by different types of springs and dampers. These springs and dampers represent the structural characteristics of the line element. Each deformation direction has its own spring and damper. A visual representation of a line element in OrcaFlex is given in figure 3.9.
The drill string in real life consists of bolted together segments of 3 meters, in OrcaFlex the drill string is modelled as one continuous pipe. Airlift within the pipe is approximated by letting the content of the drill string in the model have the same air density. The material used for the drill string is S690 steel. The values for the added mass and drag coefficient are derived from the offshore hydromechanics book by Journée and Massie [20] and the derivations are added in appendix E.

Drill String Property	Symbol	Value	Unit
Inner Diameter	D_{in}	292	mm
Outer Diameter	D_{outer}	324	mm
Material Density	ρ	7.85	te/m^3
Young's Modulus	E	212	GPa
Yield Strength	σ_y	690	MPa
Poisson Ration	ν	0.293	-
Added Mass Coefficient	C_a	1	-
Drag Coefficient	C_d	1.2	-
BHA weight	m_{BHA}	70	te

Table 3.3: Drill string parameters used in OrcaFlex

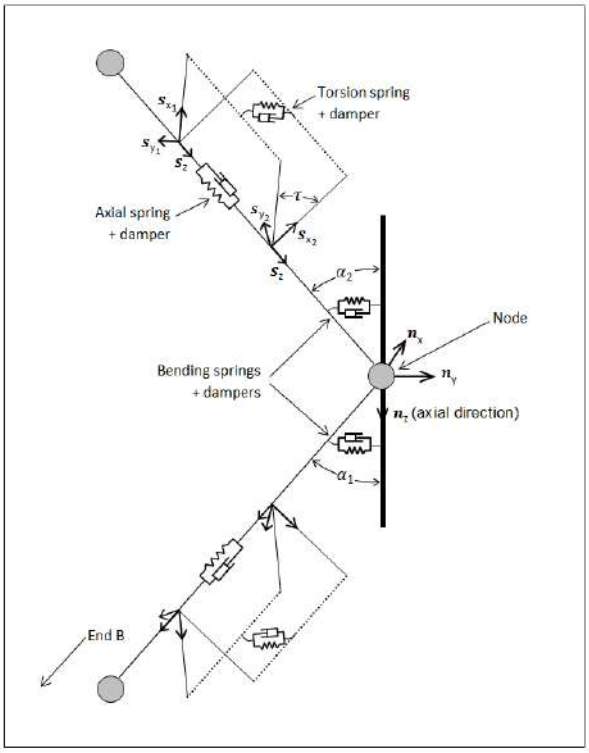

Figure 3.9: Schematic overview of a line element model in OrcaFlex [23].

Boundary conditions are an essential part of the dynamic characteristics of the drill string. The drill string model uses a total of four boundary conditions, the boundary conditions are commonly used in drill string analysis and can be found in the paper by Ghasemloonia et al. (2015) [11]. The boundary conditions are summarised below in section 3.3.4. The boundary condition at the top varies from concept to concept and will be discussed in section 3.3.5. In addition, a schematic overview of the structural model is given in figure 3.10.
The length of the drill string depends on water depth at which the operation is executed. The water depths that are considered are 50 metres, 100 metres, and 200 metres. 50 metres is relatively shallow and could be done using a jack-up vessel, however, the aim is to create an all-round solution to reduce costs. In figure 3.10, d represents this water depth and leads to drill string lengths of 73, 123 and 223 metres, respectively. The drill string model is divided into segment lengths of 1m, this has good accuracy without introducing higher calculation times. Longer drill strings in this case do have more segments, requiring more computational time.

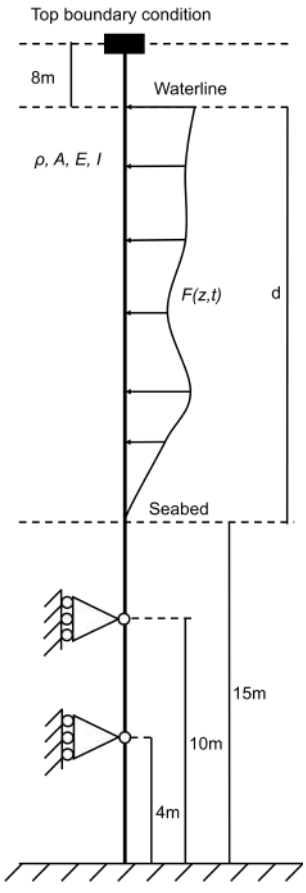

Figure 3.10: Schematic overview of the structural drill string model.

There are of course shortcomings in the way of modelling the drill string like this. An aspect missing is the coupling between vibration modes. OrcaFlex does not have a detailed mesh of the considered drill string, but springs that represent the structure. These springs are only for the dedicated direction of deformation. This means that complex vibration modes that may occur will not be modelled. Another weakness is that the drill string is modelled as a continuous pipe. The flanges and bolt connections are not taken into account, and these aspects may change characteristics like the bending stiffness or increase stresses due to stress concentrations

at the flanges. A final remark is that the bottom boundary condition where the drill string is fixed to the bottom is only valid when no liftoff occurs. If lift-off occurs, it will result in high stresses as a result of the sudden switch from partly compression to full tension.

Boundary condition	Constraint motion	Description	Location
Simply supported	X,Y	Upper Stabiliser	10m above bottom
Simply supported	X,Y	Lower Stabiliser	4m above bottom
Fixed	All directions	Interface at bottom	Borehole bottom

Table 3.4: Boundary conditions of the drill string

Initial Conditions

The initial conditions are based on the desired mean properties during drilling. The most important factor that determines this is the WoB goal. The weight on bit goal is set to be 75% of the weight of the BHA. This ensures that the drill string itself is under tension, which improves the verticality of the drilled hole. These conditions remain constant at the beginning of all simulations.

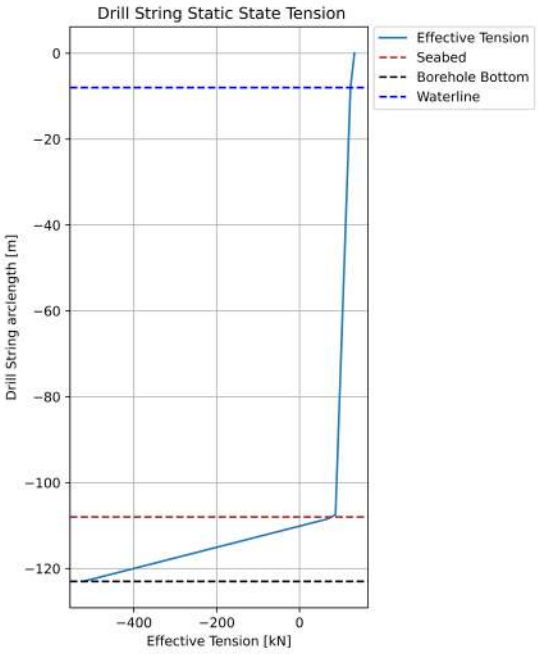

Figure 3.11: Tension distribution in the static state for a water depth of 100m.

3.3.5. Compensation models

There are two different compensation models in this thesis. One for passive systems and one for active systems. Each model has its own set of assumptions and boundary conditions. These models are designed to work in series. In other words, there is one imaginary actuator per degree of freedom that is either active or passive. This actuator works only for its designated degree of freedom. So, for example, for the 3DoF Rotation concepts, there is one cylinder compensating for heave, one cylinder compensating for roll, and one cylinder compensating for pitch. In reality, such a system is analogous to the Barge Master system shown in figure 2.5a. Here, there are three vertical cylinders working together to compensate for all these motions, and thus this system is parallel. Parallel systems are systems that can exist relatively easily in the real world. Serial systems would take up a lot of space and rotational cylinders would be very complex systems.

Passive compensation

Passive compensation are physical low-pass filters consisting of springs and dampers [33]. These springs are as mentioned inchapter 2 gas springs. In the OrcaFlex models, passive systems are mod-

elled as constraint elements with specific stiffness and damping. The horizontal and vertical compensator stiffnesses are different from each other, since in the vertical direction there is a constant opposing force, which is the weight of the drill string. The different stiffnesses are split by stacking two constraints on top of each other. Stiffness and damping in the vertical direction are based on the passive heave compensation system mentioned in the book Motion Control in Offshore & Dredging by Albers [2]. The damping here is inherent to the hydraulic gas spring stiffness, these are created by factors such as friction and flow losses. All parameters are assumed to be constant except the initial gas pressure. Parameters are given in table 3.5. The stiffness is then assumed to be linear on the basis of the linearisation provided by Woodacre et al. [33]. This stiffness is given as:

$$k = \frac{np_0A^2}{V} \tag{3.7}$$

In this linearisation, n is the polytropic index, which is 1.3, p_0 is the initial gas pressure in the system, A the diameter of the piston, and V the total gas volume. In theory the ideal passive compensator has an almost constant force for every actuator position, if equation (3.7) is considered, increasing the airbank volume will decrease the stiffness. This is thus feasible for passive heave systems.

$$F_0 = F_{g,DrillString} - F_{WoB,goal} \tag{3.8}$$

In this equation, F_0 is the initial force in the compensator, $F_{g,DrillString}$ the weight of the drill string and $F_{WoB,goal}$ the objective force on the soil. The weight of the drill string varies for different water depths, thus for every depth, the initial pressure must be adjusted. The lateral stiffnesses are chosen to be as low as possible, since there is no mean force on the drill string in that direction combined with the principle that the best passive compensator has a constant force for every position. However, zero stiffness is not possible because the drill string would not hold at the specific place on the vessel if any excitation occurred.

The rotational stiffness is again a special case. For compensation in the yaw direction, no compensation is necessary, as the drill string is already rotating itself during the drilling process. The other two directions are assumed to have the same stiffness. In this case, no stiffness is assumed since the drill string acts as a pendulum that rights itself downward. Therefore, the rotational stiffness is set to zero. The system is assumed to be infinitely stiff if the direction is not compensated for. For example, passive 1DoF has only stiffness in the z-direction, the other directions are infinitely stiff. The top boundary condition is then if rotation compensation is included as a hinge or free rotation.

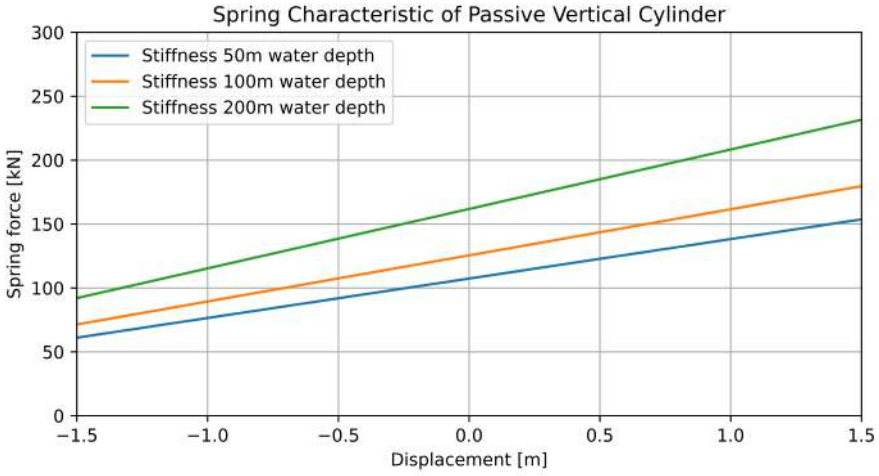

Figure 3.12: Linearised spring characteristic, based on passive system found in Motion Control in Offshore & Dredging [2].

Parameter	Symbol	Value	Unit
Cylinder Diameter	D	0.36	m
Average external load	F	107.309, 125.463, 161.77	kN
Average gas volume	V	0.485	m
Polytropic gas constant	n	1.3	-
Damping	b	5.8	kN/s

Table 3.5: Parameters of considered gas spring

Active compensation

The active compensation model, in this thesis active position-based systems are considered, is relatively easy compared to all complex control schemes used in the industry. Since it is important to keep the performance of each concept the same for comparability, it is not chosen to include control in the active compensation. In theory, controllers can be as accurate as one would like, given that the system does not include any losses. Thus, to make an accurate representation, it is necessary to model aspects of the system, such as frictional or fluid losses. This varies for every system. Thus, every system would need to be accurately modelled. To avoid this and generalise an active system, it is chosen to summarise the performance of active compensation in a compensation efficiency. This compensation efficiency determines the residual motion based on the ship motion, this efficiency is defined as:

$$\eta_{compensation} = 1 - \frac{\text{Residual Motion}}{\text{Ship motion}} \times 100\% \tag{3.9}$$

Here, a compensation of 100% means that there is no residual motion left and that the motion of the specific point is fully decoupled from the motion of the ship. Compensation efficiency numbers are based on those found in the literature [19][9]. In this way, the performance of each active compensation concept is comparable. In OrcaFlex this is modelled as a constraint with imposed motion that has a fraction of the ship motion. In the models used in the analysis an efficiency of 95% is assumed. As for structural boundary condition, it is fixed at a point on the vessel, only that point imposes a motion on the top of the drill string. Each fictional hydraulic cylinder that controls motion is assumed to have infinite stiffness. That is why it is assumed to be fixed at the point where the motion is imposed.

Now, the model is explained, and next, it will be explained how the performance of all the concepts will be determined. It will include how these parameters are derived and what their physical meaning is with respect to the drilling process.

3.4. Key Performance Indicator selection

To assess the performance of each concept, important quantitative key performance indicators (KPI) must be determined. These KPIs are based on physical parameters in the system and are carefully chosen to cover the most critical aspects of the system. The first important aspect that will be explained is weight on Bit (WoB), followed by a structural integrity indicator, and finally a factor that indicates the fatigue strength of the system.

3.4.1. Weight on bit

One of the important factors in the drilling process is the weight on bit, which means how much force is exerted on the rollers by the BHA and the drill string. This force determines the production of drilling process, the better the ability to control this force, the more efficient production is possible. Since the drill string is in motion at the top in all directions, the force on these rollers will vary. Controlling this force refers to keeping the variation of this force as low as possible. A low amplitude means that the force can be set accurately for optimised production. Since regular waves are used for this analysis, the time series of this weight on bit will be regular as well. Therefore, the value that will be used here is the amplitude of this time series. For this KPI it is thus important to keep this amplitude as low as possible, a lower amplitude means a better performing concept. An important aspect of the weight on bit that must be avoided at all times is the lift-off of the drill bit. This means that the drill bit is cleared of the ground, followed by the drill bit being smashed back onto the ground. This behaviour is very destructive to the drilling equipment and will most likely create a less accurate borehole shape. Thus, if

this behaviour is noticed once, it means that the corresponding concept is not suitable for that specific environmental condition. This behaviour can be noticed by checking if the weight on bit value becomes negative. The weight on bit is measured in the system by taking the vertical end force at the lowest fixed boundary condition, a positive value means a downward force or compression, and a negative force implies an upward force, this means lift-off and full tension in the drill string. An example of a time series can be seen in figure 3.13, notice the lift off that occurs as the WoB becomes negative. This means that this concept is not suitable for this specific environmental condition.

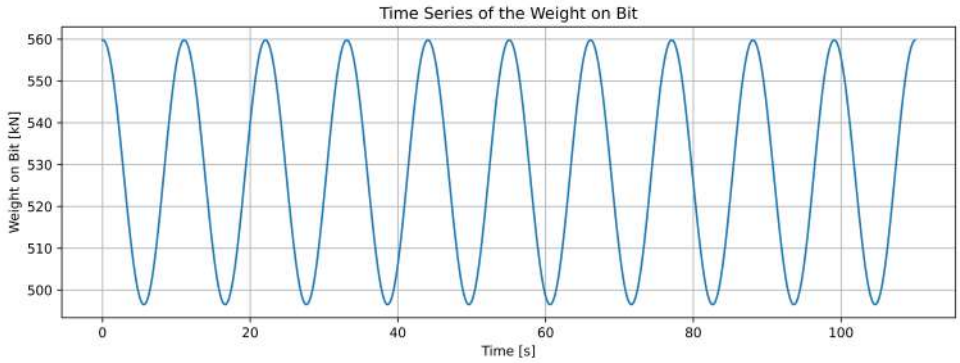

Figure 3.13: An example of a time series of WoB, for this case its 1DoF Active 200m water depth with a wave period of 11s.

3.4.2. Structural integrity

To ensure that the drill string does experience plastic deformation, the maximum stress level within the drill string should be lower than the yield strength of the material. The material is S690 steel, as mentioned before, this steel has a yield strength of 690 MPa, as the name suggests. The criterion that is used to check this is the Von Mises yield criterion. The von Mises stress should be lower than the yield stress to avoid plastic deformation of the drill string. The Von Mises stress is calculated in the following way:

$$\sigma_{VonMises} = \sqrt{\frac{1}{2}\left[(\sigma_{11}-\sigma_{22})^2 + (\sigma_{22}-\sigma_{33})^2 + (\sigma_{33}-\sigma_{11})^2\right] + 3\left(\sigma_{12}^2+\sigma_{23}^2+\sigma_{31}^2\right)} \tag{3.10}$$

Here, the stresses indicated with two 1s, 2s, or 3s are the axial stresses in the X, Y, and Z directions. The other three stresses are the shear stresses in each plane. In OrcaFlex, the Von Mises stress can be directly gathered from the results. The maximum Von Mises stress is obtained by taking the maximum value of a range graph for the drill string. The range graph plots the minimum, maximum, and mean values of a specific parameter for the drill string, then in Python it is relatively easy to determine what the maximum Von Mises stress is. The maximum Von Mises stress is only considered in the drill string, thus excluding the bottom hole assembly. This is because the exact geometry of the bottom hole assembly is unknown and it is assumed that the drill string is the most critical aspect [27]. Moreover, since no torsion is included in this model, the shear stress in the x-,y plane is lower, and thus the calculated Von Mises stress is also lower.

3.4.3. Fatigue strength

The drilling process is a time-intensive process, with drilling rates of around a metre per hour [4], drilling a hole can take up to a day. During this time, the drill string experiences many changes in bending stress and many torsional rotations to rotate the drill bit. Fatigue failure is the main cause of failure 65% in time during drilling[27]. Therefore, it is important to analyse some form of capacity of the compensation system to keep fatigue damage as low as possible. A large contributor to fatigue damage in drill strings is the rotation of the drill string itself. If there is constant bending stress in the drill string, the drill string rotates through the stress range at all rotations [18]. Then the number of stress cycles increases greatly. However, since drill string rotation is not taken into account in OrcaFlex, another way to calculate this effect is necessary. To do this, the time series of the bending stress is multiplied

by a sine with the frequency of the rotation speed. This then simulates the extra effect of the rotation on the bending stress. However, this only gives the contribution to fatigue by the bending stress, other aspects such as the variation in tension or shear is not taken into account, but they are assumed to be small compared to the fatigue from rotating bending stress.

Fatigue damage is calculated using an S-N curve, and the S-N curve links for every stress amplitude how many cycles the material can experience to reach failure. The S-N curve of S690 steel is given in figure 3.14. For this analysis, the S-N curve with a safety factor of 1 is used, but a line is drawn at $d = 0.1$, the damage cannot exceed 10% of the fatigue failure damage. In terms of the load case, all concepts and water depths are tested with the same one. A 1-hour sea state represented by the JONSWAP spectrum with $H_s = 2.5m$, $T_p = 10$, and $\gamma = 1$ (A JONSWAP spectrum with $\gamma = 1$ is a Pierson-Moskowitz (PM) spectrum). This results in damage caused by the rotating bending stress. Finally, this is transformed into a damage per year value for when the system would operate year-round in the set sea state. Additionally, a stress concentration factor (SCF) of 2 is used to take into account the stress concentrations that occur at the flanges at each end of the drill pipe.

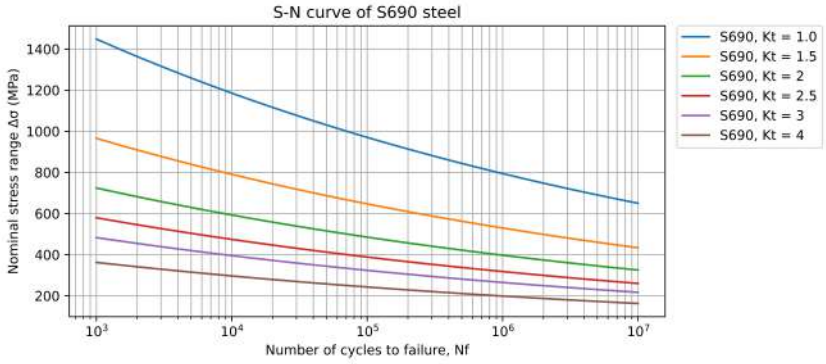

Figure 3.14: S-N curve of S690 steel with different stress concentration factors Kt.[7]

Fatigue damage is calculated by first extracting the location of the maximum bending stress in the drill string. It is assumed that at that place the maximum fatigue damage occurs. At this location, a point is taken at the outer diameter of the drill string is taken. At this point, the bending stress time series is extracted. Now, to add the rotation to this, the signal is multiplied by a cosine with a frequency of $2\pi/3rad/s$ or 20 rpm. This creates the effect as if the point is rotating through the bending stress time signal, this increases the number of cycles the point experiences and thus gives a more accurate representation of the fatigue damage, since bending stress combined with rotation is a great contributor tho the fatigue damage.
Since bending stresses play an important aspect in fatigue damage, additional cases are considered [18]. The extra cases consist of a DP offset, a current, and both at the same time. These effects create a mean bending stress in the drill string. The time series is still 1 hour long in the same sea state. This gives an indication of to what extent an increase in mean bending stress reduces fatigue life. The DP offset is the same as in figure 3.8, the current is defined as a linear decreasing current velocity with a velocity of 1m/s at the sea surface and zero velocity at the seabed. The moonpool again protects the drill string from the current near the surface. The results are given in the same type of graph as described earlier, a damage per year for that specific load case.

3.5. System Characteristics identification

Finally it is important to have good knowledge of global system characteristics, in this case a very important aspect is the natural frequencies of the system. Natural frequencies are important to know because destructive amplification of vibrations can occur if the system is excited at the same frequency. The natural frequencies of the proposed concept will vary from concept to concept and with different water depths. The most important modes of vibration are lateral vibrations as these are the only forms of vibration where their corresponding natural frequencies could coincide with the wave frequency band, other natural frequencies such as axial natural frequencies are too high to be excited by the waves for drill strings of this length. It should also be noted that lateral vibration has more damping due to the larger lateral velocities, drag coefficient, and frontal area, which increase hydrodynamic drag substantially compared to, for example, axial vibrations.

Natural frequencies are derived from the system using the OrcaFlex modal analysis tool and are verified by performing free vibration tests. First, the motion of the ship is taken out of the equation because the ship motion will create varying tension in the drill string, which changes the natural frequency. The modal analysis tool in OrcaFlex analyses the undamped version of the system, therefore it does not capture the shift in natural frequency due to damping. Therefore, the damping ratios are estimated using the logarithmic decrement, this method is explained later. In addition, the tests are performed with different levels of damping. The following scenarios are considered with this free vibration test.

- Full damping, damping is kept the same as in the first simulations
- Passive cylinder damping removed, the motion compensators are springs only
- Hydrodynamic drag removed, the cylinder damping is kept but the drag force is set to zero
- No damping at all, hydrodynamic drag and cylinder damping is removed.

The free vibration tests are based on the fact that a structure in free vibration oscillates in a combination of all modal shapes the system has. Therefore, if a spectral density is taken from a specific point on the drill string, clear peaks should emerge at specific frequencies if the system does not have too much damping. These frequencies are the natural frequencies of the modes of the system. For each mode, the damped and undamped natural frequencies can be compared. If equation (3.13) is used, the damping ratio for each mode is used. As said above, damping influences the natural frequency, and increasing damping decreases the natural frequency, as can be seen in equation (3.13). An increase in damping also reduces the peaks of a spectral density and spreads it out over a wider frequency band, this can be seen in figure 3.15, if too much damping is present in the system, it is hard to observe these peaks.

$$\omega_{n,undamped} = \sqrt{\frac{k}{m}} \tag{3.11}$$

$$\xi = \frac{c}{c_{critical}} \tag{3.12}$$

$$\omega_{n,damped} = \omega_{n,undamped}\sqrt{1-\xi^2} \tag{3.13}$$

In these equations, $omega_n$ is the natural frequency in rad/s, k is the spring stiffness, m the vibrating mass, c the damping coefficient and ξ the damping ratio.
The results of this analysis is a table that has the first five natural periods for the lateral vibrations of all concepts and water depths. These are supported by the time series of specific nodes for all the concepts and water depths as well. From this dampened out lateral response, the periods between the peaks are derived as well as the logarithmic decrement which estimates the damping ratio based on the reduction in response amplitude between a specific amount of periods. The logarithmic decrement calculation is as follows:

$$\Delta_N = \frac{1}{N} \ln \frac{u(t)}{u(t+NT_d)} \tag{3.14}$$

$$\xi = \frac{\Delta_N}{\sqrt{4\pi^2 + \Delta_N}} \tag{3.15}$$

Here, Δ_n is the logarithmic decrement, N is the number of periods taken between the considered values, t the time in s, T_d the period in s. From the derivation of this damping ratio, the damped natural

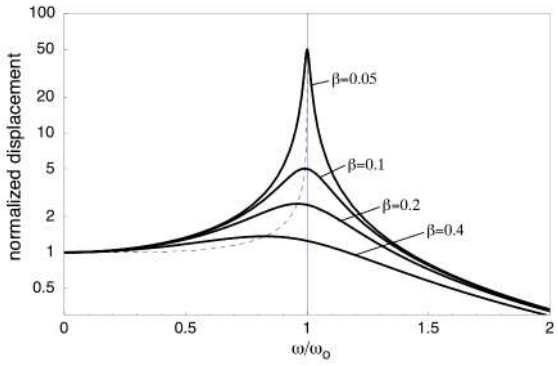

Figure 3.15: Characteristic of natural frequency peaks for different damping ratios for a mass-spring-damper system [30].

frequency can be determined if high damping ratios are present, this can be based on equation (3.13). It has to be noted that the logarithmic decrement method is meant for 1DoF oscillators such as a simple mass-spring-damper system, but it still gives a good estimation of the level of damping that can be expected in the system. Estimating the damping ratio in the overall system in this paper is hard, since the drag in OrcaFlex is calculated with the Morison equation, which results in non-linear damping. Obtaining this estimate of the damping ratio would also indicate whether the choice of damping in the passive systems is adequate.

4. Concept Identification Results

In this chapter, the results of the first analysis are discussed, and the result for each KPI introduced in chapter 3 will be discussed separately. Based on the values of these KPIs for all concepts, the best performing concept is chosen. Furthermore, the results of the natural frequencies will be presented to see whether problematic behaviour can or has occurred during the analysis. This part is followed by the optimisation of the result of the best-performing concept.

4.1. Compensation type identification

In this section, the results of the concepts are discussed. Each KPI is discussed individually, additionally notable observations are made. Finally, a conclusion is drawn on the basis of these KPIs and other important aspects.

4.1.1. Weight on bit performance

First the weight on bit performance is considered, the results will display a WoB amplitude. An amplitude is chosen since the WoB time series is regular, this is because the input is also regular. The lower the amplitude, the better the performance is considered. The amplitude is plotted against the wave period. And for each water depth, a separate plot is given containing every concept. First, a plot containing all without a DP excursion is shown, then divided into active and passive concepts, and now the DP excursion is included. In every plot, the mean of the WoB signal is plotted, which can be recognised as a faded line in the plot. If the WoB amplitude is above the mean, a lift-off occurs.

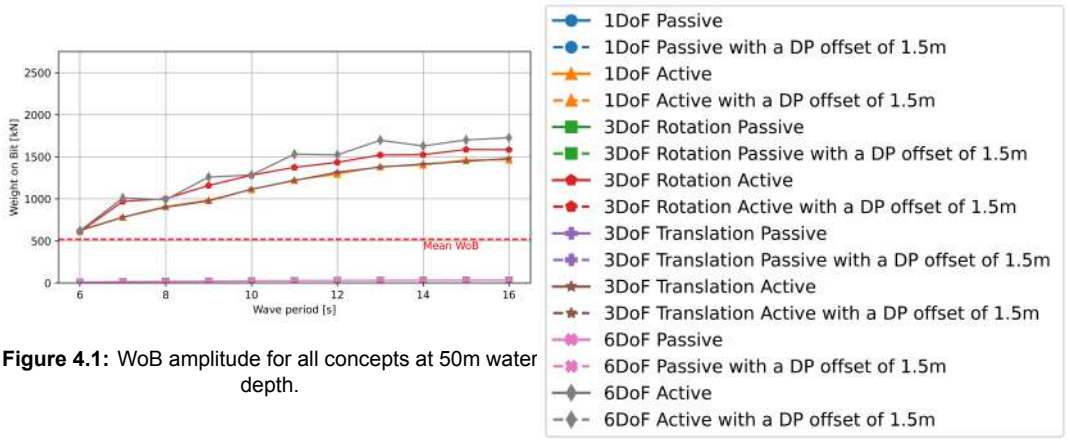

Figure 4.1: WoB amplitude for all concepts at 50m water depth.

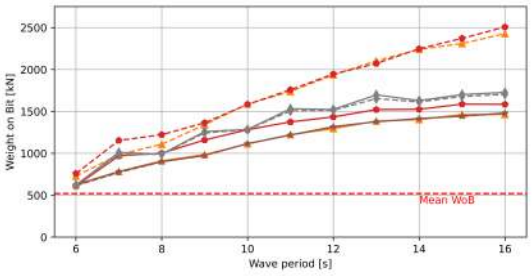

Figure 4.2: WoB amplitude for all active concepts at 50m water depth including a DP offset.

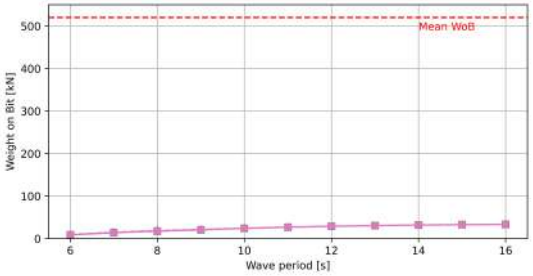

Figure 4.3: WoB amplitude for all passive concepts at 50m water depth including a DP offset.

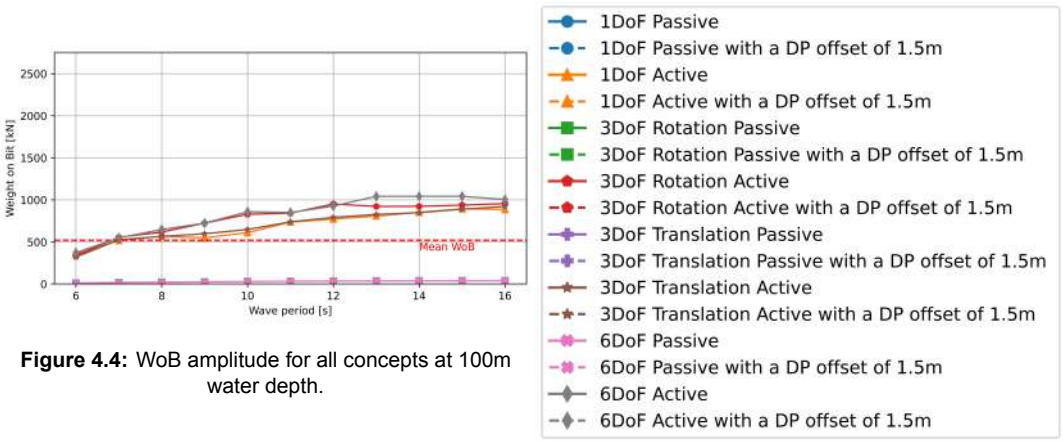

Figure 4.4: WoB amplitude for all concepts at 100m water depth.

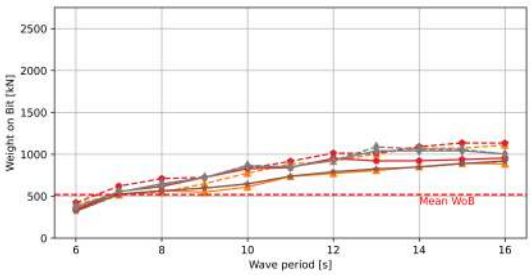

Figure 4.5: WoB amplitude for all active concepts at 100m water depth including a DP offset.

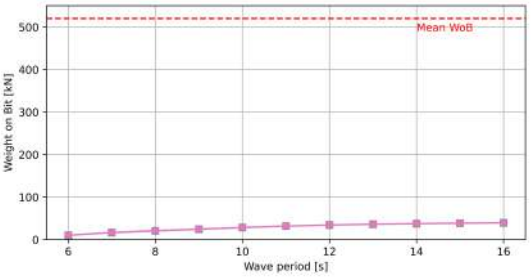

Figure 4.6: WoB amplitude for all passive concepts at 100m water depth including a DP offset.

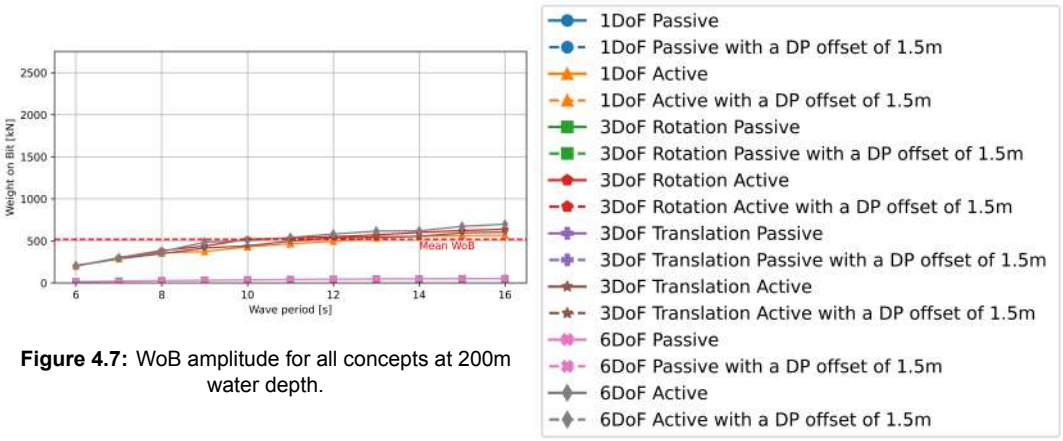

Figure 4.7: WoB amplitude for all concepts at 200m water depth.

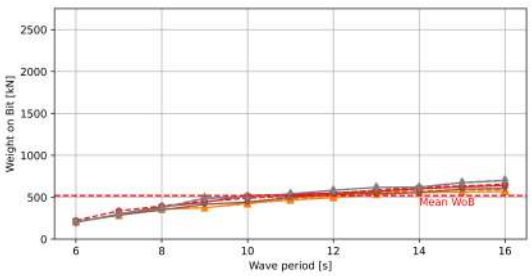

Figure 4.8: WoB amplitude for all active concepts at 200m water depth including a DP offset.

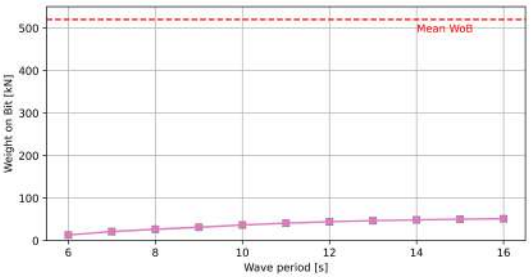

Figure 4.9: WoB amplitude for all passive concepts at 200m water depth including a DP offset.

The first observation that can be made is that the WoB amplitude for active systems is very high compared to passive systems. The amplitude line is above the mean WoB line for most of the wave periods, and only at low wave periods and deeper waters does lift-off not occur. Therefore, active position-based controlled concepts are not suitable for this application. This is mainly because these systems are very stiff in the vertical direction. The performance of these systems must be very high to reduce the residual vertical motion to a level that is in the range of axial deformations of the drill string. The overall performance of the passive systems is very similar, and here no lift-off occurs at all. It can also be seen that horizontal active position-based compensation completely reduces the effect of a second-order excursion, while for passive systems, this is not the case. Second, it can be observed that the WoB amplitude increases as the wave period increases. This can be traced back to the ship RAO, where motions increase for longer periods. This is mostly caused by the heave motion, as this is the most problematic motion of the vessel. What is also interesting is that the order of the water depth is flipped. For active position-based systems, shallower waters have higher WoB amplitudes, whereas for passive systems, this is flipped. The longer the drill string, the lower the stiffness, so more vertical motion can be absorbed by it, it would then suggest that for longer drill strings the WoB amplitude would thus be lower. This is still the case for passive systems, but the stiffness of the gas spring has a greater influence on the WoB. If the drill string is longer, it becomes heavier. It is necessary to change the increase pressure of the system if the piston area remains constant, this increases the system stiffness given that the gas volume remains the same. This relation is given in equation (2.11). Therefore, for larger water depths, the stiffness increases here, and thus also the WoB amplitude. Another conclusion can be made here that the ideal passive system would have zero stiffness, a constant force will then be acting on the system for all displacements. In theory, this was achieved by increasing the accumulator volume to infinity. The conclusion based on the WoB amplitude KPI is that active systems are not suitable with the current proposed efficiency and wave conditions, and passive systems are very suitable, but all have the same performance.

4.1.2. Structural performance

The structural performance is displayed in the same way as the WoB amplitude, different lines for different water depth, and on the horizontal axis the wave period. On the vertical axis is the maximum Von Mises stress that occurs during the simulation. Stress is evaluated only on the drill string since this is the limiting factor. The stress in the bottom hole assembly is not evaluated, as the exact geometry is not known. One side-note to this result is that the stress in real life will probably be higher, this is because in the simulation rotation and torque are not included in the model. Additionally, the drill string is modelled as a continuous pipe, so there may be places where stress concentrations can occur that are not modelled now. This again was analyses using regular waves similar to earlier.

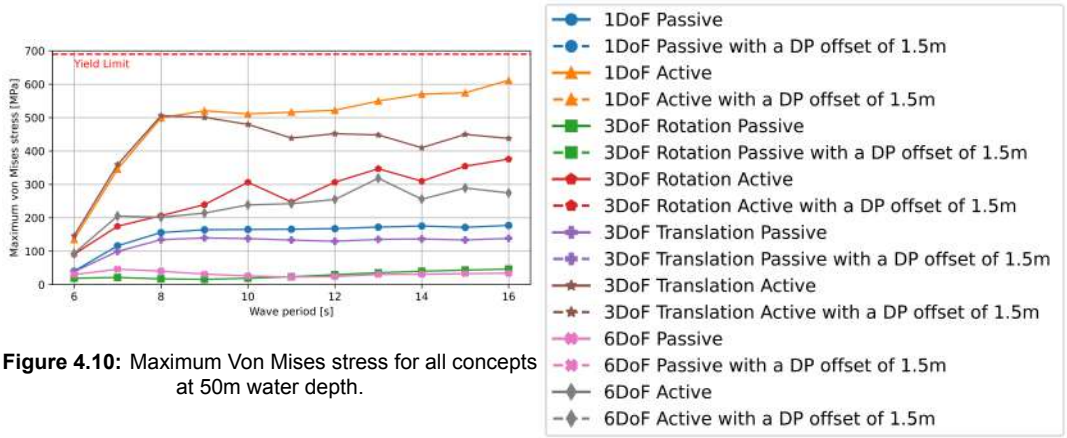

Figure 4.10: Maximum Von Mises stress for all concepts at 50m water depth.

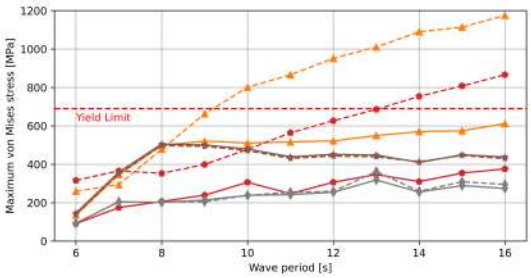

Figure 4.11: Maximum Von Mises stress for all active concepts at 50m water depth including a DP offset.

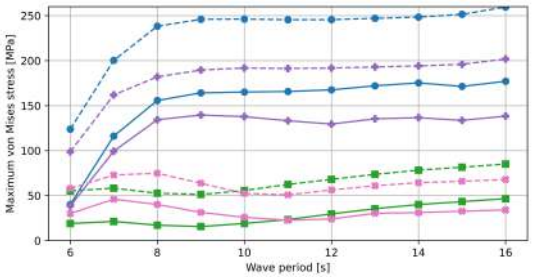

Figure 4.12: Maximum Von Mises stress for all passive concepts at 50m water depth including a DP offset.

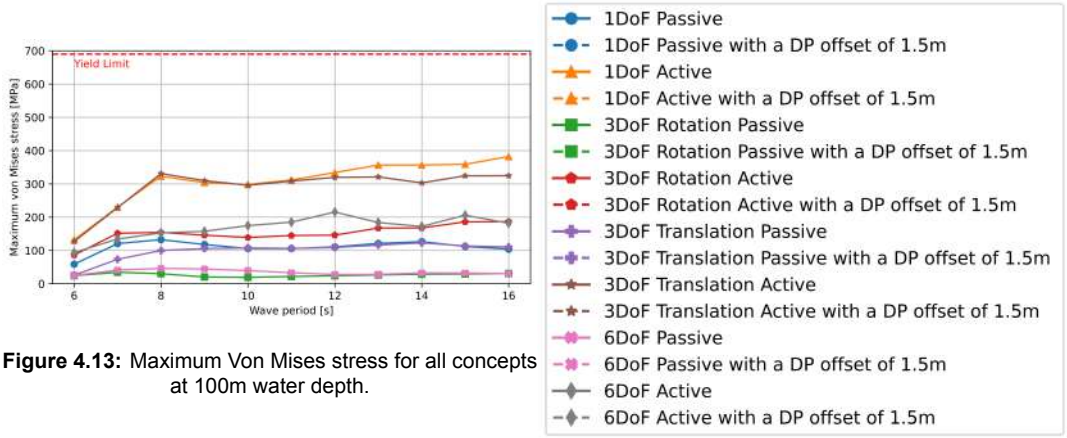

Figure 4.13: Maximum Von Mises stress for all concepts at 100m water depth.

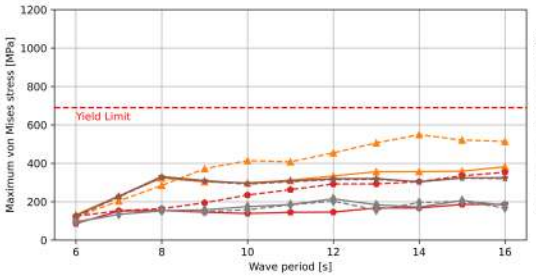

Figure 4.14: Maximum Von Mises stress for all active concepts at 100m water depth including a DP offset.

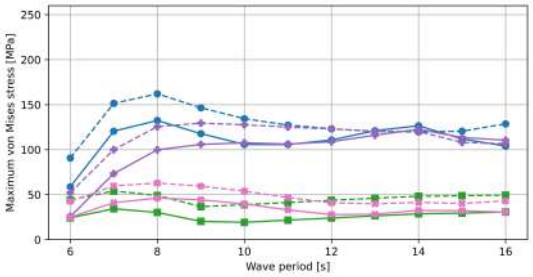

Figure 4.15: Maximum Von Mises stress for all passive concepts at 100m water depth including a DP offset.

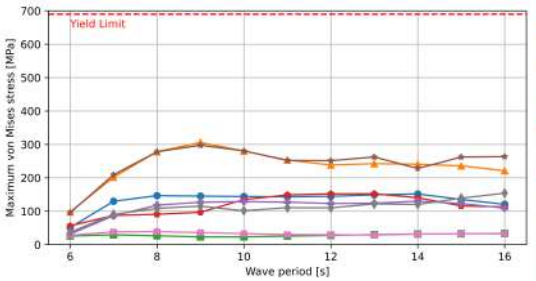

Figure 4.16: Maximum Von Mises stresse for all concepts at 200m water depth.

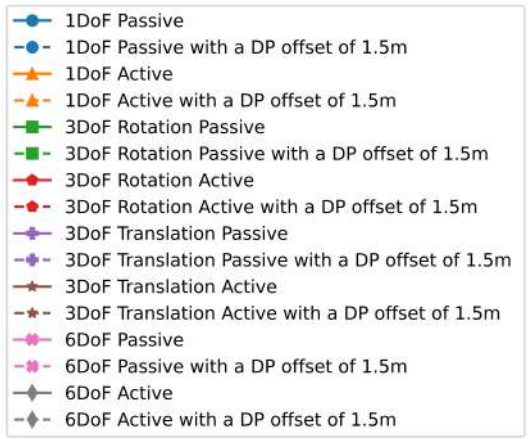

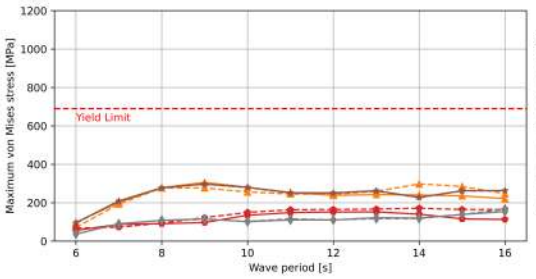

Figure 4.17: Maximum Von Mises stress for all active concepts at 200m water depth including a DP offset.

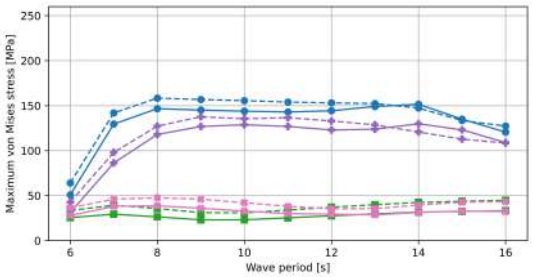

Figure 4.18: Maximum Von Mises stress for all passive concepts at 200m water depth including a DP offset.

Here, it can be seen that, for active systems, the stress is significantly higher than for passive systems. It can be seen that for shallow waters that if a second-order excursion is evaluated, the von Mises stress even exceeds the yield strength of 690 MPa of the material, and thus drill string failure occurs here. Also, again, if active translational compensation is present, the extra excursion is compensated for and there is no extra stress present. What can be seen is that now for passive systems, the stress differs between different concepts. The stress is lower for concepts where the roll and pitch rotation is compensated for. Also, for larger depths or longer drill strings, the difference between with and without constant ship excursion becomes smaller. This is mainly because when the length of the drill string increases, the bending and axial stiffness decrease, for the same displacement, there are lower forces and thus less stresses. The bending stiffness depends on the force and boundary conditions but generally follow the same structure, examples are given in figure 4.19. The axial stiffness is described by the following.

$$k_{axial} = \frac{EA}{L} \tag{4.1}$$

Here k is the stiffness, E is the Young's modulus, and A is the area. In figure 4.19, I is the area moment of inertia.

Edge Conditions and Loading Diagrams	Elastic Stiffness, K_e	Elasto-Plastic Stiffness, K_{ep}	Equiv. Elastic Stiffness, K_E
L	$\frac{384EI}{5L^4}$	—	$\frac{384EI}{5L^4}$
P, L/2, L/2	$\frac{48EI}{L^3}$	—	$\frac{48EI}{L^3}$
L	$\frac{185EI}{L^4}$	$\frac{384EI}{5L^4}$	$\frac{160EI^*}{L^4}$
P, L/2, L/2	$\frac{107EI}{L^3}$	$\frac{48EI}{L^3}$	$\frac{106EI^*}{L^3}$
L	$\frac{384EI}{L^4}$	$\frac{384EI}{5L^4}$	$\frac{307EI^*}{L^4}$
P, L/2, L/2	$\frac{192EI}{L^3}$	$\frac{48EI^{**}}{L^3}$	$\frac{192EI^*}{L^3}$
L	$\frac{8EI}{L^4}$	—	$\frac{8EI}{L^4}$
P, L	$\frac{3EI}{L^3}$	—	$\frac{3EI}{L^3}$
P/2, P/2, L/3, L/3, L/3	$\frac{56.4EI}{L^3}$	—	$\frac{56.4EI}{L^3}$

Figure 4.19: Bending stiffness for beams with different loading conditions and boundary conditions

Based on the stress analysis, it can be seen that the best performing concepts are 3DoF Rotation Passive and 6DoF Passive. These concepts include the ability to compensate for roll and pitch rotation, which greatly reduces the bending stress at the top, since the boundary condition results in zero moment at the hinged position. And with reduced moments, the overall stress levels are reduced.

4.1.3. Fatigue life performance

The fatigue results are the damage caused by the load case described in section 3.4.3. The results are given as damage per year, and the red line is a total damage of 1/3. Generally, a safety factor of 3 is used in fatigue analysis, as the probability of failure increases with greater accumulated damage. This ensures that the maximum probability that a failure can occur is 2.3% [12] [32].

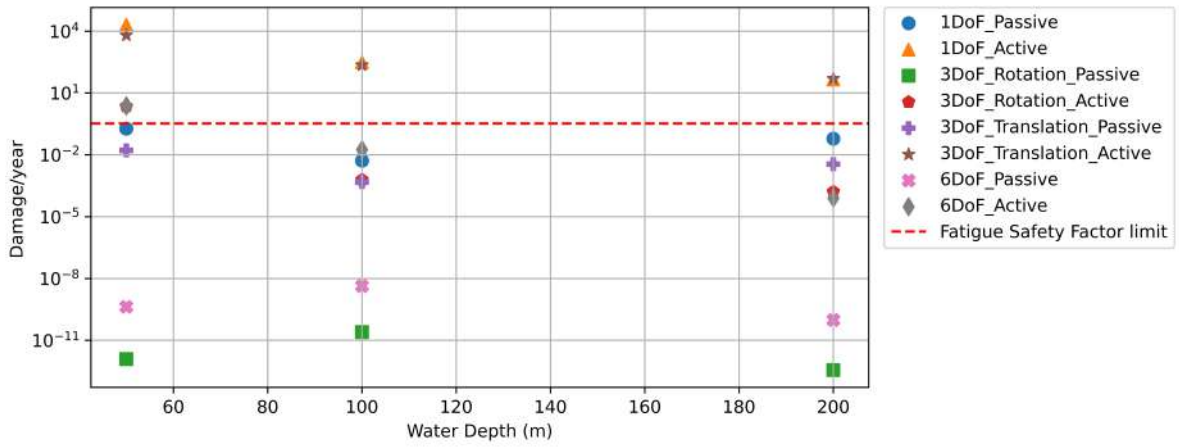

Figure 4.20: Rotational bending fatigue damage per year in a sea state with $H_s = 2.5m$, $T_p = 10s$, $\gamma = 1$.

From figure 4.20 it can be seen that fatigue damage in passive concepts that have rotation compensation is much lower than in the rest of the concepts. Other concepts score worse, and some even fail multiple times during one year of drilling in this sea state. This comes from the fact that the passive rotational compensation is modelled as a hinge. There are thus small bending moments at the top, in fact the maximum bending stress for the 3DoF Rotation Passive and 6DoF Passive occurs above at the interface with the bottom hole assembly.

A correlation between fatigue damage and maximum bending stress can be observed by plotting the max bending stress from each simulation against the fatigue damage. It is expected that as the bending stress increases, the fatigue damage will also increase. A function can be fitted to the data which can be used to estimate the fatigue life based on the maximum bending stress. The equation for this is:

$$\frac{\text{Damage}}{\text{Year}} = 1.004\sigma_{bend,max}^{0.0028} \tag{4.2}$$

It has to be noted that this is very specific to the rotation speed, for this fatigue analysis a rotational speed of 20 rpm was used.

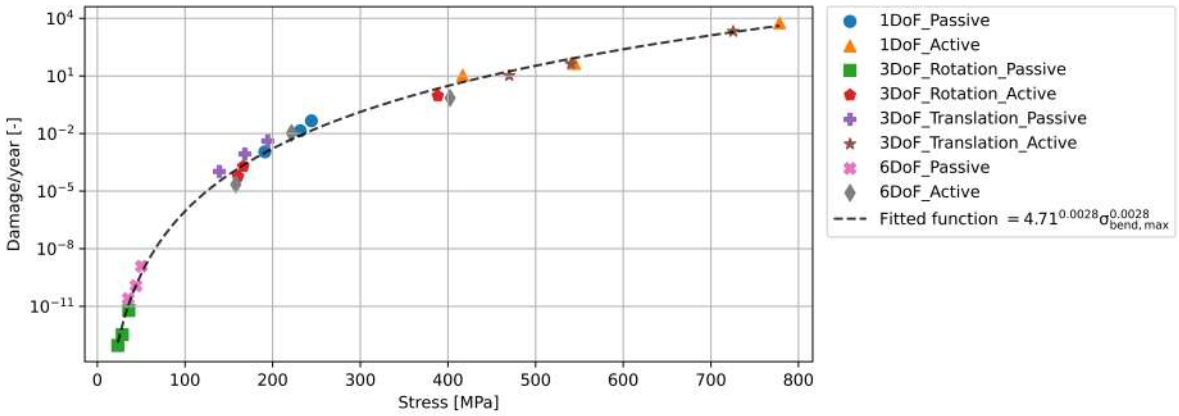

Figure 4.21: Correlation between the maximum bending stress and fatigue damage/year when considering the load case described in chapter 3

4.1.4. Natural frequency

Natural frequencies are determined as discussed in section 3.5. The power spectral density is taken of node number 25 on all of the drill strings, this position does not coincide with a node of any of the first five modal shapes, here a node is meant as a point that is stationary during vibration. In appendix H this can be recognised as a point that is on the zero line on the x-axis. The power spectral densities are

found in appendix G. Peaks are found using a peak-finding algorithm from the SciPy library available in Python. The periods are given in table 4.1. The corresponding mode shapes are given in appendix H.

Concept	# mode	50m	100m	200m
1DoF Passive	1st	2.47	6.36	14.59
	2nd	1.01	2.63	6.68
	3rd	0.61	1.45	3.98
	4th	0.38	0.94	2.65
	5th	0.24	0.68	1.89
3DoF Translation Passive	1st	4.10	7.77	15.84
	2nd	1.61	3.58	7.47
	3rd	0.82	1.98	4.61
	4th	0.52	1.21	3.15
	5th	0.33	0.83	2.25
3DoF Rotation Passive	1st	3.25	7.61	15.78
	2nd	1.17	3.03	7.23
	3rd	0.68	1.62	4.30
	4th	0.43	1.03	2.85
	5th	0.27	0.72	2.02
6DoF Passive	1st	4.27	8.64	16.93
	2nd	1.70	3.61	7.82
	3rd	0.90	2.01	4.70
	4th	0.58	1.27	3.15
	5th	0.37	0.87	2.25
Active concepts	1st	2.40	6.63	14.45
	2nd	0.96	2.70	6.63
	3rd	0.58	1.48	3.96
	4th	0.38	0.95	2.64
	5th	0.25	0.69	1.89

Table 4.1: The 5 first natural periods in seconds for lateral vibration at different water depths for all concepts.

It can be seen in the tables that there are some natural periods of lateral vibration that are within the frequency band of the waves. Therefore, resonance can occur when excited by waves or vessel motion. However, these wave frequencies are considered in regular wave analysis, and some regular wave frequencies are close to the natural frequencies of the system. However, destructive behaviour cannot be seen, for example, in the stress graphs. This is mainly due to the non-linear damping that increases rapidly when the lateral velocities increase. A more detailed analysis of the damping is given in appendix I. The periods of active position-based systems are very similar to passive compensation systems, although they are much stiffer. It is actually much stiffer in the vertical direction, and this has a small influence in the natural periods of lateral vibration. It is actually quite comparable in lateral stiffness to the 1DoF Passive system. For both systems, the drill string mounting point is assumed to be not able to move in the horizontal direction. And the low vertical stiffness does not influence the bending stiffness much.

4.1.5. Final concept selection

Now that all KPIs have been discussed, it can be concluded what the best-performing concept is. First, based on the WoB amplitude needing to be as small as possible, passive concepts are the only concepts that have desired characteristics. Passive compensation systems have the ability to deal with larger vessel motions while keeping the force constant, in other words, a low stiffness. Low stiffness is especially helpful in the Z-direction. The performances of these passive concepts are very similar. It can be seen directly that active position-based systems are not suitable for this application, as lift-off occurs in almost every simulation. This is caused by the fact that the residual motions of the motion-compensated point are high enough to cause full tension in the string. Then, based on the stress KPI, the 3DoF Rotation Passive and 6DoF passive concepts showed the lowest maximum stress. For some concepts, the plastic deformation limit was reached, these are mostly active concepts in shallow waters

with a DP excursion. Finally, based on the fatigue KPI the 3DoF Rotation Passive and 6DoF passive concepts are again the best with similar performance. Thus, these two concepts are suitable and best performing for this application. The final conclusion is then based on the complexity of the system, the 6DoF system is more complex than the 3DoF system, and the performance is almost equal. Then it is better to have a less complex system. Another advantage of the 3DoF system is that it used fewer gas spring cylinders, thus fewer failure points and components that need servicing. The concept that is selected to be optimised further is thus the 3DoF Rotation passive concept.

	Depth [m]	**50**	**100**	**200**
3DoF Rotation Passive	WoB amplitude [kN]	67	79	102
	Max Von Mises Stress [MPa]	46	30	50
	Fatigue damage/year	1×10^{-12}	1×10^{-11}	1×10^{-12}
6DoF Passive	WoB amplitude [kN]	67	108	103
	Max Von Mises Stress [MPa]	34	31	50
	Fatigue damage/year	1×10^{-9}	1×10^{-8}	1×10^{-9}

Table 4.2: Comparison of the maximum values found for each KPI at every water depth for the 3DoF Rotation Passive and 6DoF Passive systems.

4.2. Discussion

This section discusses the result of this chapter, mainly how specific assumptions lead to this result and what the result means for the application of certain motion compensation devices.

The results derived from the simulations indicate that a 3DoF Rotation passive system is the best type of motion compensation for the considered drilling operation. This is a system that compensates for vertical vessel motion as well as roll and pitch motions. This is mainly based on the performance related to bending stress reduction compared to other passive systems. It is observed that active position-controlled systems are not suitable for this application. As the residual motions are too large in the used environmental conditions.

This result of passive systems is as expected, but the second result regarding active position controlled systems is actually contradicting. Floating drilling using the RCD method has been done once in a similar setting using a 3DoF Rotation Active system, the Barge Master compensation system. The ships used in this case were a barge and a diving support vessel. However, it should be noted that the environmental conditions considered in this research are more severe than those encountered during the drilling operations already performed. Therefore, the results suggest that there is a physical limit for the environmental conditions in which active position-based systems work, this is also shown in appendix D.
The results achieved by this investigation are, of course, influenced by the assumptions made. Here, some of these critically important assumptions that have a great influence on the result are discussed. First, when it comes to the chosen boundary condition of the lower part of the drill string, the connection between the drill bit and the soil. In this research, this is modelled as a fixed connection. This fixed boundary condition assumes that, in theory, the soil is infinitely stiff. Additionally, the drill bit cannot lift off the ground, and this part needs to be in compression otherwise the boundary condition of fixation is not valid anymore. The assumption of infinitely stiff soil also results in larger variations in the vertical direction. However, this negatively impacts all motion compensation systems and is thus a save assumption. It could be said that active systems suffer more from these boundary conditions, since it is a very stiff system. Moreover, assuming a finite soil stiffness would reduce the WoB spread for active systems. But it would not reduce the effect of lift-off, therefore the choice of this boundary condition would not change the outcome when it comes to the unsuitability of active systems, however it can overestimate the severity of the behaviour observed for active systems.

Another aspect that has a significant influence on the performance of active systems is the compensation efficiency. The compensation efficiency dictates the ability of active compensation to reduce the motion of the ship. This efficiency was chosen to be 95%, increasing the efficiency would increase the

performance and thus decrease the WoB variation, stresses and fatigue life. Efficiency was chosen on the basis of values found in the literature and the manufacturers of motion compensation systems. However, as shown in appendix D simply increasing the efficiency to 100% is not even sufficient when only the vertical motion is compensated. This analysis shows that the system is too stiff for the application. Still, this analysis is only done for the 1DoF active system, and doing this for the other concepts may show that more degrees of freedom with slight efficiency increase suddenly would make active systems usable in the considered conditions. But again, these concepts perform better than passive concepts that do not require energy input and are generally less complex. Even if the difference in performance was smaller, the advantages of passive systems are superior to those of active position-based systems in this application. Therefore, changing efficiency would most likely not change the outcome of this research.

On the other hand, passive systems are chosen to have linear spring stiffness and damping characteristic. This is not true in real life, hydraulic gas spring cylinders have a non-linear spring characteristic, this characteristic gives different behaviour whether the cylinder is contracting or extending, the difference can be seen in figure 4.22. This means that the cylinder actually has a lower stiffness than when in compression. The stiffness when in compression is almost half the stiffness when in tension, as can be seen in figure 4.22. But actually a lower spring stiffness is actually favourable for passive systems, therefore this assumption actually lowers performance for the assumed passive systems. The same is true for the damping in the passive systems, these are taken from [2], but are in reality also nonlinear. Damping in the motion compensation system has a large influence on the performance of the system. High damping results in a system with overall worse performance than for a system without damping. In this case, the level of damping is also very important, it dictates the amplitude of the response of the system, and if modelled in this research too high could hide the effects of exciting the system close to its natural frequency. A careful analysis of the natural frequencies of the system and the level of damping has been carried out. These are found in chapter 4 and appendix I.

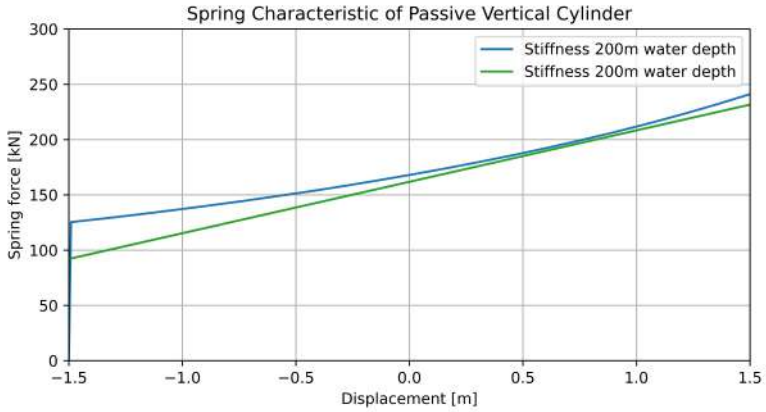

Figure 4.22: Non-linear and equivalent linear stiffness for the hydraulic gas spring.

5. Concept Realisation Results

In the previous chapter, it was concluded that the 3DoF Rotation Passive concept that compensates for the vertical motion of the vessel, as well as the pitch and roll, showed the best performance in the range of performance indicators. In this chapter, it will be derived how this concept can be realised. First, it will explain what some systems will look like and what they consist of. Then, a partial design of both systems is done. For one system it is straightforward, for the other a multi-objective optimisation is used to determine the design. After that, the systems are evaluated in a detailed irregular wave analysis and compared to the results of the concept identification. Finally, the results of this realisation are discussed.

5.1. Concept variations

There exist multiple ways to achieve a system that has the three specific degrees of freedom derived in chapter 4. The number of degrees of freedom for a system can be derived using the following equation [15]:

$$F = 6\,(n-1) - \sum_{1}^{g} (6-f) \tag{5.1}$$

Here, F is the number of degrees of freedom, n the number of links in the system, g the number of joints, and f the number of degrees of freedom of the joints. F has to be equal to three for the potential realisations of the system, this can be achieved by many different combinations of number of links, hinges. The most obvious two choices are:

- Vertical cylinder and a universal joint.
- Three independently moving cylinders with universal joints connecting a platform.

The first realisation is relatively simple, which requires the drill string to be suspended by a gas spring and a universal joint at its interface. This is given in figure 5.1.

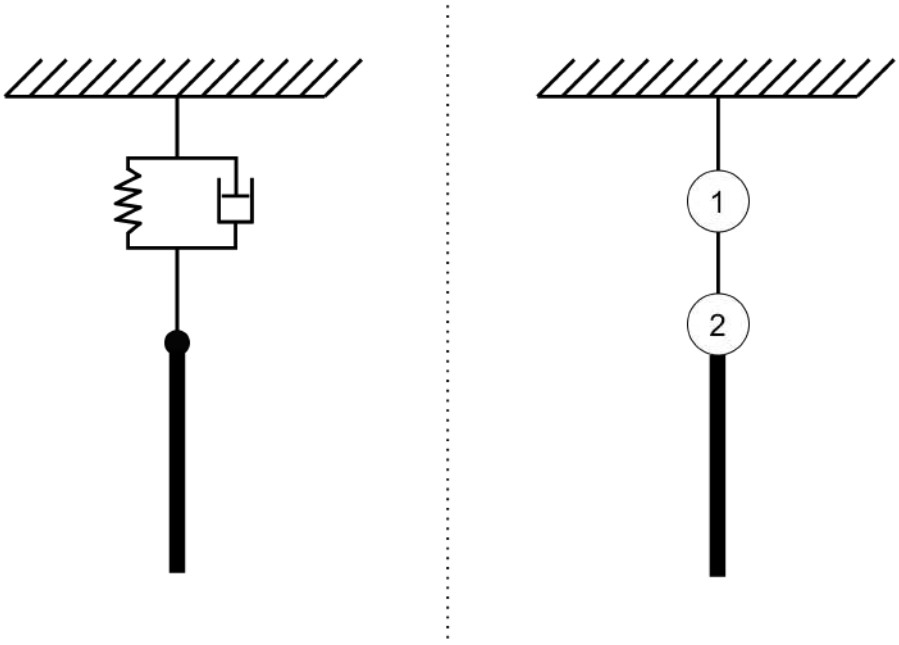

Figure 5.1: Schematic overview of the first realisation

Considering equation (5.1) for this realisation. The degree of freedom of the system can be calculated as three. The hydraulic cylinder acts as a prismatic joint that connects two bodies. The third body, the drill string, is connected by a universal joint to the actuator. Here $n = 3$, $g_1 = 5$ and $g_2 = 4$. This gives $F = 3$, a system with three degrees of freedom.

An alternate method of constructing a three-degree-of-freedom system is to use three parallel cylinders that move a platform in a vertical direction. A diagram of this system is presented in Figure 5.2.

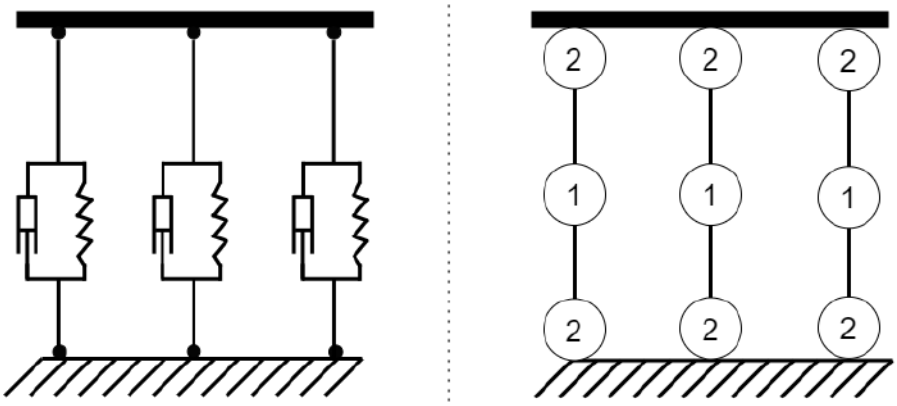

Figure 5.2: Schematic overview of a 3DoF platform

Again considering equation (5.1), the number of bodies can be counted as $n = 8$, then there are again two types of joints, 3 prismatic joints with one degree of freedom and 3 universal joints with two degrees of freedom. So $g_1 = 5$ and $g_2 = 4$. If this is all plugged in, the amount of degrees of freedom for this platform becomes three. The only thing that needs to be added are the long control arms that are connected to the vessel and platform that prevent the top platform from rotating and falling down. This concept is very similar to the Barge Master concept, except that this is a pure passive system [19]. An example of this system can be seen in figure 2.5a. Note the long white control arms that connect from the vessel to the platform. Concepts are integrated with the moonpool and examples of them can be seen in figure 5.3.

5.2. Realisation

Both concepts are considered viable solutions as motion compensation systems. Both systems are optimised and then finally compared to assess their performance. In the following subsections, the optimisation of each concept will be explained, followed by the evaluation of the optimisation process for each concept. Finally, an analysis is done to verify the performance of the system and compare the two. Then a final conclusion can be drawn as to what the best concept is. Both concepts are realised with a water depth of 50 metres, as this is the limiting water depth with respect to stress and fatigue. The weight on bit performance showed that across all depths, this was similar.

5.2.1. Vertical Cylinder concept realisation

The single vertical cylinder is similar to the 3DoF Rotation Passive concept presented in the identification phase and thus remains almost unchanged in this phase. Only the drill rig is added, the weight of the drill rig is 28 tonnes [1], and its moment of inertia is assumed to be that of a solid cylinder with a diameter of 2.5m and a height of 4m, which is $48.27t.m^2$. The mean force of the hydraulic cylinder is adjusted to account for the additional weight. It is assumed that the drill rig rotates along with the drill

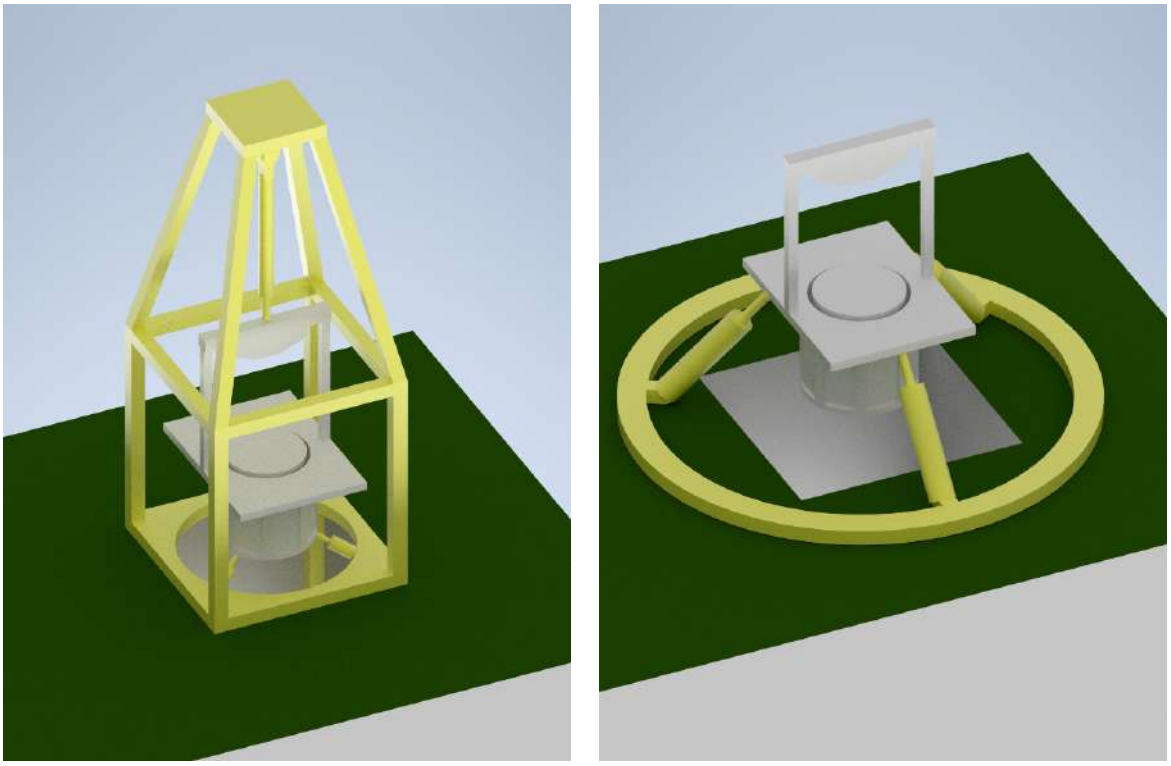

(a) An example of the vertical cylinder and universal joint concept.

(b) An example of the platform concept.

Figure 5.3: Two examples of realisations of concepts that represent a 3DoF system integrated with a moonpool.

Parameter	Value	Unit
D	0.360	m
V	1.07	m^3
b	5	kNs/m

Table 5.1: Gas spring parameters used in the hinge concept realisation.

string in the roll and pitch direction. The stiffness is again linearised and is based on equation (2.11). The diameter is based on the gas cylinder used in the identification phase [2]. The initial pressure p_0 is based on the mean force. The volume of the gas is increased to $1.07m^3$ in order to maintain the same stiffness as in the identification phase. This stiffness is approximately $47.97kN/m$.

5.2.2. Platform concept realisation

The realisation for this concept is more complex, there are more parameters that can be changed, and the result of these changes is less straightforward than for the other concept. Therefore, this is optimised parametrically. The exact orientation of the cylinders can be changed to effectively change the characteristic of rotational and vertical stiffness. Therefore, the optimisation algorithm can find the optimal geometry of the system, as well as the corresponding stiffness and damping. The optimisation algorithm used is a multi-objective genetic algorithm, this exact method is explained later. The following parameters can be varied, and an overview can be seen in figure 5.4:
All varying parameters have an upper and a lower limit. These boundaries are given in table 5.2. The upper radius R_{upper} is determined by the vessel and drill rig used, with the minimal value being the drilling diameter, as the drill rig is clamped to pipe with the drill diameter. The upper limit is set so that no motion compensation structure can interfere with the deck infrastructure, which is 7.7 m. The lower radius is determined by the diagonal of the moonpool, which is 4.94m. The upper limit is the same as the upper radius. The height of the platform is kept at a minimum height during the simulation to avoid having tall structures on the deck. This height required is based on the maximum heave amplitude that can be expected, which is 1.8m, resulting in a full range of 3.6 m. Taking into account the DNV-OS-

Parameter	Symbol	Unit
Lower radius	r_{lower}	m
Upper radius	r_{upper}	m
Cylinder height	$h_{cylinder}$	m
Piston diameter	$D_{cylinder}$	m
Total gas working volume	V	m^3
Cylinder damping coefficient	b	kNs/m

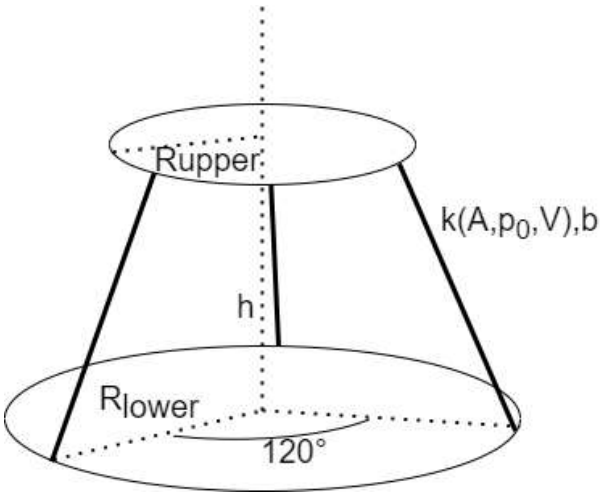

Figure 5.4: 3DoF platform with the varying parameters

Parameter	Lower boundary	Upper boundary	Unit
R_{upper}	1.25	7.7	m
R_{lower}	4.94	7.7	m
$h_{cylinder}$	4.28	6.25	m
D	0.1	0.75	m
V	0.1	10	m^3
b	5	100	kNs/m

Table 5.2: Upper and lower limits for the varying parameters for the optimisation algorithm

H101 [13], it must be divided by 0.84, resulting in a minimum full stroke of 4.28m. The cylinder diameter has no theoretical limits, but cannot be zero, and is capped at 0.75 m to avoid the algorithm generating very large unrealistic cylinder sizes. A buckling constraint is added to ensure that the cylinder cannot buckle, and the algorithm is penalised if buckling could occur. The diameter of the rod is assumed to be $1.2D_{rod} = D_{Cylinder}$, the cylinder rod must be able to resist buckling, so using the Euler buckling formula together with the area moment of inertia of a solid rod, the constraint becomes as follows.

$$D_{cylinder} > 1.2\sqrt[4]{\frac{F_{axial}L^2}{\pi^3 E_{steel}/64}} \tag{5.2}$$

The gas volume of the system is limited to a range between $0.1m^3$ and $20m^3$ to prevent a division by zero and to avoid the need for large tank structures on board, respectively. The damping is kept relatively unrestrained and can be adjusted in reality by adding a pure damping cylinder to the system, which adds to the damping already present in the hydraulic cylinder. The lowest damping that is assumed to be possible is close to the value specified in the book Motion Control in Offshore & Dredging [2]. The stiffness in this scenario is again calculated using the linearised stiffness equation equation (2.11). Additionally, the platform in this scenario is given a mass of 20 tonnes and a corresponding moment of inertia based on a flat cylinder with a radius of the upper-radius position of the cylinder. The drill rig is modelled as a 28-tonne solid cylinder with a diameter equal to the drilling diameter and a height of 4 metres; this gives a rotational inertial around the X and Y axes of $48.27tonnesm^2$. The environmental

Parameter	Value	Unit
H_s	2.5	m
α	165	degrees
T_p	10	s
γ	1	-
d_{water}	50	m
$t_{simulation}$	3000	s

Table 5.3: Simulation parameters used in the simulations for the multi-objective optimisation.

conditions used in the simulation are given in section 5.2.2.
The used algorithm for this optimisation is the NSGA-II algorithm, it is a non-dominated classification genetic algorithm based on Deb et al. (2002)[8]. It is a multi-objective evolutionary algorithm that uses a population of potential solutions and mutating the optimal ones in each population. This results in a Pareto-optimal front, this is a boundary which consists of all the most optimal solutions found by the algorithm. These solutions are called non-dominated solutions, which means that no solution in this set is worse than any other in all objectives.

For each generation, the best performing solutions are used to make combinations of the parameters that will be assessed in the next generation, these offsprings are also mutated to increase the probability of better performing individuals. If the solutions are of the same rank, it will choose the individual to reproduce based on its crowding distance. The individual which is most isolated from other non-dominated solutions is then preferred. This ensures a good spread in the search for optimal solutions and increases the likelihood of finding a wider range of optimal solutions. Furthermore, the algorithm uses elitism, this means that it takes a few of the best performing solutions to the next generation to ensure that good solutions are not lost and the algorithm always goes forward in finding the most optimal solutions. The selection process for the mutation is displayed in figure 5.5. The algorithm eventually stops when it reaches a stopping criterion, which can be set to a specific number of generations or to a convergence of the solution to a specific value.

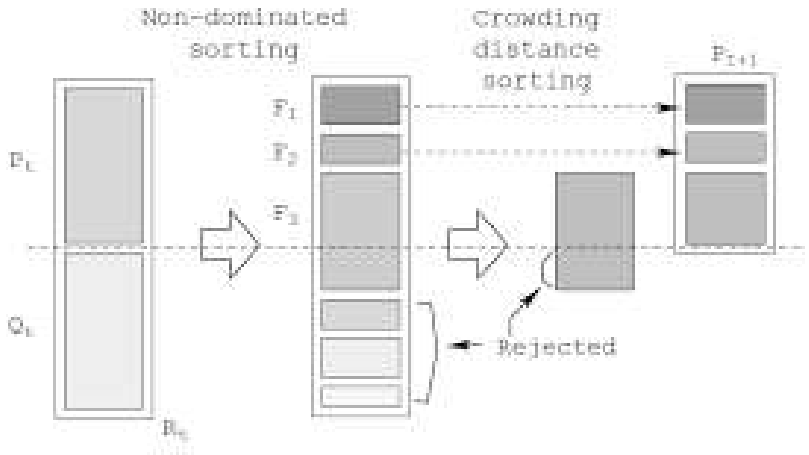

Figure 5.5: Sorting rules applied by the NSGA-II algorithm [8]

The case study involved running a simulation with a population size of 30 for 30 generations, resulting in a total of 900 simulations. The objectives were to minimise the standard deviation of the Weight on Bit (WoB) signal and the maximum bending stress. The results yielded a Pareto front with optimal objectives, as shown in figure 5.6. The parameters corresponding to these outcomes were divided into two sets based on the upper radius, one with approximately 1.4 metres and the other with 1.6 metres or larger. The larger upper radius set, although smaller with only six variants, generally had higher stresses but lower weight on bit. The other set demonstrated that damping played a significant role in

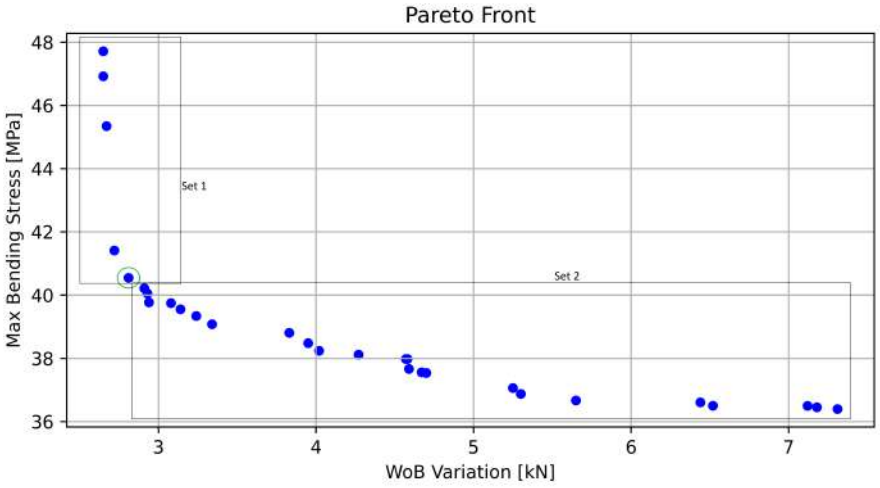

Figure 5.6: Pareto front of a calculation with 30 generations and a population size of 30.

the trade-off between low WoB deviation and maximum bending stress. The results also showed that the bending stress was generally higher than in the 3DoF Rotation Passive concept due to rotational stiffness in the platform concept and the inertia of the platform. The diameter of the cylinder was relatively large in the optimisation results. This is most likely due to the fact that the piston diameter is 1.2 times the diameter of the rod. And the rod diameter is determined by the buckling check equation (5.2), this value 1.2 could be on the high side, therefore resulting in relatively high diameters. However, the diameter can be adjusted with volume by equation (2.11) to keep the spring stiffness constant, and a new buckling check should be performed if the rod diameter is also changed.
The optimisation algorithm ended up with two sets of similar solutions; the main differences in these two sets are the upper and lower radius. Set 1 has an upper radius of 1.6m or larger, this is paired with a generally smaller lower radius than set 2. This set is characterised by having a smaller WoB standard deviation but higher maximum bending stresses. The spread in the WoB standard deviation for this set is small, while the maximum bending stress range is relatively large. Set 2 is characterised by having an upper radius that is around 1.4m for all solutions and also a larger lower radius than set 1, for set 2 the performance regarding the max bending stress is better than for set 1 but in return for this the WoB standard deviation is relatively larger. Additionally, the spreading of performance for this set is the other way around compared to set 1. Both sets are visualised in figure 5.7.

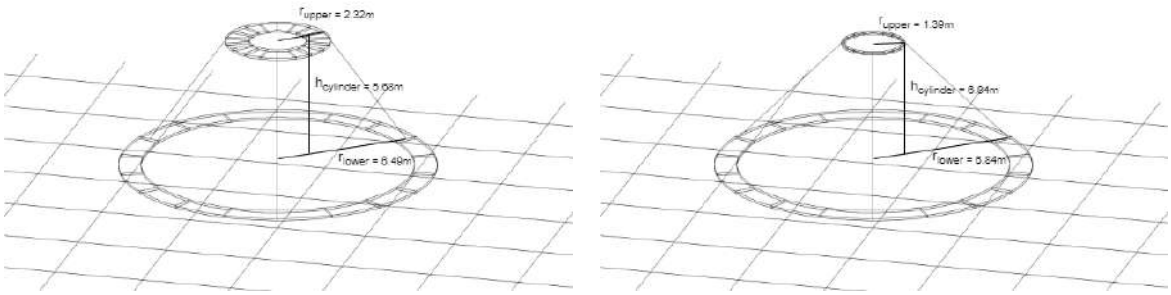

(a) Set 1 **(b)** Set 2

Figure 5.7: Two examples that are found in set 1 and set 2

The chosen parameters for final evaluation is realisation 11, which is mainly because it has the lowest deck footprint, this is a radius of 6.49m, additionally the upper radius of 2.32m leaves more space for the cylinder mountings and platform-drill rig connections than for a smaller diameter. The exact values and the corresponding results are in table 5.4. The corresponding point is also encircled in green in the Pareto front in figure 5.6.

Realisation	WoB SD (kN)	$\sigma_{\text{bend,max}}$ (MPa)	r_{upper} (m)	r_{lower} (m)	h_{cylinder} (m)	d (m)	V (m^3)	b (kNs/m)
11	2.81	40.55	2.32	6.49	5.68	0.62	4.73	5.02

Table 5.4: The final chosen parameters in the Pareto-Front.

The parameters for the final evaluation were chosen from set 11. The exact values and the corresponding results are given in table 5.4. The parameters obtained from the optimisation algorithm can be justified. For example, all optimal sets had a low upper radius, close to the lower boundary set for optimisation, to reduce the inertia of the platform and make the system less affected by residual platform motions. The height of the cylinder converged to around 5.5 metres to improve the buckling strength of the cylinder. The cylinder diameter was relatively high, but this was explained earlier. The volume was around $4.73m^3$ which had to be available for the three gas cylinders, resulting in a total gas volume of $14.19m^3$ on the deck. The volume is relatively high, creating a very low spring stiffness ideal for the application. The damping was kept low to improve the WoB characteristic, although it was observed that high damping decreased the maximum bending stress at the cost of an increased WoB standard deviation.

5.3. Optimised concept analysis & Results

For this analysis, both finalised concepts are subjected to a sea state of 3 hours with a $H_s = 2.5$ and a peak period of 10 seconds. Performance is measured in the same way as in the identification phase: WoB deviation, maximum Von Mises stress, fatigue strength analysis, and natural period analysis. The final results are given in maximum and significant amplitudes for the WoB variation, a maximum stress, and fatigue damage per year accompanied by a maximum bending stress. Finally, the natural periods corresponding to the first five modes are given. The most important aspect that is kept constant across the two realisations is the stiffness and damping in the vertical direction, as this determines the WoB performance the most. The scenarios considered are similar to the identification phase. Two different water depths are considered, the stress-limiting 50m water depth, and to check performance for longer drill strings, a 200m water depth. Additionally, an identical DP offset is used, and here the effect of a current on the system is also considered. This current is defined in the same way as in chapter 3.

5.3.1. WoB performance

The WoB performance is the most important parameter when it comes to production or, in other words, the drilling distance per hour. As mentioned above, the results are given as standard deviation. Although this does not have physical meaning, it indicates the average deviation of the signal. For an irregular signal like this, minimising this will reduce the spread of the signal around the mean. Lower spread means that the WoB can be better controlled, and thus increase production. The values are summarised in figure 5.8. The values are sorted per final concept, water depth, and peak period. Additionally, the mean, min, and max values are given for all scenarios considered to give a clearer picture of the WoB characteristic.

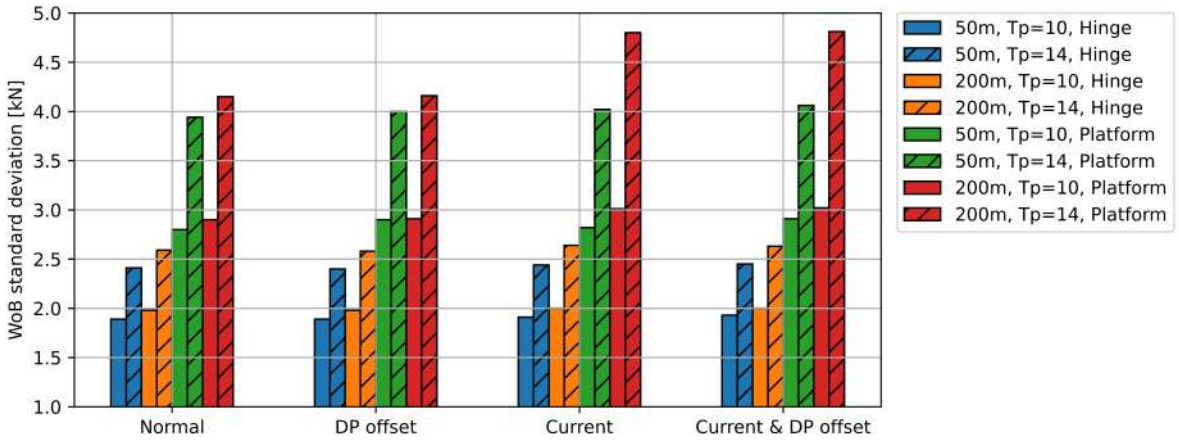

Figure 5.8: WoB standard deviation for the final concepts in different scenarios for different water depths and peak periods

This graph shows that the values are quite low. The platform has higher values than the hinge concept. Although the vertical stiffness is similar, the damping is much higher mainly due to the lower damping, as the platform has only one gas spring cylinder instead of three. The standard deviation increases when different scenarios are taken into account, such as increasing the top displacement or adding extra force to the drill string. These deformations affect the WoB signal at the bottom. The most significant decrease in deviation is seen when the current is taken into account. Both systems perform adequately under a variety of environmental conditions and the WoB is controllable for both. Another important aspect of these data is the fact that when the peak period increases, the standard deviation of the WoB increases. This is mainly due to larger vessel motions for longer wave periods, this can be seen in the RAOs in appendix C. The RAO value increases for most motions as the wave period increases. To get a clearer overview of the WoB behaviour, the mean, min, and max are given. The mean WoB values for different operating conditions are given in figure 5.9 below.

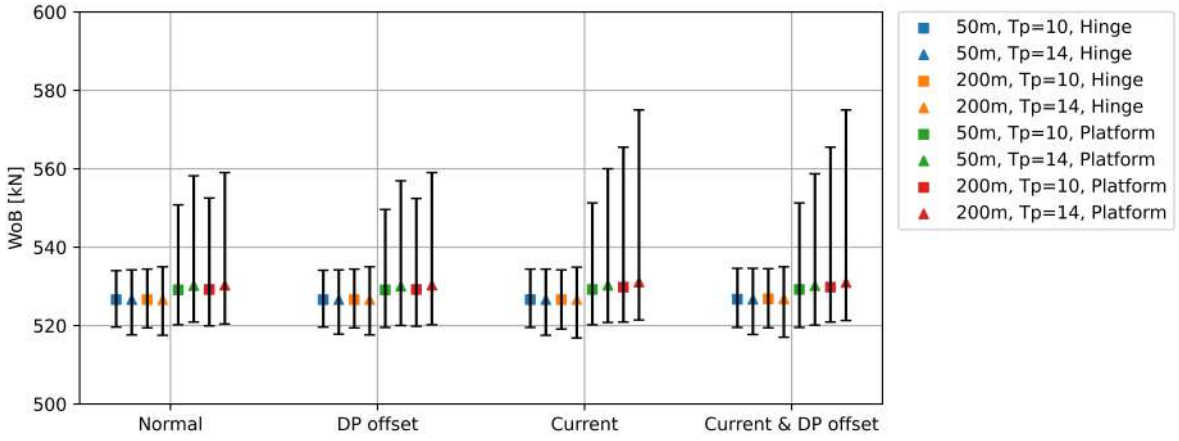

Figure 5.9: WoB mean, min and max for the final concepts in different scenarios for different water depths and wave periods.

What can be observed here is that the mean is very consistent under all operating conditions. Even when a current is applied to the system. A current increases loading and deformation in the drill string; this increases tension in the system. But the motion compensation device deforms to return the tension level to the same level as the scenario without current. Only a slight increase in the mean value can be seen in the concept of the platform at a water depth of 200 m. Longer drill strings suffer more from current loads because they have a larger submerged surface area. Thus, more total forcing, additionally, the lever arm becomes larger for longer drill string. The moment thus increases rapidly for longer drill string because of the increased forcing and lever arm. Also, the platform concept is not free in rotation at the top. The rotational stiffness created by the three cylinders creates extra forcing

in the drill string, this is then seen in the mean value of the WoB signal. The mean between the two concepts is slightly differing, this because of the not perfect calibration of the initial forces in the gas spring cylinder in the models. However, it is only 0.6%, so the difference can be neglected.
If the min in figure 5.9 is considered, it can be seen that the range between min and max for the platform is generally larger than for the hinge concept. Around 30 kN compared to 17 kN. Thus, there are higher extremes for the platform concept. Additionally, for both concepts, the minimum value remains relatively constant for the different scenarios considered, the maximum however increases more as additional sources of mean bending stress are introduced. The phenomenon can be explained by looking at the vertical displacement of the mounting point of the drill string. This is given in figure 5.10. The difference between the min and max values is lower than in the first scenario, this comes from the fact that the frequency where the maximum amplitude occurs in the regular wave analysis is 16 seconds this is much higher than observed here in the used JONSWAP spectrum. And by the use of RAOs from appendix C it can be seen that longer period waves will result in greater motions, especially for the heave motion which is the motion that influences the WoB the most.

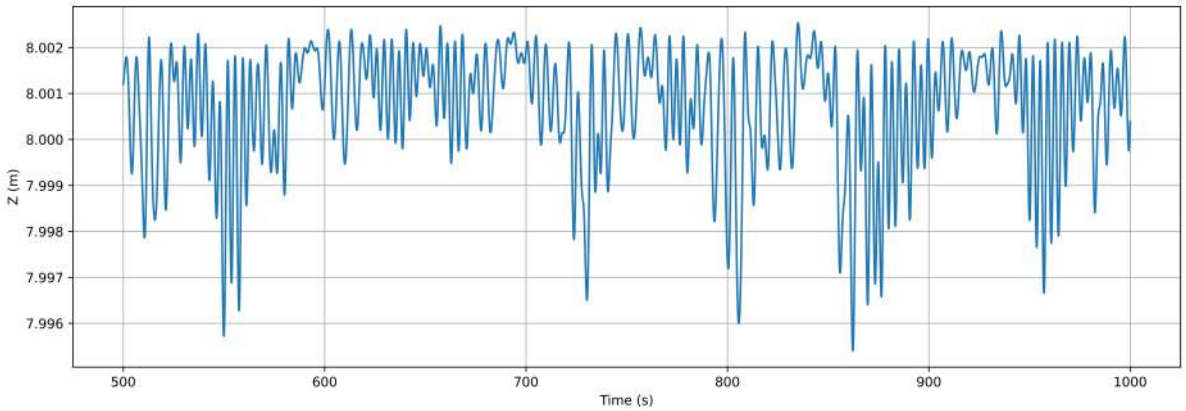

Figure 5.10: Drill string top displacement for the 3DoF hinge concept at 50m water depth with a wave spectrum of $H_s = 2.5m$ and $T_p = 14s$ between 0 and 1000s. (needs to become a python made plot)

The displacement is mostly downward and never exceeds the initial position of $z = 8m$, and the system actually has a different stiffness in different directions. The drill string is in tension during the drilling, it wants to contract, so when the mounting point moves downward the tension decreases rapidly, more rapidly than the motion compensator can increase its force. Thus, the point moves downward for a relatively large distance. The other way around, when the point wants to move up, the tension in the drill string increases while the vertical force in the motion compensator decreases, and given that the drill string tension increases more due to the stiffness of the drill string, the mounting point does not move upward. This eventually leads to the effect that the minimum WoB value is relatively constant compared to the maximum value for different scenarios.

Overall, the WoB performance of both concepts is satisfactory and very similar to each other. Based on the WoB only, there cannot be one better performing concept chosen. This will be further investigated by looking for stresses that occur in the drill pipe.

5.3.2. Structural performance

The drill string must remain intact without plastic deformation during the drilling process. It was checked in the identification phase, and it was shown that in this compensation type, no problematic stress levels were observed, but this was only in regular waves. It is not expected to result in problematic stress levels, as preliminary results were already low. But it is still important to check this. Furthermore, statistical extremes of the Von Mises stress are also evaluated. Note that again during this simulations only axial and lateral vibrations and thus corresponding stresses exclude torsional effects.

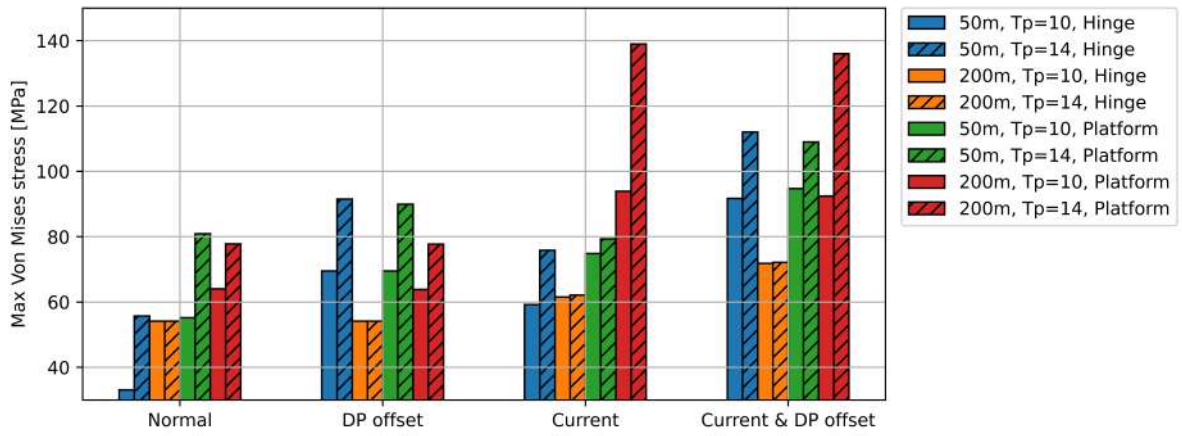

Figure 5.11: Maximum Von Mises stress for the final concepts in different scenarios for different water depths and peak periods.

As the data in figure 5.11 show, the maximum stress is not problematic. The behaviour is quite similar to the first identification phase. The most important aspect here is that the stress in the platform concepts is generally larger than for the hinge concept, especially at 200m water depth when a current is present in the scenario. In these scenarios the location of the maximum stress is different, for the platform concepts it is mainly at the top, while for the hinge concept it is always at the bottom. The change in the maximum stress location between concepts and scenarios is the main reason why the results differ for some combinations or why they are the same, for example the DP offset at 50m with $T_p = 10s$, this is the same for both the hinge and platform concept. Here, for both systems, the maximum stress location is at the bottom. This cannot be seen for the same scenarios at 200m water depth, this is because here the maximum stress location is again at the top. A DP offset has a larger contribution in shallower waters, as the drill string is less flexible, so the same DP offset will result in lower stresses for the more flexible, and thus here longer drill string. In this scenario the Maximum von Mises stress is actually mostly higher than in the identification phase, this can be explained by the fact that here the wave spectrum is used with a $H_s = 2.5m$. This means that there can be waves higher than 2.5m that could introduce higher stresses in the drill string, resulting in a higher Von Mises stress.

5.3.3. Fatigue performance

The fatigue life is evaluated in the same way as in the identification phase, it takes into account the rotation of the drill string and extrapolates the damage in the scenario to a damage/year. Although this value was very low in the identification phase, it still has to be checked. The data of the fatigue analysis are shown in figure 5.12 below.

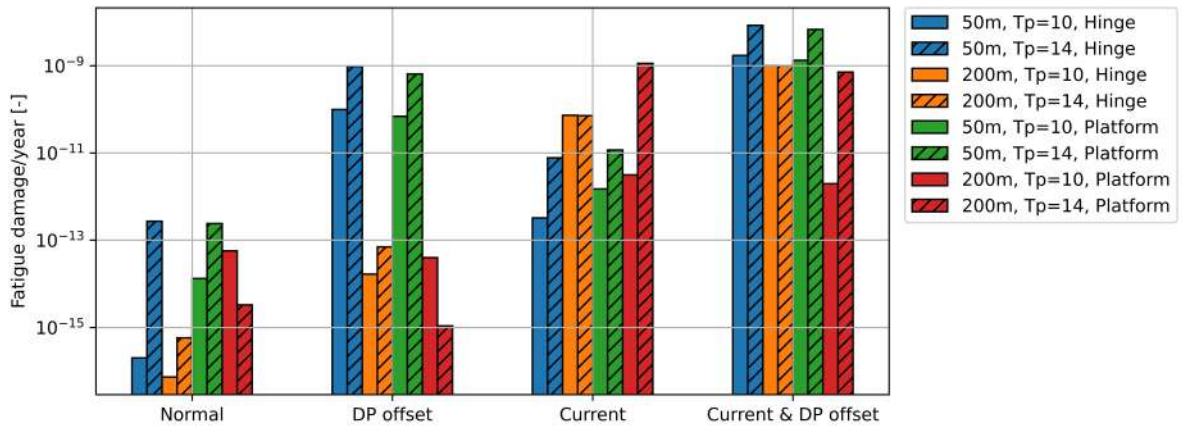

Figure 5.12: Fatigue damage per year for the final concepts in different scenarios for different water depths and peak periods.

Overall the fatigue resistance of the hinge concept is better than the platform concept. This does not actually make a big difference since all the values are very low. Even for the concept that performs the worst, it is possible to continuously drill for 10^9 years before failure. Note that this estimation uses a stress concentration factor of 2, if a higher stress concentration factor is necessary, fatigue life will decrease. These fatigue values exclude changes in shear stress due to bending and torque, and changes in axial stress due to tension differences. The fatigue damage when considering these effects may be different from that derived here. This fatigue damage per year is very low, similar to the first identification phase.

5.3.4. System characteristics

In this section, other effects that were observed in the final simulations are discussed. These include buckling, the effect of current on the system, and finally the natural frequencies of both systems. First, the natural frequencies, the natural frequencies are derived and checked in the same manner for the identification phase as mentioned in chapter 3.

Concept	**# mode**	**50m**	**200m**			**50m**	**200m**
Hinge	1st	3.28	15.71	**Platform**	1st	3.48	15.82
	2nd	1.22	7.21		2nd	1.54	7.27
	3rd	0.71	4.29		3rd	0.96	4.34
	4th	0.50	2.85		4th	0.62	2.91
	5th	0.35	2.02		5th	0.40	2.1

Table 5.5: First five natural periods of the final realisations.

The natural frequencies are very similar to what is expected, since they represent the same motion compensation system, the values are also very similar to the initial 3DoF Rotation Passive concept, and this again shows that these two systems represent this kind of system well. The mode shapes of the drill string are given in appendix H.
Additionally, the addition of current loading on the system comes with additional effects on WoB and compensation characteristics. Current loading has a larger effect on longer drill strings as there is more area to exert the force on. This results in higher loads and deformations. The extra load induced by the current also has an effect on the motion compensation system. First of all, it induces a sag and tilt of the drill rig when it is in the static state. For this sag and tilt, the forces in the motion compensator are also different, which results in different mean WoB and overall compensation characteristics. This sag and tilt is mainly the result of an increase in tension along the drill string.

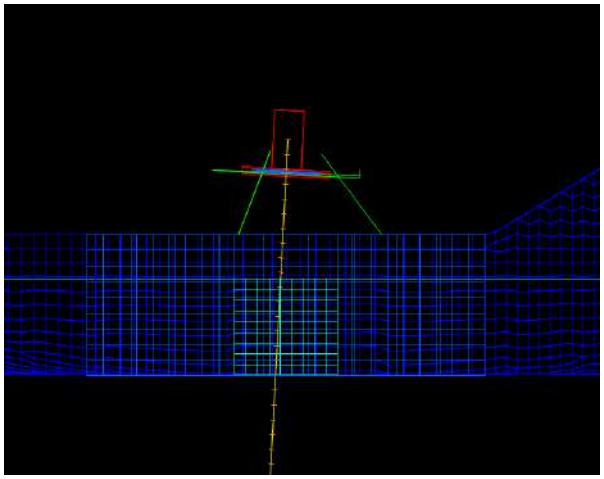

Figure 5.13: Platform tilt and sag due to current loading on the drill string

The sag and tilt in the concepts can be reduced by increasing the stiffness and initial pressure in the system, this however, needs to be done carefully since this will have an effect on the WoB characteristics of the system. This must be carefully calibrated for the desired drilling production and rock type.

In all simulations, the drill string was consistently under tension, so no buckling occurred and therefore was not taken into account.
Furthermore, the inertia of the drill rig is observed to have little influence on the behaviour of the system. Although the platform concept has more inertia in the system (the platform), it does not have a significant influence on performance. The accelerations of the drill rig and platform are relatively low, in the 3 hour simulation with $T_p = 14s$ the maximum rotational acceleration is 0.043 rad/s^2 and a translational acceleration of 0.45 m/s^2. These low accelerations result in relatively small forces compared to the tension in the drill string.

5.3.5. Statistical Analysis

The wave spectrum used in all simulations was the same, only for sea states with a higher peak period, the spectrum was shifted to lower frequencies. Additionally, the surface elevation for every simulation was the same. The same seed that generates the surface elevation from the wave spectrum is used. This makes it easier to compare the results directly with each other as done above. However, how do the maxima in wave spectrum generated relate to the most probable maximum values for this specific wave spectrum, in other words, are the maxima observed in this spectrum relatively high and low? For this, the extreme value analysis tool from OrcaFlex is used. It is assumed that the wave elevation follows a Rayleigh distribution [17].

	Highest value observed	**3-hour return level**
Maximum surface elevation	2.88m	2.39m
Minimum surface elevation	-2.34m	-2.39m

Table 5.6: Statistical wave elevation data of the wave spectrum with $H_s = 2.5$, $T_p = 10s$, $\alpha = 165°$

	Highest value observed	**3-hour return level**
Maximum surface elevation	2.11m	2.33m
Minimum surface elevation	-2.10m	-2.33m

Table 5.7: Statistical wave elevation data of the wave spectrum with $H_s = 2.5$, $T_p = 14s$, $\alpha = 165°$

From these tables it can be observed that the wave spectrum describes the wave spectrum relatively well and that the minima and maxima do not differ too much from the 3-hour return level. Only for the maximum observed in the wave spectrum with a peak period of 10s, a relatively large deviation is seen. This means that the maximum values observed in the simulation are higher than the most probable maximum, and this maximum is also significantly higher than the maximum value observed in the surface elevation of the spectrum with $T_p = 14s$. However, no notable differences are seen in the maximum and minimum values between the spectrum with $T_p = 10$ and $T_p = 14$.

5.3.6. Initial Concept Comparison

It is important for both systems to compare performance with the system proposed in the first identification phase. For this, the same analysis is done for these two systems as in this phase. A regular wave analysis is applied to the realised systems to compare them with the original version. The KPIs that are considered here are only the WoB amplitude and the maximum von Mises stress.

First, when considering the WoB performance, for which the comparison is given in figure 5.14 and figure 5.15. It is observed that the WoB amplitude first of all is much lower than in the reference case, which is mainly due to the lower stiffness that is used in the realisation phase. The stiffness is better optimised to lower values, resulting in smaller force disturbances due to the extension and retraction of the hydraulic gas spring. Furthermore, the effect of an increase in WoB amplitude with increasing period is also visible, but this is more due to the fact that the RAO value for heave increases with increasing period. So regarding the WoB performance this is similar behaviour as in the identification phase, but this comes mainly from the fact that it is a passive system that has all very similar performance regarding this performance indicator.

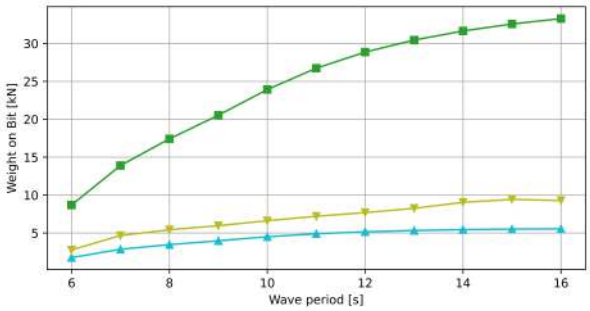

Figure 5.14: WoB amplitude for all 3DoF Rotation Passive concepts at 50m water depth.

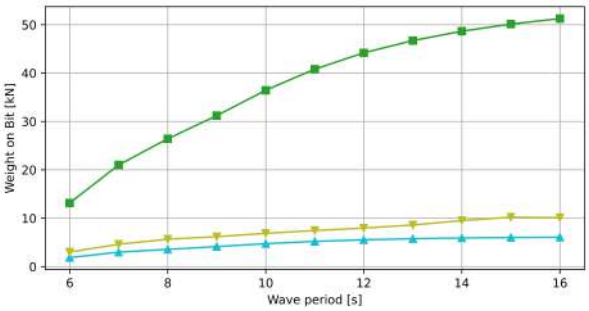

Figure 5.15: WoB amplitude for all 3DoF Rotation Passive concepts at 200m water depth.

Now regarding the maximum Von Mises stress, this time it is split into a maximum stress at the top of the drill string (see figure 5.16 and figure 5.17, which is the mounting point on the vessel to the compensator, and at the bottom, which is at the interface of the bottom hole assembly (BHA) (see figure 5.18 and figure 5.19. This makes comparison easier since the location of the maximum stress can vary between the top and bottom, as experienced during the 3 hour storm simulation. It also gives a clear picture of the main differences between the two realised concepts. If the stress at the top is considered, it can be observed that the stress for the platform concept is higher than that for the other two, which comes from the fact that there is a rotational stiffness created by using three offset gas springs. The boundary condition is no longer free rotating and the boundary condition becomes:

$$M = \theta k_{rotational}(z, \theta) \tag{5.3}$$

The rotational stiffness is not constant, but is actually a complex function that depends on the heave position and the combined roll and pitch angle. But the stiffness is nonzero opposite to a free hinged drill string, and thus the moment is also nonzero. This introduces thus bending stresses in the top of the drill string and thus the total stress is higher. If the maximum stress at the bottom is considered, it is observed that this is relatively similar to the 3DoF Rotation Passive concept proposed in the identification phase.

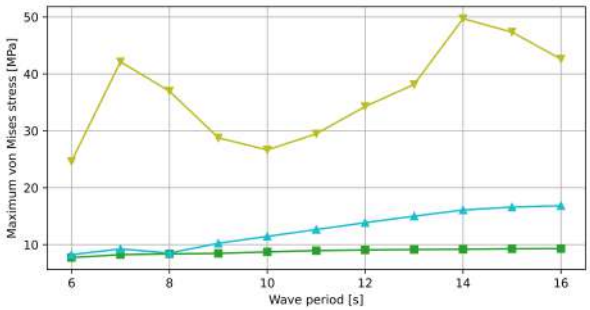

Figure 5.16: Maximum Von Mises stress at the drill string mounting point for all 3DoF Rotation Passive concepts at 50m water depth.

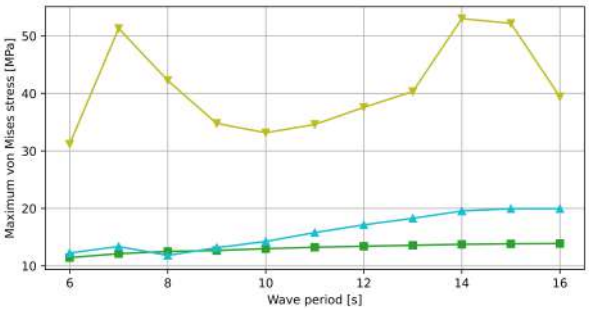

Figure 5.17: Maximum Von Mises stress at the drill string mounting point for all 3DoF Rotation Passive concepts at 200m water depth.

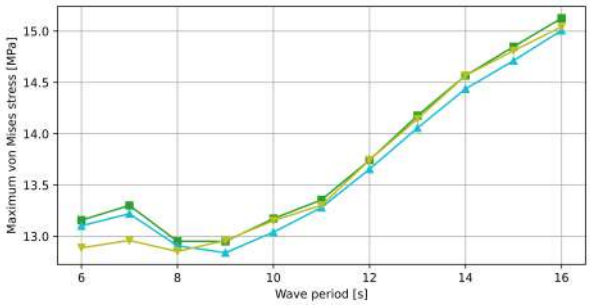

Figure 5.18: Maximum Von Mises stress at the BHA interface for all 3DoF Rotation Passive concepts at 50m water depth.

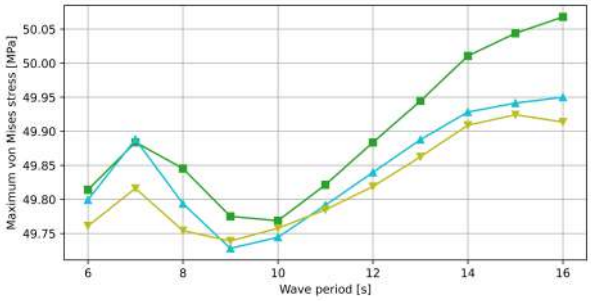

Figure 5.19: Maximum Von Mises stress at the BHA interface for all 3DoF Rotation Passive concepts at 200m water depth.

Overall, the performance is quite similar, and when taken into account the natural periods and mode shapes (see appendix H), which are very similar, it can be concluded that these two realisations accurately represent the 3DoF Rotation Passive system proposed in the identification phase.

Concept	# mode	50m	200m
Hinge	1st	3.28	15.71
	2nd	1.22	7.21
	3rd	0.71	4.29
	4th	0.50	2.85
	5th	0.35	2.02
Platform	1st	3.48	15.82
	2nd	1.54	7.27
	3rd	0.96	4.34
	4th	0.62	2.91
	5th	0.40	2.1
3DoF Rotation Passive	1st	3.25	15.78
	2nd	1.17	7.23
	3rd	0.68	4.30
	4th	0.43	2.85
	5th	0.27	2.02

Table 5.8: First five natural periods of the final realisations and the 3DoF Rotation Passive concept.

5.3.7. Physical characteristics

The two proposed concepts represent a 3DoF Rotation Passive system, both approach this in different ways, performance wise these two concepts are similar as they represent the same system. However, due to their different approach each concept has their own set of physical advantages and disadvantages, in this section these attributes are explored. This gives more of an indication which is more practical to integrate on the a vessel and with off the shelf drill rigs. It is first described what components each system has and then what the influence of these components is on aspects like maintenance, deck space and other characteristics. The most important aspects are also summarised in table 5.9.

Hinge concept

The hinge concept consists only of one gas spring and a universal joint. This concept requires less maintenance compared to the platform concept due to its single cylinder design. And also requires only one set of gas tanks for the accumulator volume, it is a set of gas tanks so that the backed up volume can be controlled by closing or opening additional tanks in the set. However this system would be a taller system than the platform system, the drill rig is suspended and combined with a max expected

heave amplitude of 1.7m and full stroke of 3.4m in spectra with a $T_p = 14s$ appendix D. This results in the drill rig top point being roughly 7.5m above the deck, and on top of that a structure has to be build above it from which the drill is suspended. It is possible for the drill rig to be suspended using a cable, instead of directly to the gas spring, allowing the gas spring cylinder to be laid horizontally on the deck. This eliminates the need for the gas spring cylinder to be positioned above the drill rig, resulting in a taller overall height. The cable length can be varied by laying it over a winch connected to the gas spring. This is drawn in figure 5.20. This does however, increase the use of the deck space again.

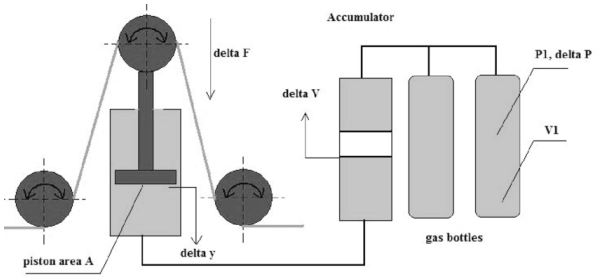

Figure 5.20: Visualisation of the use of a cable in combination of a gas spring [16].

Additionally, integrating this concept with standard RCD drill rigs is relatively complex. The current interface of the drill rig is at the bottom, it is usually clamped on a pipe that is stationary on the soil. This can be seen in figure 5.21. The drill rig will need to be connected at the top, it is unknown whether this part of the drill rig is structurally strong enough to transfer all forces from the drill pipe to the motion compensation device. In addition, a universal joint has to be integrated in this, increasing the height of the support structure even more. It could be considered to place the universal joint in the drill rig between the drive system and the top drill pipe segment. However, when removing or adding drilling pipe segments to the drill string, the drill string must be disconnected from the drive system. The drill string is then held at the bottom of the drill rig in a clamping system. During this part of the operation, the universal joint is also disconnected and the compensation for roll and pitch is then lost, which could lead to undesirable stress levels in the clamped part of the drill string.

Figure 5.21: Example of a Wirth drill in operation on top of a pipe [1].

Platform concept

The platform concept has three cylinders instead of one, which means three times the maintenance on the cylinders, which will most likely come with higher operating costs, and moreover for each cylinder a set of gas bottles is necessary to function as an airbank. Three times the volume on deck compared to the hinge concept. On the other hand, this time the drill rig is supported from the bottom, and this has some other advantages. First, the structure around the drill rig is less tall than for the hinge concept, but since there are now three cylinders present, the system has a larger footprint on the deck. For the platform concept proposed in this chapter, the footprint is a circle with a radius of 6.5 m. Second, supporting the drill rig from the bottom simplifies the connection between the motion compensation device and the drill rig, and the tube to which the drill rig is clamped can be integrated into the platform structure. This also mitigates changes to the current design of the drill rig that will most likely require new certification.

Component	Hinge Concept	Platform Concept
Hydraulic Cylinders	Less maintenance due to a single cylinder design. Can be positioned horizontally to reduce height.	More maintenance due to three cylinders. Larger footprint on deck.
Airbank/Gas Accumulator	Only one set of gas tanks is needed. Reduced deck space necessary	Three sets of gas bottles required. Larger area necessary on deck.
Piping System	Less piping, can be further reduced by using cables and placing cylinder on deck Less flow losses	More piping More flow and piping leads to more flow losses in the system.
Joints	One large joint with large bearing capacity. No redundacy but less maintenance and failure rates	Many small joints at each cylinder Redundancy but higher failure rates.
Mounting Structures	Taller system overall. Increased use of deck space with horizontal positioning.	Less tall structure. Larger footprint due to three cylinders.
Total Number of Moving Components	Fewer moving components, simpler design.	More moving components, more complex design.
Drill Rig Integration	More complex due to top connection and potential structural issues.	Relatively easy integration due to use of original drill rig mounting point

Table 5.9: Comparison practical aspects of Hinge and Platform concepts.

While this section and table 5.9 give information on the practical aspects of each system, there is no clear advantageous concept. Each concept has its own advantages that are hard to compare with, it has to come down to hard restrictions like no drill rig modifications or this much deck space can be used. System specifications like this are currently unknown, but will make the difference in which system is preferable.

5.4. Discussion

When considering the optimisation of the platform concept, it was observed that during all iterations, the algorithm was very sensitive to user input. Mainly how the system was parameterised. The algorithm converged in some cases to very similar solutions. For example, the inertia of the platform and drill rig was combined in one; the algorithm converged to a single geometry that tries to reduce that inertia. Thus, careful consideration is necessary when parameterising the platform. It also shows that small assumptions can sometimes create a very biased solution to the problem. However, in this research, the result showed several different types of optimal geometries, indicating that there is no strong bias. Furthermore, the analysis and comparison to the hinge concept shows that the performance is very similar, and thus shows an optimal solution for the platform concept that represents the 3DoF Rotation Passive concept.

Moreover, the optimisation has only been done under one condition, as shown in section 5.2.2. The system is thus optimised for only this simulation. This is of course not the only scenario that the system will encounter, therefore the system was tested with additional environment effects such as a current, a stationkeeping offset and different peak periods. This showed that the system works under these conditions, but it is probably not optimal performance under these conditions. Therefore, it might be essential to run the optimisation process for various additional environmental conditions and assess the resulting geometries and stiffnesses. In doing so, it is possible to determine and verify the most suitable configurations.

6. Conclusion & Recommendation

In this study, the focus was on motion compensation for large diameter floating drilling to increase operational efficiency and enable economically feasible execution. The objective was to identify the type and number of degrees of freedom that need to be compensated for and to design systems that represent the selected concept. The research was divided into two phases: identification and realisation.

First, the conclusion on the first phase is explained followed by the conclusion on the second phase, which is then summarised in a final conclusion that answers the research question. Finally, some recommendations are made for further research.

6.1. Concept identification

During the concept identification phase, the objective was to determine which type of system is the best suited for the drilling process. Here, a wide variety of motion compensator types with different degrees of freedom compensated were assessed, and for each type, active position-based and passive versions were assessed. Passive systems are all very similar in performance with respect to weight on bit characteristics, whereas active position-controlled systems all resulted in lift-off of the drill bit from the borehole. This has mainly to do with the fact that residual motions are too large, these residual motions create drill string deformations that lead to an increase in axial force and thus lift-off. Passive systems have the ability to deal with large vessel motions, and thus gas spring deformations, while keeping the force relatively constant, and these systems have a low stiffness in the vertical direction. Thus, passive compensation is at least necessary when the drilling method is performed under more challenging environmental conditions. But when considering performance related to stress, there was a clear difference between passive concepts. Mainly the variants that included compensation for a rotation, the free rotation at the top greatly reduces the bending stress, as this boundary condition results in zero moment at that point. Furthermore, the influence of a DP offset on the drilling process and the corresponding motion compensator was investigated. This showed that at shallower water depths, the effect of a DP offset was larger, especially for heave-only compensated systems. Furthermore, active position-based translational compensation was able to fully remove the effects of DP offset on the system. Active position-based systems were also shown to be not completely unusable. Analysis showed that for small wave heights, the system can operate without problems as the vessel motions are smaller in smaller waves and thus the residual motion imposed on the drill string. However, for the most severe desired conditions, passive systems are usable only. The concepts that were finally considered the best were the 3DoF Rotation Passive and the 6DoF Passive. And based on the fact that less degree of freedom compensation is generally less complex, the 3DoF rotation concept was chosen.

6.2. Concept realisation

The 3DoF Rotation passive concept was realised in a system that can physically exist. Two types were considered, a platform type with three cylinders and a type with a heave compensator and universal joint. The universal joint was kept almost the same as in the identification phase, only changing the stiffness and damping. The platform type was optimised using the NSGA-II multi-objective optimisation. The resulting geometry was used for a final evaluation in which the two systems were compared.

Based on the performance that can be seen in the graphs in chapter 5, both are considered suitable for the drilling process. They have good WoB performance, stress is well below the plastic deformation limit, and fatigue life is not problematic. A final conclusion on the best-performing concept is not straightforward since they perform very similar. As some advantages and disadvantages are given for each system, the final decision will depend on the practical characteristics demanded by the designers of the motion compensation system.

What can be concluded from this final phase is what the most critical scenarios are in which the system may need to work. The most critical aspect is operating at shallow depths, especially when it comes to offsets that originate during station-keeping. It showed that the stresses in the lower part of the drill string will increase when an offset is introduced. This may scale non-linearly, so while only 1.5-metre offset will result in 70MPa of bending stresses, 2 metres could double it. Furthermore, if this case is combined with a current, this stress increase can only be exacerbated.

6.3. Final conclusion

Overall, a variety of types of motion compensation were evaluated for suitability in the drilling process. The performance of these systems was evaluated on the basis of the weight on bit amplitude, maximum Von Mises stress, and fatigue life. Passive systems were found to perform similarly, while active position-controlled systems often resulted in lift-off of the drill bit from the borehole. However, passive systems that included rotational compensation showed a significant reduction in bending stress. The 3DoF Rotation Passive and 6DoF Passive concepts were identified as the best, and the 3DoF Rotation concept was chosen for its lesser complexity.
Finally, in the concept realisation phase, the 3DoF Rotation passive concept was physically realised in two forms: a three-cylinder platform type and a universal joint with a heave compensator type. Both systems performed well in terms of weight on bit, stress levels, and fatigue life. However, a definitive conclusion on the best-performing concept could not be drawn based solely on these factors. Other practical aspects such as operational cost, system complexity, effect on ship motions, and integration on deck should be considered.

As a result of this research and answering the research question: What is the most effective compensation methodology for large-diameter drilling from an offshore construction vessel in relatively shallow waters? It is concluded that the 3DoF Rotation Passive and 6DoF Passive systems are the best when considering their performance, it was then decided to further develop the 3DoF Rotation Passive system. The two systems serve as a basis for the design of a system that could be designed in the future. For the platform concept, this is mainly on what the geometry should look like.

6.4. Recommendations

This research made simplifications, some of which the effect could lead to the discovery of new challenges regarding this subject, therefore other effects can be taken into account to further enhance the research. These aspects can show other possible solutions to this problem and provide more information on other effects that could influence the system or be problematic. One such aspect is the exploration of active force control within the drilling process. Focussing on force control instead of displacement control could improve overall performance for active systems and increase overall operational efficiency. Of course, energy consumption must then be taken into account if that would be a better performing system than currently proposed, since active systems do require external energy input.

Another promising solution is the investigation of a combined system that combines active and passive elements. For instance, the integration of the 3DoF Rotation passive concept with horizontal compensation could enhance performance. The 3DoF Rotation passive concept could be effectively combined with horizontal active compensation to create a motion compensation system that is better able to compensate for station keeping inaccuracies.

It is also crucial to consider other aspects of the drilling operation when deciding on the final concept. For example, during the drill string build-up phase, a different type of motion compensation may be necessary. This phase, which involves the assembly and installation of the drill string, can introduce unique challenges and requirements that may not yet be adequately addressed by the motion compensation systems derived in this research. Similarly, the landing operation of the bottom hole assembly on the seabed could require a unique approach to motion compensation. This operation, which involves placing the bottom hole assembly on the seabed, can be particularly challenging as a result of the transient effects of this operation. Therefore, it may be necessary to develop a specific motion compensation

approach that includes one of these scenarios. Alternatively, other solutions could still be found using the motion compensation device proposed in this research.

Another significant factor to consider is the drift of the ship, particularly in scenarios where the DP system fails. Ship drift, which refers to the unintentional movement of a vessel due to wind, currents, or other forces, can introduce unwanted movements and forces into the drilling process. It would be beneficial to investigate the maximum driftoff that each motion compensation device could handle and develop mitigation strategies for such occurrences. Integration of these strategies into the motion compensation system will significantly improve the safety and reliability of the system.

Furthermore, a production estimation model could be included to predict production based on variations in the vertical of the bottom. This model could take into account factors such as the type of cutter, the characteristics of the soil at the drilling site, and the performance of the motion compensation system. By providing a reliable estimate of production, this model could help decide the optimal strategy when performing this operation on a project.

The introduction of torque and rotation into the system could also be considered. Torque and rotation are fundamental aspects of the drilling process. By incorporating these elements into the motion compensation system, exact stresses and fatigue life can be estimated more accurately than in this research.

Additionally, the hydrodynamic effects that occur when a drill string is rotating in water, such as the Magnus effect, could be taken into account. The Magnus effect, which refers to the force exerted on a rotating object moving through a fluid, can introduce unwanted forces and movements into the drilling process. By understanding and accounting for these effects, the performance of the motion compensation system could be improved.

In addition, a more detailed analysis of vortex-induced vibrations (VIV) could provide valuable information on potential challenges and solutions in the drilling process. VIV, which refers to vibrations caused by vortexes in a fluid, can cause unwanted movements and forces in the drilling process. By understanding these vibrations and developing strategies to mitigate them, the efficiency and safety of drilling operations could be significantly improved.

Lastly, an aspect that could be further investigated is the interaction between the motion compensator, the drill string, and the ship. In the current analysis, the assumption is that the motion of the vessel remains unaffected by the forces exerted by the drill string. Although this assumption holds during the drilling operation, it may not be true during the buildup of the drill string. During this phase, there is a large mass suspended connected by a rigid pipe below the ship, which could potentially influence the ship's motions or the performance of the motion compensator. This suspended mass could introduce additional forces and motions that are not considered in the current research.

Furthermore to check the results of this investigation, the data obtained should be compared with the data from the real world. However, it was found that real-life data did not exist. Another option for extra verification of the results of scale model tests. But constructing models for all considered concepts is a challenge, it could only be done for the final two concepts considered in the research. Model tests will, of course, be less costly than performing full-scale tests to verify the data. Alternately, a pilot project can be setup to test a motion compensation device and fine-tune the models to correspond to that obtained data.

To end up with a system that is most suitable for this operation, a detailed analysis of the practical aspects is needed, and only a small part of this thesis is dedicated to this. The exact demands of the design will be different for each vessel that will be used eventually. Additionally, the integration of the drill rig has to be discussed in more detail with the drill rig suppliers. For example, what modifications are possible for the drill rig and is the proposed connection practical? These aspects will most likely make the final decision as to what of the final two proposed concepts the system will look like. The final decision on what system to use for the application thus comes down to additional aspects. But

when the desired aspects are known it is possible to start the design of either one of the two proposed concepts, this will end up in a more detailed design, where losses and actual stiffnesses are more accurately known, and it is recommended then to again validate the design by altering the proposed concept in the used OrcaFlex files.

In conclusion, there are several promising directions for further enhancement of this research on motion compensation for floating drilling and derive the best motion compensation system for this application. By exploring these areas, we can continue to improve the efficiency, safety, and productivity of drilling operations. This will not only benefit the innovation of motion compensation technology but also contribute to the acceleration of the floating wind industry.

References

[1] Aker-Wirth. *Wirth Pile Top Drill Rigs*. 2012. URL: https://www.pilingplaza.com/wp-content/uploads/2016/02/wirth-drills.pdf.

[2] P. Albers. *Motion Control in Offshore and Dredging*. Jan. 2010. DOI: 10.1007/978-90-481-8803-1. URL: https://doi.org/10.1007/978-90-481-8803-1.

[3] *Ampelmann*. URL: https://www.ampelmann.nl/.

[4] R. Bekkers. *Modelling of the drilling rates for large diameter offshore foundation piles*.

[5] *BUMA Construction Equipment*. URL: http://www.bumace.com/product/product01.html#.

[6] A. Cuesta et al. "Why offshore wind energy?" In: *Renewable Energy* 36.2 (Feb. 2011), pp. 444–450. DOI: 10.1016/j.renene.2010.07.009.

[7] Abílio M.P. De Jesus et al. "A comparison of the fatigue behavior between S355 and S690 steel grades". In: *Journal of Constructional Steel Research* 79 (Dec. 2012), pp. 140–150. DOI: 10.1016/j.jcsr.2012.07.021. URL: https://doi.org/10.1016/j.jcsr.2012.07.021.

[8] Kalyanmoy Deb et al. "A fast and elitist multiobjective genetic algorithm: NSGA-II". In: *IEEE Transactions on Evolutionary Computation* 6.2 (Apr. 2002), pp. 182–197. DOI: 10.1109/4235.996017. URL: https://doi.org/10.1109/4235.996017.

[9] K.D. Do and J. Pan. "Nonlinear control of an active heave compensation system". In: *Ocean Engineering* 35.5-6 (Apr. 2008), pp. 558–571. DOI: 10.1016/j.oceaneng.2007.11.005. URL: https://doi.org/10.1016/j.oceaneng.2007.11.005.

[10] Odd M. Faltinsen. *Sea loads on ships and offshore structures*. Oct. 1990. URL: http://fipak.areeo.ac.ir/site/catalogue/18314286.

[11] A. Ghasemloonia, D. Rideout, and S. Butt. "A review of drillstring vibration modeling and suppression methods". In: *Journal of Petroleum Science and Engineering* 131 (July 2015), pp. 150–164. DOI: 10.1016/j.petrol.2015.04.030. URL: https://doi.org/10.1016/j.petrol.2015.04.030.

[12] DNV GL. *Fatigue design of offshore steel structures*. Tech. rep. RP-C203. June 2014. URL: https://www.dnv.com/.

[13] DNV GL. *Marine operation and marine warranty*. Tech. rep. ST-N001. June 2016. URL: https://www.dnv.com/.

[14] DNV GL. *Wave Loads*. Tech. rep. DNVGL-CG-0130. Jan. 2018. URL: https://www.dnv.com/.

[15] Paul Grodzinski and Ewen M'Ewen. "Link mechanisms in modern Kinematics". In: *Proceedings - Institution of Mechanical Engineers* 168.1 (June 1954), pp. 877–896. DOI: 10.1243/pime\{_}proc\{_}1954\{_}168\{_}079\{_}02. URL: https://doi.org/10.1243/pime_proc_1954_168_079_02.

[16] Jerzy Herdzik. "UTILIZATION OF AN ACTIVE AND/OR PASSIVE HEAVE COMPENSATION IN THE EQUIPMENT OF DYNAMIC POSITIONING VESSELS". In: *Journal of KONES* 21.2 (May 2014), pp. 89–95. DOI: 10.5604/12314005.1133875. URL: https://doi.org/10.5604/12314005.1133875.

[17] L. H. Holthuijsen. *Waves in Oceanic and Coastal Waters*. Cambridge University Press, Feb. 2010.

[18] T. Inoue et al. "Fatigue Strength Evaluation of Drill Pipe Constantly Bent In Strong Current". In: *Proceedings of the Eighth (2008) ISOPE Pacific/Asia Offshore Mechanics Symposium* (Jan. 2008). URL: https://onepetro.org/ISOPEPACOMS/proceedings/PACOMS08/All-PACOMS08/ISOPE-P-08-023/25777.

[19] F. Jaouen et al. "How Does Barge-Master Compensate for the Barge Motions: Experimental and Numerical Study". In: July 2012. DOI: 10.1115/omae2012-83045. URL: https://doi.org/10.1115/omae2012-83045.

[20] J.M.J. Journée and W.W. Massie. *Offshore Hydromechanics*. 1st ed. Delft University of Technology, Jan. 2001.

[21] JPE. *Structural damping definitions - JPE*. Oct. 2020. URL: https://www.jpe-innovations.com/precision-point/structural-damping-definitions/.

[22] U.A. Korde. "Active heave compensation on drill-ships in irregular waves". In: *Ocean Engineering* 25.7 (July 1998), pp. 541–561. DOI: 10.1016/s0029-8018(97)00028-0. URL: https://doi.org/10.1016/s0029-8018(97)00028-0.

[23] Orcina Ltd. *OrcaFlex*.

[24] K.G. MacDonald and J.V. Bjune. "Failure analysis of drillstrings". In: *Engineering Failure Analysis* 14.8 (Dec. 2007), pp. 1641–1666. DOI: 10.1016/j.engfailanal.2006.11.073. URL: https://doi.org/10.1016/j.engfailanal.2006.11.073.

[25] Barge Master. *Barge Master Motion Compensation Systems*. URL: https://www.barge-master.com/.

[26] Bernard Le Méhauté. *An introduction to hydrodynamics and water waves*. Jan. 1976. DOI: 10.1007/978-3-642-85567-2. URL: https://doi.org/10.1007/978-3-642-85567-2.

[27] M. Moharrami and H. Shiri. "Fatigue Reliability Assessment of Drill String Due to Stick-Slip Vibrations and Wave-Frequency Vessel Motions". In: *The 31st International Ocean and Polar Engineering Conference* (June 2021). URL: https://onepetro.org/ISOPEIOPEC/proceedings/ISOPE21/464703.

[28] J. Morison, J. R. Johnson, and S. A. Schaaf. "The Force Exerted by Surface Waves on Piles". In: *Journal of Petroleum Technology* 2.05 (May 1950), pp. 149–154. DOI: 10.2118/950149-g. URL: https://doi.org/10.2118/950149-g.

[29] *NG-20000X Self-propelled jack-up | NOV*. URL: https://www.nov.com/products/ng-20000x-self-propelled-jack-up.

[30] Dan Russel. *Regions of Resonance*. June 2019. URL: https://www.acs.psu.edu/drussell/Demos/Resonance-Regions/Resonance.html.

[31] A. R. Southerland. "MECHANICAL SYSTEMS FOR OCEAN ENGINEERING". In: *Naval Engineers Journal* 82.5 (Oct. 1970), pp. 63–74. DOI: 10.1111/j.1559-3584.1970.tb04361.x. URL: https://doi.org/10.1111/j.1559-3584.1970.tb04361.x.

[32] A. Stacey and J. V. Sharp. "Safety factor requirements for the offshore industry". In: *Engineering Failure Analysis* 14.3 (Apr. 2007), pp. 442–458. DOI: 10.1016/j.engfailanal.2005.08.003. URL: https://doi.org/10.1016/j.engfailanal.2005.08.003.

[33] J. Woodacre, R. Bauer, and R. A. Irani. "A review of vertical motion heave compensation systems". In: *Ocean Engineering* 104 (Aug. 2015), pp. 140–154. DOI: 10.1016/j.oceaneng.2015.05.004. URL: https://doi.org/10.1016/j.oceaneng.2015.05.004.

[34] N. Woodall-Mason and J.R. Tilbe. "Value of Heave Compensators to Floating Drilling". In: *Journal of Petroleum Technology* 28.08 (Aug. 1976), pp. 938–946. DOI: 10.2118/5267-pa. URL: https://doi.org/10.2118/5267-pa.

[35] X. Wu et al. "Foundations of offshore wind turbines: A review". In: *Renewable & Sustainable Energy Reviews* 104 (Apr. 2019), pp. 379–393. DOI: 10.1016/j.rser.2019.01.012.

A. Boka Falcon Data

Boskalis

EQUIPMENT SHEET

BOKA FALCON
MULTIPURPOSE DP2 OFFSHORE CONSTRUCTION VESSEL

CONSTRUCTION / CLASSIFICATION	
Vessel built by	Drydock World, Singapore
Year of built	2011
Classification	Offshore support vessel (Anchor handling; Fire-fighting 1 -water spraying; Supply HNLS; TUG) Unrestricted navigation AVM-DPS, AUT-UMS, SYS-NEQ-1, SYS-IBS, MON-SHAFT, GREEN PASSPORT, CLEANSHIP, DYNAPOS AM/AT R
Flag	Belgian
Port of registry	Antwerp

FEATURES	
Accommodation	100 berths, 14 x single cabins & 9 x double cabins & 17 x 4 person cabins, all with private facilities
Bunker capacity	1,049 m^3 1,761.3 m^3 (including Methanol tanks and combination tanks mud/brine)
Other tanks for cargo	Potable water: 1,088.8 m^3 Drill water / SWB: 2,661.5 m^3 Liquid mud / base oil / brine: 712.3 m^3 Chain locker: 797.4 m^3 Methanol: 196.8 m^3
Discharge capacity	Fuel oil 1 x 250 m^3/hr @ 9 bar Potable water 1 x 250 m^3/hr @ 9 bar Drill water 2 x 250 m^3/hr @ 9 bar Liquid mud 2 x 100 m^3/hr @ 24 bar Base oil 1 x 125 m^3/hr @ 9 bar Brine 1 x 75 m^3/hr @ 18 bar Methanol 2 x 100 m^3/hr @ 9 bar
Positioning	Dynamic positioning, class II, K-POS 21

MAIN DATA	
Length overall	93.4 m
Length BP	82.0 m
Breadth moulded	22.0 m
Depth moulded	9.5 m
Design draught	7.0 m
Summer draught	7.866 m
Maximum displacement	10,973 t
Lightship weight	6,888 t
Gross tonnage	6,776 GT
Netto tonnage	2,032 NT
Bollard pull	403 t
Deck area	815 m^2

PROPULSION AND MAIN SYSTEM	
Main engine (Hybrid)	2 x MAK 16M32C, 10,728 BHP each
PTI Booster motor	2 x 3,000 kW = 8,046 BHP
Total BHP	29,502 BHP

Boskalis

BOKA FALCON
MULTIPURPOSE DP2 OFFSHORE CONSTRUCTION VESSEL

Propeller	2 x CPP, Ulstein
Azimuth thruster (FWD)	1 x Ulstein Aquamaster TCNS 92/62-220, 1,500 kW, Swing Up, CPP
Bow thruster	2 x 1,000 kW, Kamewa TT 2200 DPN CP
Azimuth thruster (AFT)	1 x Ulstein Aquamaster TCNS 92/62-220, 1,500 kW, Swing Up, CPP
Stern thruster	1 x 1,000 kW, Kamewa TT 2200 DPN CP
Fire fighting	FIFI CLASS (1) with water spray). Pump: 2 x 2,095 m^3/hr @ 32 m head. Monitor (water): 1 x 1,200 m^3/hr @ 12 bar

ELECTRIC POWER GENERATION

Main generator	4 x CAT 3516C rated 2,230 kW/690 V/60 Hz/3 Phh
Shaft alternator	2 x 4,000 kW/690 V/60 Hz/3 Ph
Emergency generator	1 x 370 kW/690 V/60 Hz/3 Ph

DECK EQUIPMENT

Tugger winch	2 x 24 t @ 22 m/min, Brattvaag
Tugger/mooring winch (AFT)	2 x 17 t @ 15 m/min, Brattvaag
Subsea crane	1 x HMC 3568 LKO 250-35 (1500-10), AHC crane, SWL: 150 t @ 12 m, wire length 3,000 msw
A Frame (optional)	1 x 250 t AHC capability A Frame for LAR of subsea equipment up to depth of 3,000 msw
Moonpool (optional)	7.0 m x 7.0 m

TOWING AND ANCHOR HANDLING EQUIPMENT

SPECIAL HANDLING DRUM

Brake/Pull	600 t brake, 500 t Pull
Drum capacity	14,800 m x 76 mm (Ø) Wire rope/2,180 m x 203 mm (Ø) synthetic rope
Tugger/mooring winch (AFT)	2 x 17 t @ 15 m/min, Brattvaag
Tugger winch	2 x 24 t @ 22 m/min, Brattvaag

TOWING/WORKING DRUM (PORT SIDE)

Brake/Pull	750 t brake, 450 t Pull
Drum capacity	3,500 m x 76 mm (Ø) Wire rope/490 m x 203 mm (Ø) synthetic rope
Chain gypsy	2 x 76 mm (Ø), 2 x 97 mm (Ø), 2 x 120 mm, 1 x 124 mm (Ø), 1 x 127 mm (Ø)

TOWING/WORKING DRUM (STARBOARD SIDE)

Brake/Pull	750 t brake, 450 t Pull
Drum capacity	3,800 m x 90 mm (Ø) Wire rope/800 m x 203 mm (Ø) synthetic rope
Chain gypsy	2 x 76 mm (Ø), 2 x 97 mm (Ø), 2 x 120 mm, 1 x 124 mm (Ø), 1 x 127 mm (Ø)

AFT-DECK

Karm Fork	2 x Karm Fork, SWL: 800 t
Tow pin	4 x Tow pin, SWL: 800 t
Split stern roller	2 x 2.9 x 4.5 m (Ø), SWL: 750 t

SAFETY EQUIPMENT

Life raft	12 x 25 persons, Viking RFD
Rescue boat	1 x 15 persons, Norsafe MAKO 6,55, 246 hp
Davit	NDM PRHE 35, SWL: 3.5 t

ROV SYSTEM

ROV	2 x Triton XLX 150 hp heavy work Class ROV, working up to depths of 3,000 m

NAVIGATION AND COMMUNICATION EQUIPMENT

GMDSS (Area 3)	2 x Furuno RC-1800TVHF DSC
Inmarsat	2
VSAT	1
Gyro compass	3
DGPS	2
Joystick	RRM PosCon independent joystick fitted
Anemometer	2
ECDIS	2
SAT TV System	1
MRU5	3

Boskalis

BOKA FALCON
MULTIPURPOSE DP2 OFFSHORE CONSTRUCTION VESSEL

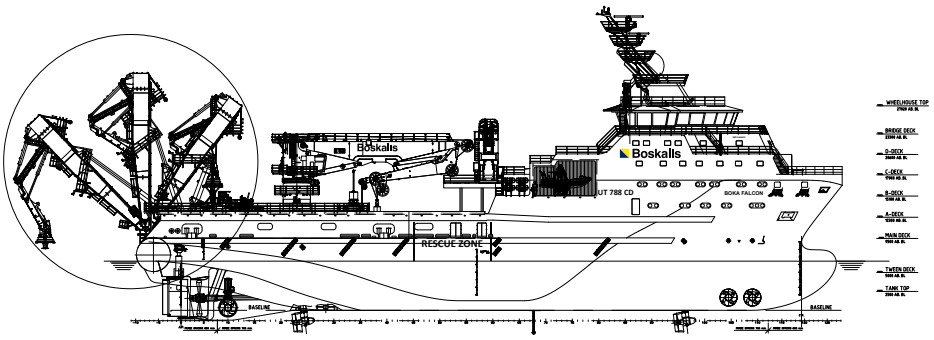

SIDE VIEW

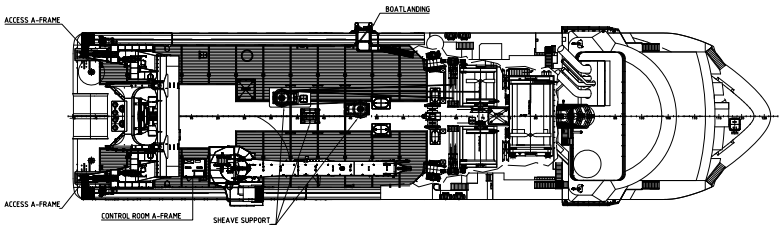

TOP VIEW

Boskalis
PO Box 43
3350 AA Papendrecht
The Netherlands
T +31 78 69 69 000
offshore.energy@boskalis.com
www.boskalis.com/offshore

B. Drill String Technical Drawing

Content in this appendix has been removed due to sensitive data.

C. BOKA Falcon RAOs

Content in this appendix has been removed due to sensitive data.

D. Sensitivity Analysis

In this appendix, the validity of the analysis of the first phase is discussed. First, a comparison will be made between the vessel motions in the regular wave analysis and the vessel motion that one can expect under the desired operating conditions. This is followed by a look at the impact of wave amplitude and active system efficiency on the final result of the compensation type selection. Then the impact of the drill string stiffness is discussed and the consequence of a changing drill string stiffness is investigated. Finally, it is recommended to what extent the first result is valuable and right for this research.

D.1. Ship motion analysis

To check whether the use of regular waves in the motion compensation type identification phase is a valid method. A comparison is made between the amplitudes of the drill string suspension point. For regular wave analysis, the amplitude of this motion is extracted from the OrcaFlex simulation files. This is compared with statistical amplitudes, and the comparison can be seen in figure D.2 to figure D.6. Statistical amplitudes are calculated using the OrcaFlex vessel response. This function calculates the significant amplitude and maximum amplitude of the ship motions based on an input wave spectrum. The input wave spectrum is a JONSWAP with values based on DNVGL-CG-0130 [14]. A JONSWAP spectrum with $\gamma = 1$ is the same as a Pierson-Moskowitz (PM) spectrum. The input parameters are given in table D.1.

Parameter	Value	Unit
H_s	2.5	m
T_p	6, 8, 10, 12, 14, 16	s
γ	3.99, 1, 1, 1, 1, 1	-
α	165	°
T_{storm}	3	hours

Table D.1: Parameters used in the vessel response wave spectrum

The statistical amplitudes in OrcaFlex are calculated by joining the wave spectrum and the ship RAO together, which results in a response spectrum for every degree of freedom. Then the significant amplitude is calculated by using the zeroth spectral moment of this response spectrum.

$$A_s = 2m_0^{\frac{1}{2}} \tag{D.1}$$

The maximum amplitude that could occur within the 3-hour duration the ship is exposed to the wave spectrum is calculated by using the significant amplitude and number of zero-up crossing periods occurring in that time frame.

$$A_{max} = A_s \left[\ln 60^2 d/T_z\right]^{-1/2} \tag{D.2}$$

From figure D.1 to figure D.6 it can be seen that the amplitude considered for the regular wave analysis causes excitations comparable to the significant amplitude that the vessel experiences in sea states with the corresponding significant wave height and peak period. The maximum amplitude that can be expected during three hours of that wave spectrum is significantly higher. This means that regular wave analysis is no indication whether the system will be able to operate under such environmental conditions, but what can be concluded is that regular wave analysis still gives an indication of the performance of such motion compensation systems, just not in these specific real wave environments. Therefore, to get a real estimate of the performance, a more detailed analysis, including wave spectra, needs to be done to finally assess whether it is suitable for the desired conditions. This is done in the second phase of this research, thus a final verification is done.

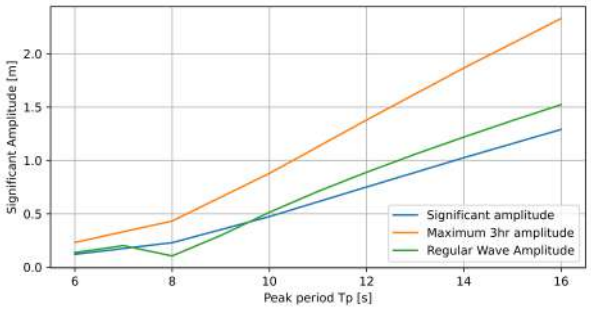

Figure D.1: Surge motion amplitudes for regular waves with $H = 2.5m$, $\alpha = 165°$ and statistical amplitudes for surge motion in a JONSWAP spectrum with $H_s = 2.5m$, $\alpha = 165°$

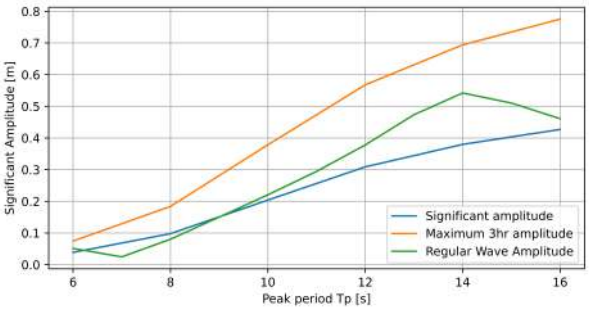

Figure D.2: Sway motion amplitudes for regular waves with $H = 2.5m$, $\alpha = 165°$ and statistical amplitudes for sway motion in a JONSWAP spectrum with $H_s = 2.5m$, $\alpha = 165°$

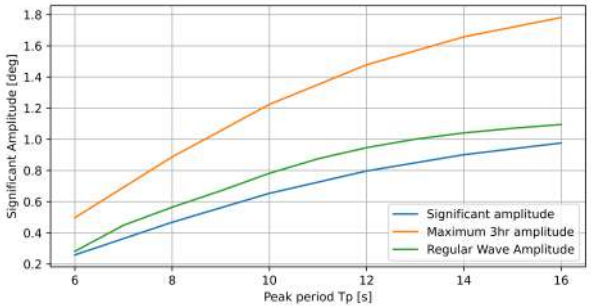

Figure D.3: Heave motion amplitudes for regular waves with $H = 2.5m$ and statistical amplitudes for heave motion in a JONSWAP spectrum with $H_s = 2.5m$

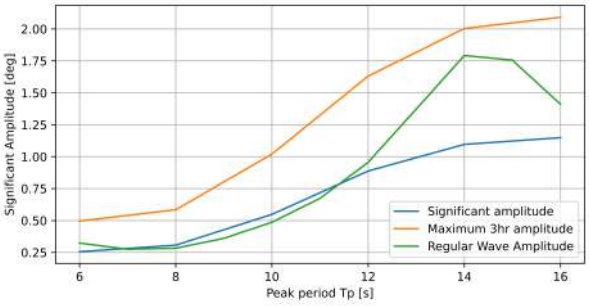

Figure D.4: Roll motion amplitudes for regular waves with $H = 2.5m$, $\alpha = 165°$ and statistical amplitudes for roll motion in a JONSWAP spectrum with $H_s = 2.5m$, $\alpha = 165°$

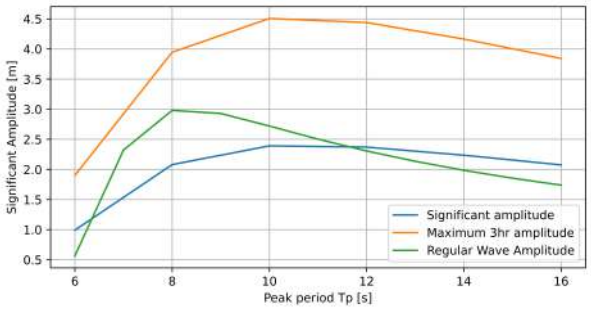

Figure D.5: Pitch motion amplitudes for regular waves with $H = 2.5m$, $\alpha = 165°$ and statistical amplitudes for pitch motion in a JONSWAP spectrum with $H_s = 2.5m$, $\alpha = 165°$

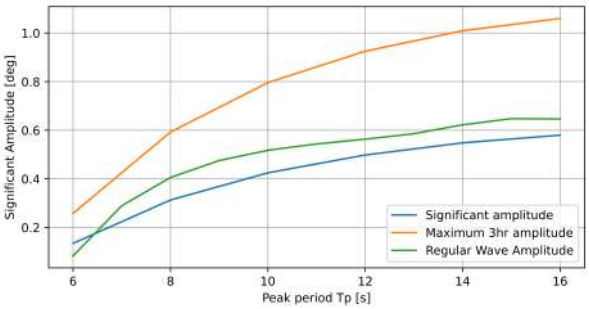

Figure D.6: Yaw motion amplitudes for regular waves with $H = 2.5m$ and statistical amplitudes for yaw motion in a JONSWAP spectrum with $H_s = 2.5m$

D.2. Wave Amplitude & Efficiency sensitivity

The performance of active systems is described by an efficiency factor. This efficiency factor is chosen as 95%. Therefore, the total residual motion is 5% of the vessel motion. Additionally, the vessel motion is calculated with RAOs and the amplitude of the ship motion is the RAO factor multiplied by the wave amplitude. Therefore, the residual motion of the suspension point depends on the efficiency and wave height chosen. There exist combinations of efficiency and wave height at which active systems do not experience lift-off. This combination gives a specific constant deformation for the drill string to achieve full tension. In this section, this limit will be calculated to see at which point active systems start to perform comparable to the passive systems.
To calculate the limit, it is necessary to vary the efficiency and wave height and apply this to a case already investigated. It can be seen in figure 4.14 that the Active compensation model of 1DoF is the least efficient concept, the performance is worst at 50m water depth since the drill string is the least flexible, and at a wave period of 16 seconds since the RAO value of the BOKA Falcon is the largest

Parameter	Value	Unit
Concept	1DoF Active	-
Water depth	50	m
Wave period	16	s

Table D.2: The case represented for the wave amplitude efficiency sensitivity analysis.

there. Thus, the scenario that is evaluated for the problem is given in table D.2.
This analysis evaluates different combinations of efficiency and wave height to determine whether the WoB time series changes signs. If so, this is noted, and the safe region for this limiting scenario is plotted in figure D.7. The dots represent the boundary where the operation can still be performed safely. Since this is a discrete analysis, there is no in-between; only success or failure. In cases where multiple combinations are limiting, there may be multiple dots vertically above each other. The boundary is linearly interpolated between the outermost points, where the operation can be safely executed.
To analyse this, combinations with different efficiencies and wave heights are evaluated. Then it is checked whether the WoB time series switches signs. If so, this is noted. With this result, the safe region for this limiting scenario can be plotted, this is done in figure D.7. The dots represent the boundary where the operation is still be able to be done safely. Since this is a discrete analysis, there is only failure or success, no in-between. There are cases where multiple combinations are limiting, there can be multiple dots vertically above each other. The boundary is linearly interpolated between the outermost points where the operation can be executed safely.

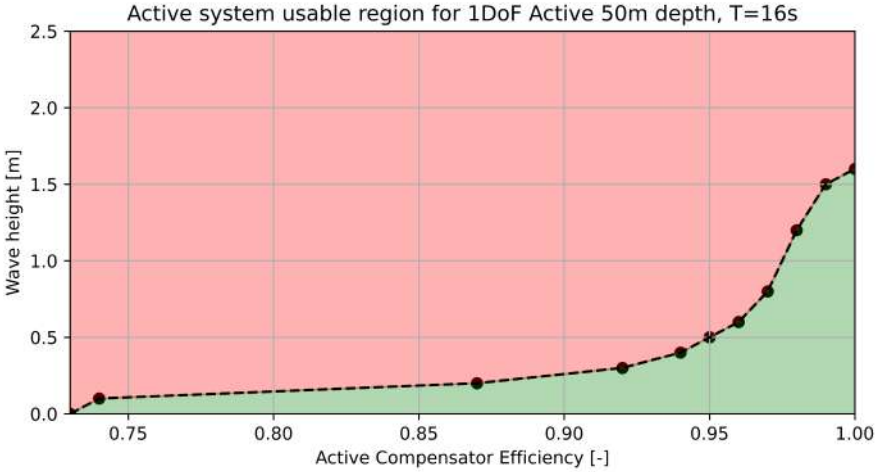

Figure D.7: The usable region depending on efficiency and wave height for the limiting active system scenario (1DoF Active 50m depth, T=16s).

It can be seen that from the wave height of around 1.6m, the operation cannot be executed. From that point on the other motions of the ship (surge, sway, roll, pitch, and yaw) are severe enough to deform the drill string in such a way that perfect active heave compensation is enough. From then on, additional degrees of freedom need to be compensated for to ensure safe operation. This means that no active heave compensator can work for the first-phase evaluated case. Then how is this possible for passive systems? Passive systems can partially compensate for other motions, if there is a rotation or horizontal deformation, the span of the drill string becomes shorter, the passive system can deform to allow for this deformation, and the active system can only compensate for the heave, and thus not change its position in response to other deformations.

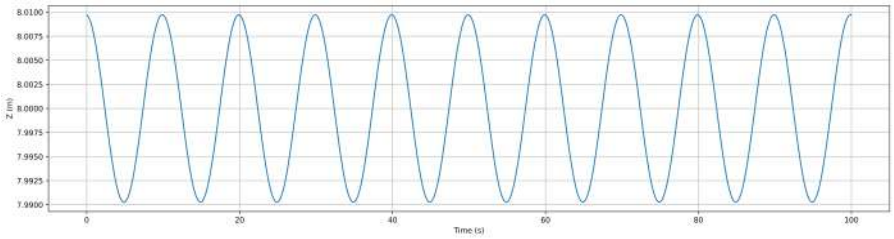

Figure D.8: Residual z-motion of the 3DoF Rotation Active case at 50m depth with a wave height of 0.625m and period of 10s.

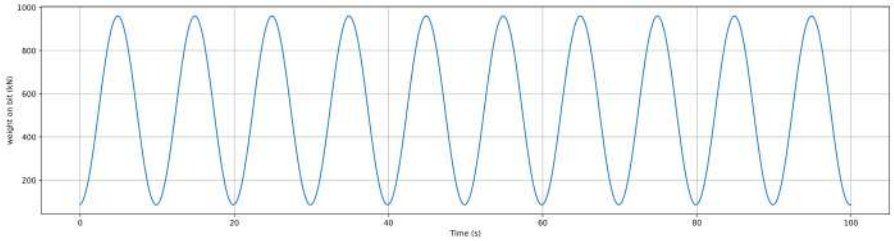

Figure D.9: Weight on bit time series for the 3DoF Rotation Active case at 50m with residual motions of $\pm$1cm.

Moreover, during the construction of the Wikinger offshore wind farm the RCD method has been executed by Boskalis using the Bargemaster motion compensation system. This is an active position-based motion compensation device that compensates the heave, roll, and pitch, just like the 3DoF Rotation active concept. Here, the drilling was excecuted well, it was reported that the residual motions at the top were $\pm$1cm maximum. This can be translated into the models proposed in this thesis, for example, the 50m water depth with the 3DoF Rotation Active System with a regular wave period of 10s. The wave height is then tuned to 0.625m. This, combined with the RAO value for the heave and the efficiency of 95%, gives a residual motion at the top of 1cm (RAO values in appendix C. The simulated time series shows that lift-off does not occur and that stresses remain below the yield limit, again this also indicates that active solutions can work and that the models proposed in this research are accurate [25], the data supporting this are given in figure D.8 and figure D.9.
All in all, active systems are not entirely unsuitable for this application. For calm seas and normal efficiencies, the system can work fine. But for the more severe desired operating conditions, it is not suitable. In addition, passive systems are usually much less complex and cheaper than active systems. An active system may then only be desirable if the compensation systems were used during other parts of the operation or completely different operations.

E. C_d & C_a Derivation

For the derivation of the C_d & C_a coefficient the books of Journée & Massie and Holthuijsen are used [20][17]. The main parameter that is important for the C_d derivation is the Reynolds number. This is:

$$Re = \frac{UD}{\nu} \tag{E.1}$$

Here, U is the undisturbed flow speed of the fluid, D the diameter of the cylinder, and ν the kinematic viscosity. The Reynolds number can be extracted directly from the OrcaFlex simulation. The maximum Reynolds number is found to occur for the smallest water depth and the longest wave period. This is displayed in figure E.1a.

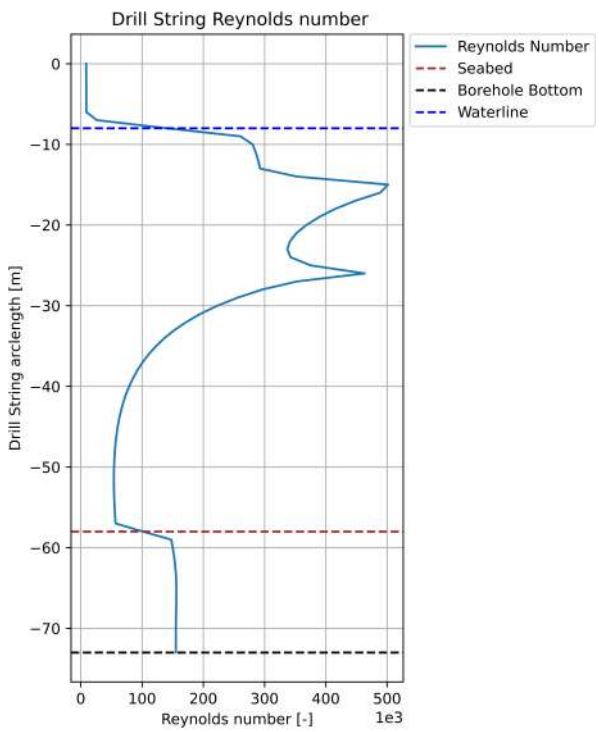

(a) Mean Reynolds number along the drill string for 1DoF passive at 50m water depth with a wave period of 16s.

Flow and Parameters	Flow Patern	Flow Description
1. Viscous *Rn < 1* *C_D > 12*	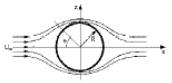	Flow is symmetric about both axes. Friction dominates.
2. Hele-Shaw *1 < Rn < 5* *12 > C_D > 4.5*		Slight separation downstream. Symmetry about flow axis only. Inertia becomes important.
3. Symmetric Vortices *5 < Rn < 65* *4.5 > C_D > 1.6*		First separation and vortices downstream. Wake unstable (turbulent) farther downstream.
4. Precritical *65 < Rn < 5 000* *1.6 > C_D > 1.2*		Vortices become unstable and alternately separate forming a Von Karman vortex street.
5. Subcritical *5K < Rn < 200K* *C_D about 1.2*		Turbulent mixing between vortices downstream. Laminar boundary layer on front of cylinder.
6. Critical *200K < Rn < 500K* *1.2 > C_D > 0.3*		Turbulent wake behind cylinder. Separation and re-attachment of boundary layer upstream of wake.
7. Supercritical *500K < Rn < 4M* *0.3 < C_D < 0.7*		Separation 'bubble' gone. Cylinder boundary layer begins to be turbulent. Wake becomes wider.
8. Postcritical *Rn > 4M* *Cd about 0.7*		Turbulence reaches the boundary layer on the upstream side.

(b) Reynolds numbers and their corresponding C_d values [20].

Figure E.1: Reynolds numbers from OrcaFlex simulations and their corresponding C_d values.

The maximum mean Reynolds number in this graph is around 500k, then in figure E.1b, it can be seen that C_d should be between 0.3 and 1.2. Then, to be conservative, the value of 1.2 is chosen. One note on figure E.1a is the increase in Reynolds number in the borehole, this is because of two reasons: the larger diameter that the drill string model in OrcaFlex has at the bottom hole assembly, and the fact that OrcaFlex here calculates the water particle orbital velocity down to infinite depth. Therefore, the velocity of the particles is not zero below the seabed. It can be set to calculate this to a specific level, but this was found late in the study, and the effect was investigated to be negligible for stresses and WoB. This is because the drill string is fixed at three locations close to each other.
For the added mass coefficient, C_a, the offshore hydromechanics book by Journée suggests that C_a will generally not be higher than the theoretical value of 1 [20].

F. VIV analysis

Vortex induced vibrations (VIV) are oscillations perpendicular to the flow around objects. It occurs when vortex shedding occurs at specific frequencies. Vortex shedding occurs when a fluid flows at relatively constant speed around objects, for example, a current. The shape considered here is a cylinder as it represents the drill string. The shedding frequency of the created vortices can be calculated considering the Strouhal number [20].

$$St = \frac{f_v D}{U} \tag{F.1}$$

Here St is the Strouhal number, D is the diameter of the cylinder in the flow, and U is the flow velocity. The Strouhal number is considered to be 0.2 for most situations, and thus also here. VIV can occur when the vortex shedding frequency is equal to or close to the natural frequency of the system. Thus:

$$f_v = f_n = \frac{StU}{D} \tag{F.2}$$

Here, f_n is the natural frequency of the cylinder. The natural frequencies considered for this analysis are the first two lateral natural frequencies for each concept and depth in the identification phase. This gives a good overview of what constant flow velocities can trigger lock-in.
In table F.1 it can be seen that the range of constant fluid flow is from 0.16m/s and higher, this means that even a small current will most likely trigger VIV, so it should be carefully considered when deploying this drilling technique in the current that VIV can occur and that possibly additional countermeasure should be taken.

Concept	Depth	Natural Period (s)	VIV Lock-in Velocity (m/s)
1DoF Passive	50	2.47	0.66
		1.01	1.6
	100	6.36	0.25
		2.63	0.62
	200	14.59	0.11
		6.68	0.24
3DoF Translation Passive	50	4.1	0.4
		1.61	1.01
	10	7.77	0.21
		3.58	0.45
	200	15.84	0.1
		7.47	0.22
3DoF Rotation Passive	50	3.25	0.5
		1.17	1.38
	100	7.61	0.21
		3.03	0.53
	200	15.78	0.1
		7.23	0.22
6DoF Passive	50	4.27	0.38
		1.7	0.95
	100	8.64	0.19
		3.61	0.45
	200	16.93	0.1
		7.82	0.21
Active systems	50	2.4	0.68
		0.96	1.69
	100	6.63	0.24
		2.7	0.6
	200	14.45	0.11
		6.63	0.24

Table F.1: The lowest and highest lateral natural frequencies of the the first two lateral natural periods for different drill strings and their corresponding VIV locking flow velocities.

G. Power Spectral Density Plots

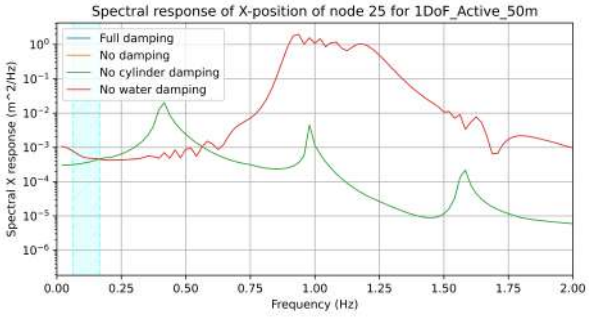

Figure G.1: Spectral density of the free lateral vibration of node 25 for the 1DoF Active concept at 50m.

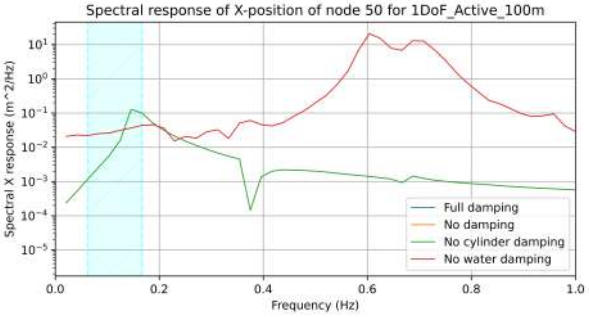

Figure G.2: Spectral density of the free lateral vibration of node 25 for the 1DoF Active concept at 100m.

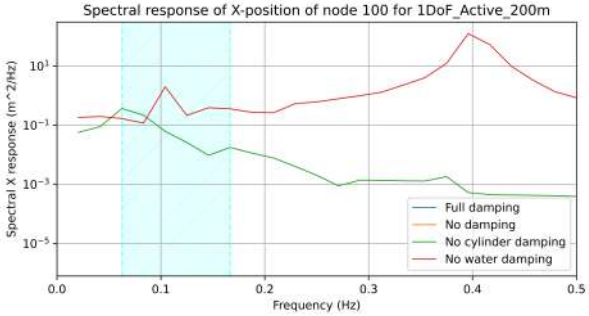

Figure G.3: Spectral density of the free lateral vibration of node 25 for the 1DoF Active concept at 200m.

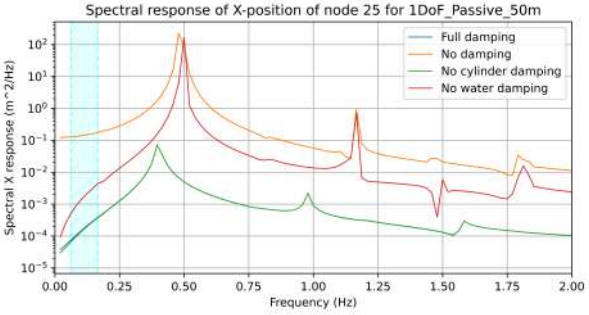

Figure G.4: Spectral density of the free lateral vibration of node 25 for the 1DoF Passive concept at 50m.

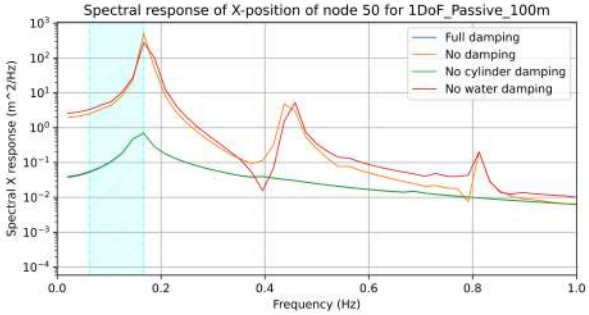

Figure G.5: Spectral density of the free lateral vibration of node 25 for the 1DoF Passive concept at 100m.

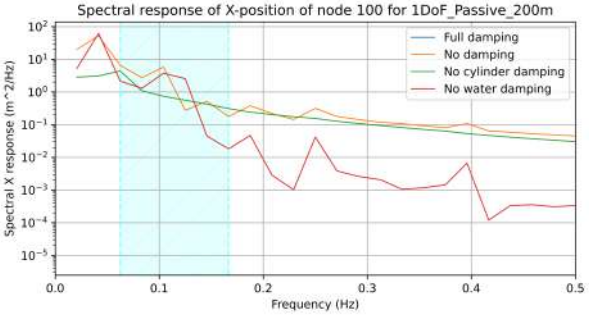

Figure G.6: Spectral density of the free lateral vibration of node 25 for the 1DoF Passive concept at 200m.

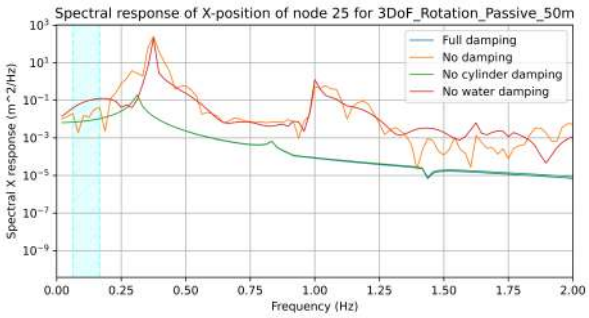

Figure G.7: Spectral density of the free lateral vibration of node 25 for the 3DoF Rotation Passive concept at 50m.

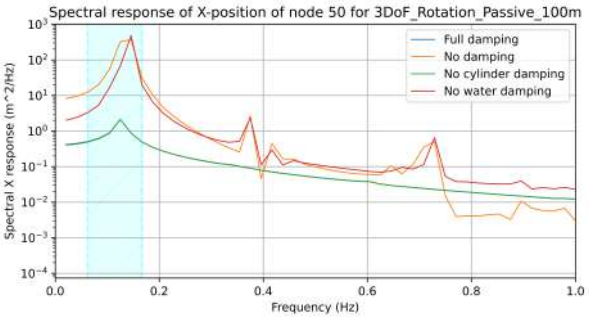

Figure G.8: Spectral density of the free lateral vibration of node 25 for the 3DoF Rotation Passive concept at 100m.

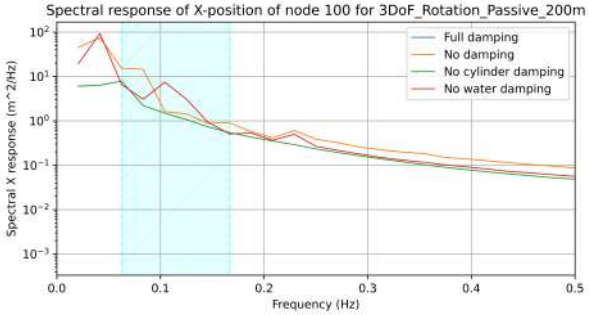

Figure G.9: Spectral density of the free lateral vibration of node 25 for the 3DoF Rotation Passive concept at 200m.

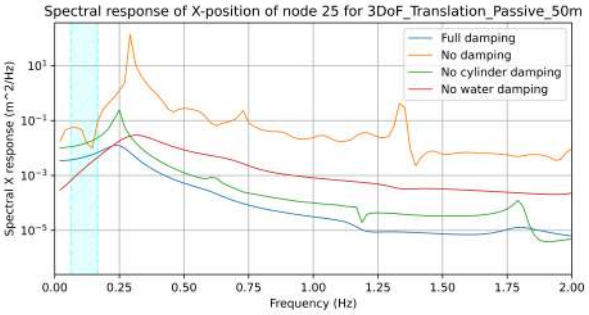

Figure G.10: Spectral density of the free lateral vibration of node 25 for the 3DoF Translation Passive concept at 50m.

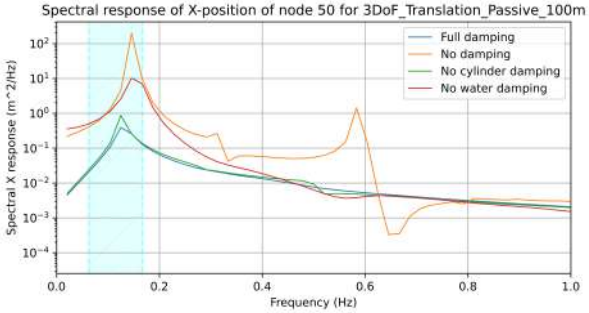

Figure G.11: Spectral density of the free lateral vibration of node 25 for the 3DoF Translation Passive concept at 100m.

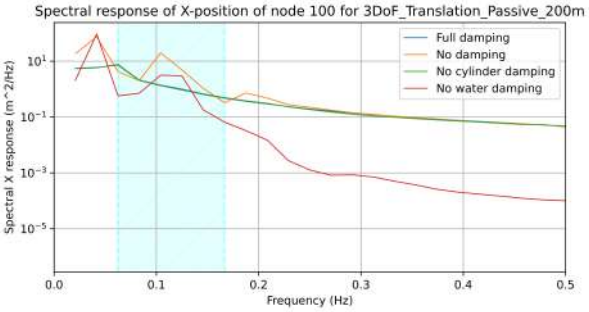

Figure G.12: Spectral density of the free lateral vibration of node 25 for the 3DoF Translation Passive concept at 200m.

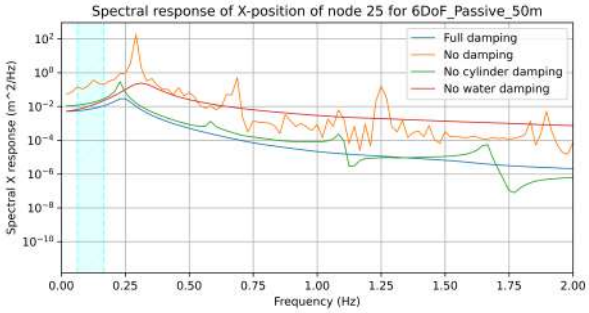

Figure G.13: Spectral density of the free lateral vibration of node 25 for the 6DoF Passive concept at 50m.

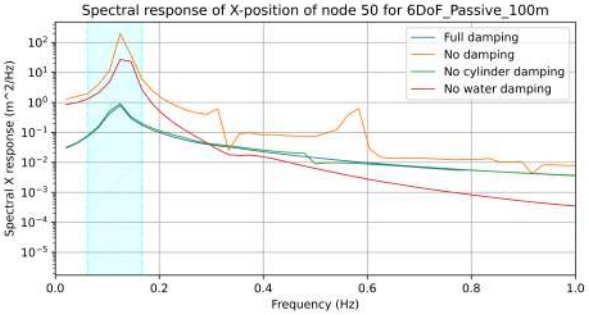

Figure G.14: Spectral density of the free lateral vibration of node 25 for the 6DoF Passive concept at 100m.

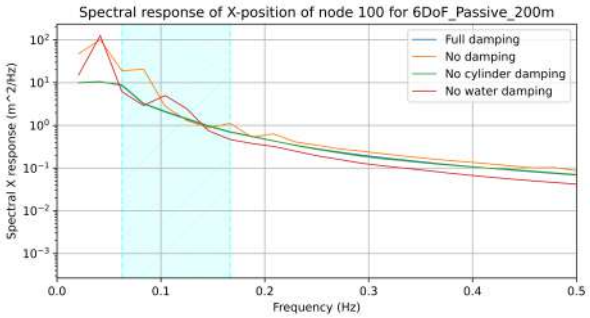

Figure G.15: Spectral density of the free lateral vibration of node 25 for the 6DoF Passive concept at 200m

H. Mode shapes

H.1. Identification Phase

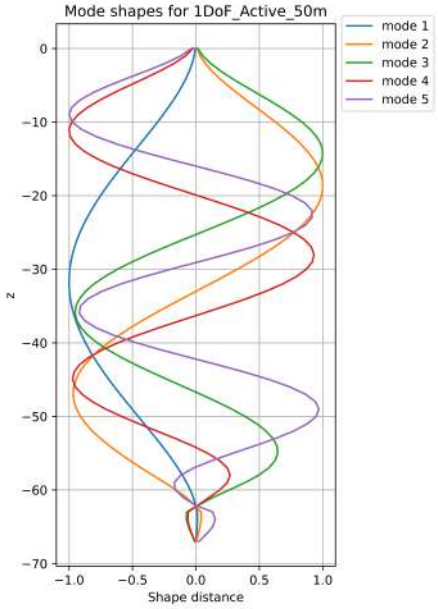

Figure H.1: Mode shapes for the 1DoF Active concept at 50m water depth.

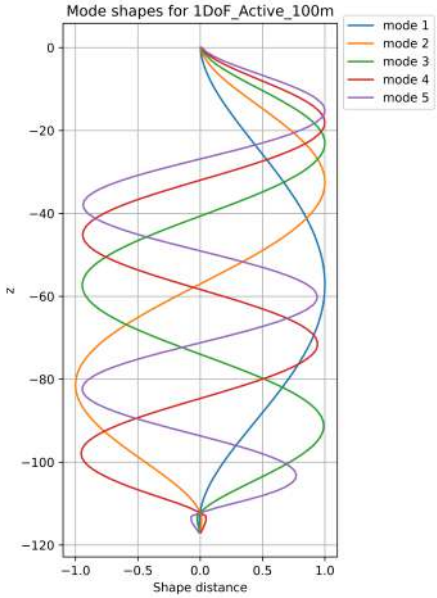

Figure H.2: Mode shapes for the 1DoF Active concept at 100m water depth.

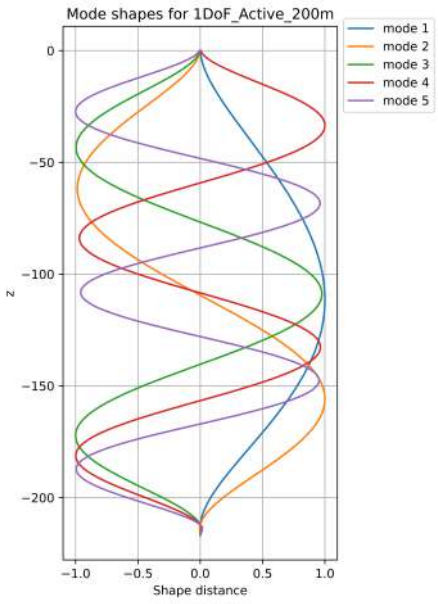

Figure H.3: Mode shapes for the 1DoF Active concept at 200m water depth.

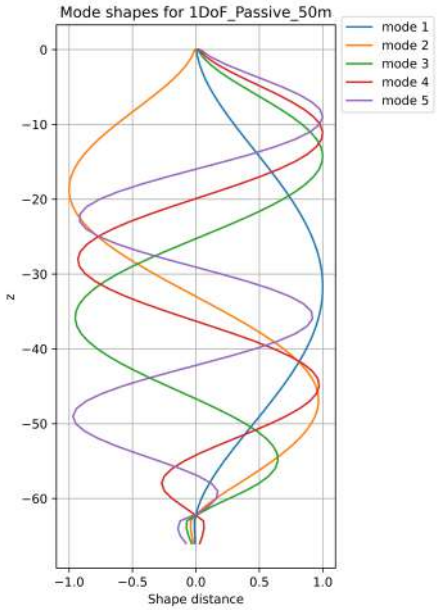

Figure H.4: Mode shapes for the 1DoF Passive concept at 50m water depth.

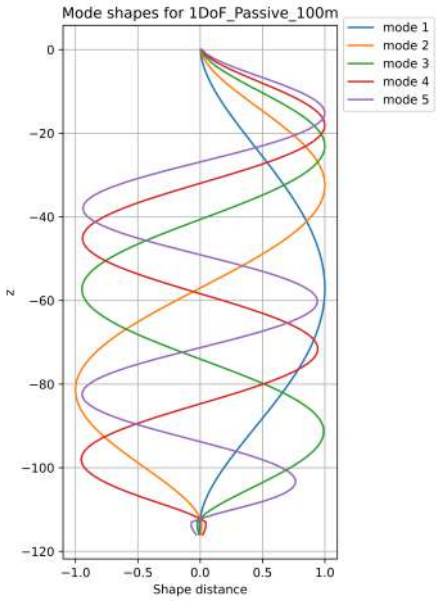

Figure H.5: Mode shapes for the 1DoF Passive concept at 100m water depth.

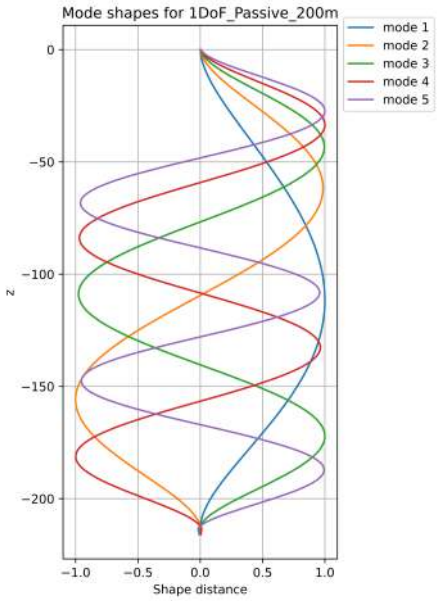

Figure H.6: Mode shapes for the 1DoF Passive concept at 200m water depth.

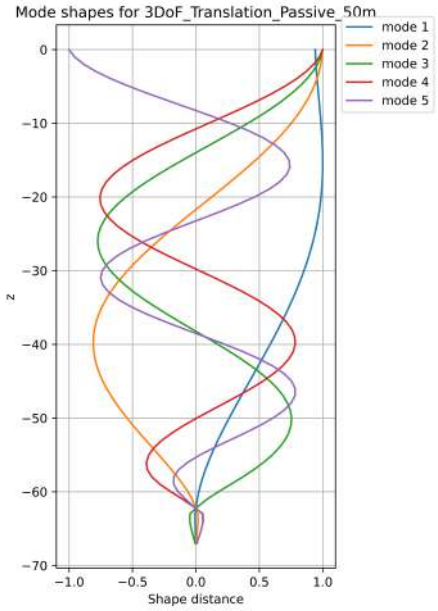

Figure H.7: Mode shapes for the 3DoF Translation Passive concept at 50m water depth.

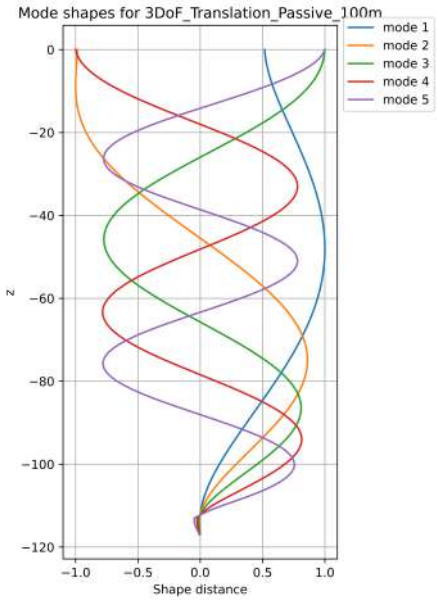

Figure H.8: Mode shapes for the 3DoF Translation Passive concept at 200m water depth.

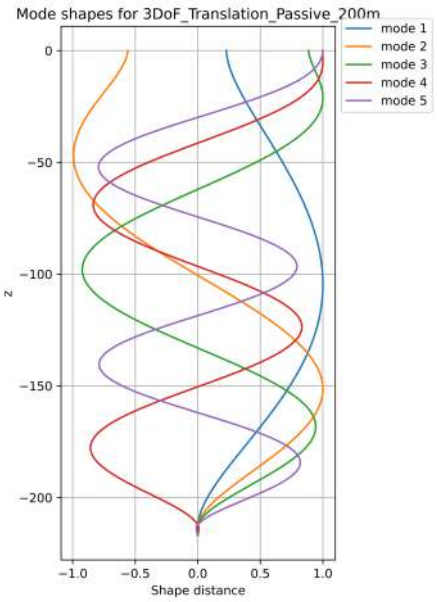

Figure H.9: Mode shapes for the 3DoF Translation Passive concept at 200m water depth.

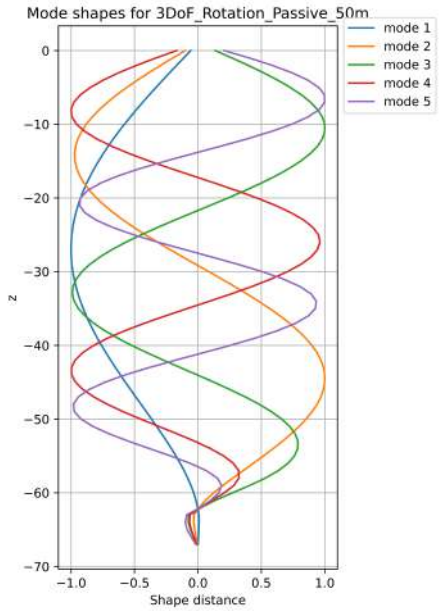

Figure H.10: Mode shapes for the 3DoF Rotation Passive concept at 50m water depth.

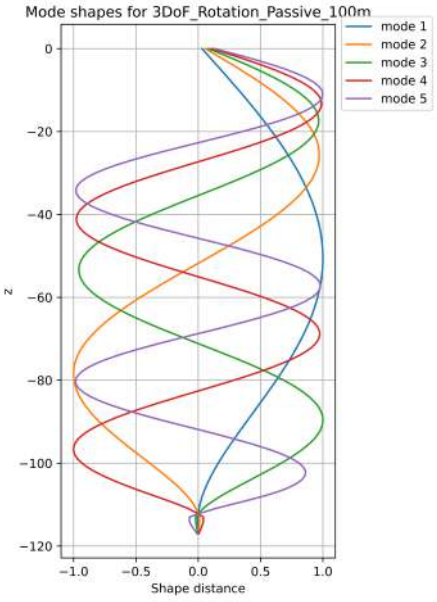

Figure H.11: Mode shapes for the 3DoF Rotation Passive concept at 100m water depth.

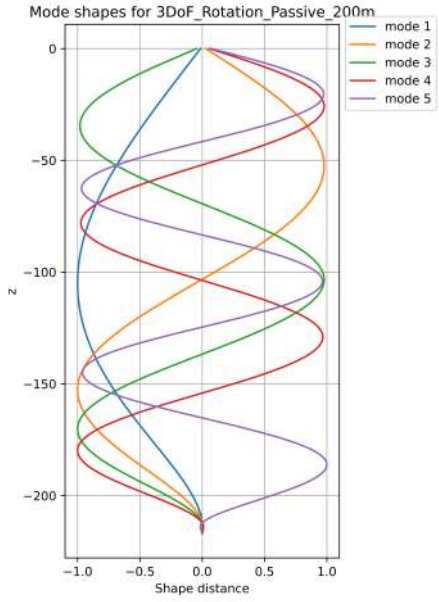

Figure H.12: Mode shapes for the 3DoF Rotation Passive concept at 200m water depth.

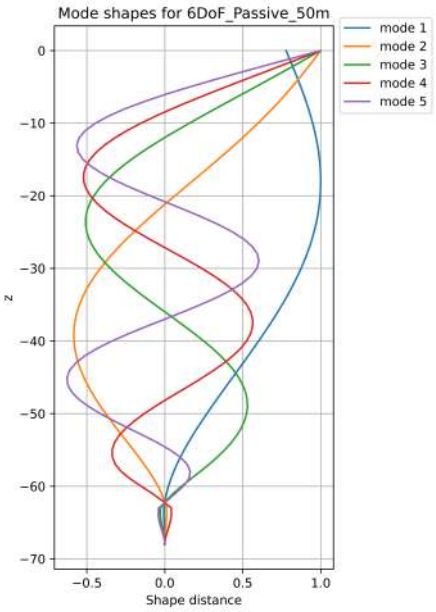

Figure H.13: Mode shapes for the 6DoF Passive concept at 50m water depth.

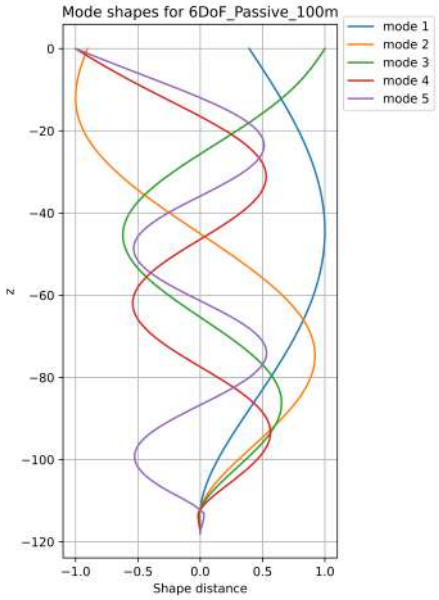

Figure H.14: Mode shapes for the 6DoF Passive concept at 100m water depth.

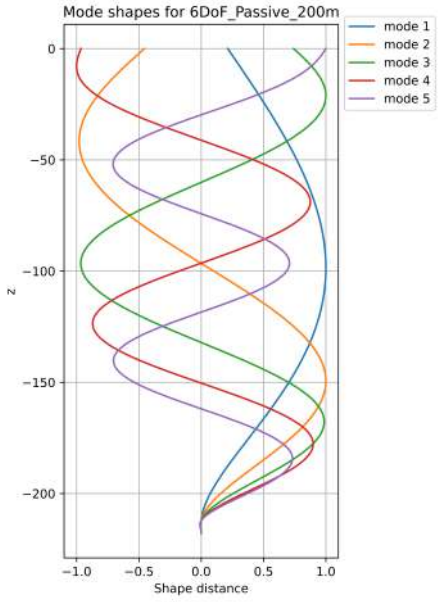

Figure H.15: Mode shapes for the 6DoF Passive concept at 200m water depth.

H.2. Realisation phase

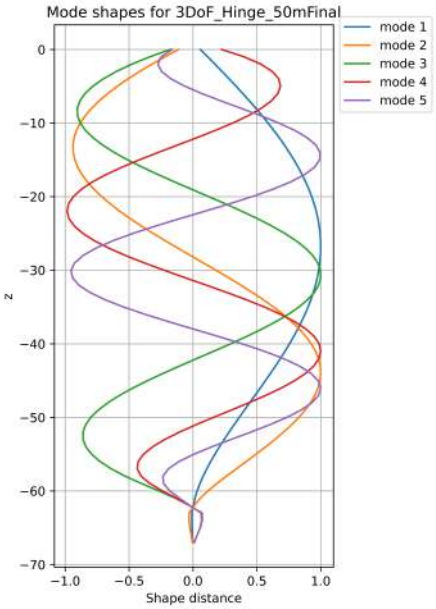

Figure H.16: Mode shapes for the 3DoF Hinge concept at 50m water depth.

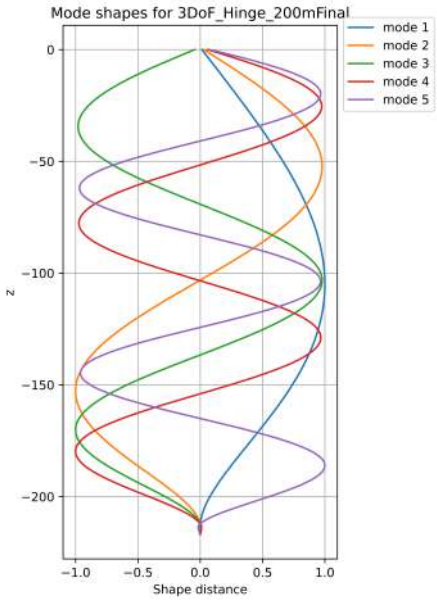

Figure H.17: Mode shapes for the 3DoF Hinge concept at 200m water depth.

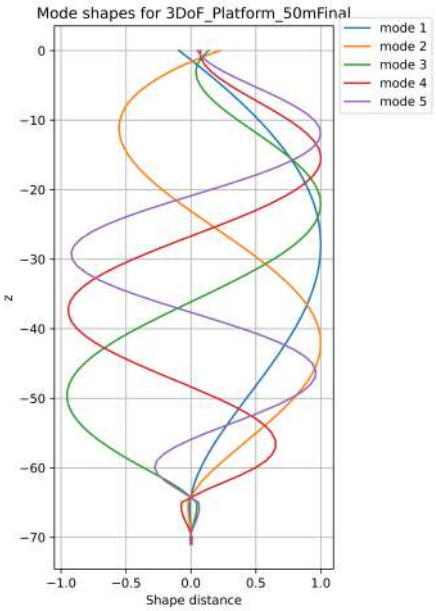

Figure H.18: Mode shapes for the 3DoF Platform concept at 50m water depth.

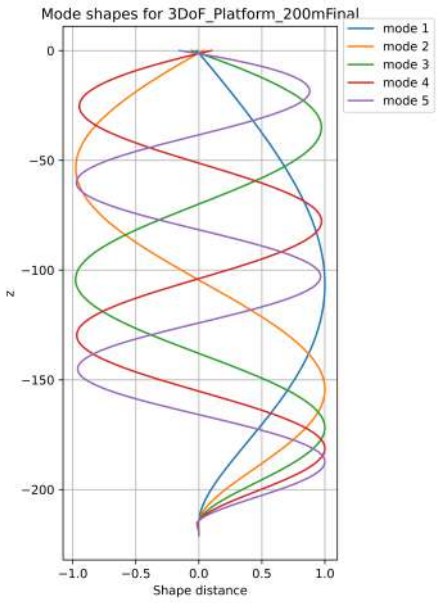

Figure H.19: Mode shapes for the 3DoF Platform concept at 200m water depth.

I. System damping analysis

Damping in the system consists of two parts, hydrodynamic drag on the drill string and damping in the passive systems imaginary linear actuators. The hydrodynamic force in OrcaFlex is described by the Morison equation, and the drag part of this equation is as follows:

$$F_{drag} = 1/2\rho A C_d u(t)^2 \tag{I.1}$$

This drag is non-linear, as it depends on the square of the water particle velocity. On the other hand, damping in passive systems is modelled as a linear dashpot. To check whether the damping in the system is too high or at a level where it can alter the natural frequencies that are calculated assuming that there is no damping in OrcaFlex, a damping analysis is performed. This is done by using the free vibration tests that are performed by pulling the drill string to the side and at a specific point and then letting go. Then a free vibration occurs that dampens the initial position. This gives a periodic decaying signal for a specific point on the drill string. From this time series the logarithmic decrement can be calculated and from this the damping ratio can be calculated, which causes this decrease in amplitude. In this analysis, the vessel motion is excluded from the system. The equation used to solve this is as follows:

$$\Delta_N = \frac{1}{N} \ln \frac{u(t)}{u(t + NT_d}} \tag{I.2}$$

$$\xi = \frac{\Delta_N}{\sqrt{4\pi^2 + \Delta_N}} \tag{I.3}$$

Additionally, the period between each of the peaks is calculated to see how it evolves over time. For each drill string, four points are taken and these values are derived from it. Not all time series are given here, but the ones that give a clear picture of the behaviour of the system in this test. In the graphs below, the segment length is 1m so, for example, node 40 is 40 metres downward along the drill string from the top.

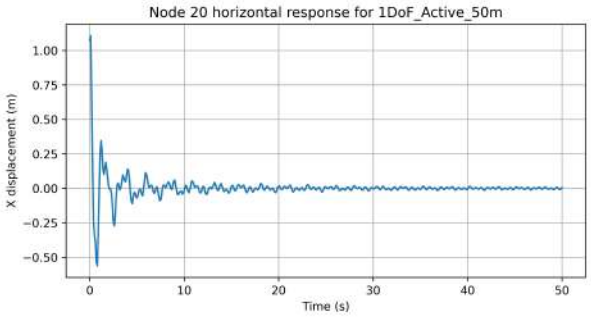

Figure I.1: Time series of the decaying periodic signal for a free vibration of node 20 of the 1DoF Active concept at 50m water depth.

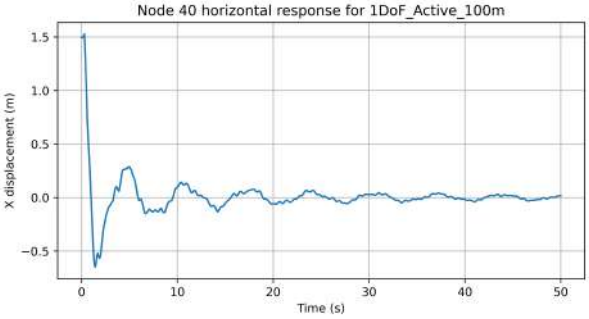

Figure I.2: Time series of the decaying periodic signal for a free vibration of node 40 of the 1DoF Active concept at 100m water depth.

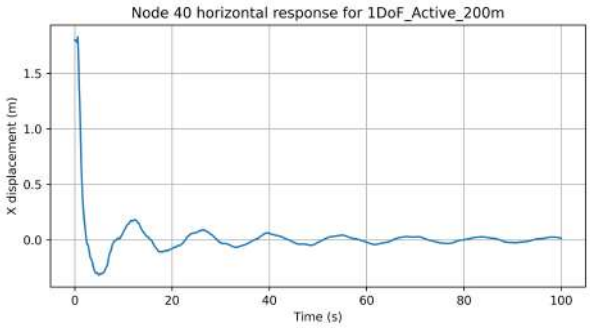

Figure I.3: Time series of the decaying periodic signal for a free vibration of node 40 of the 1DoF Active concept at 200m water depth.

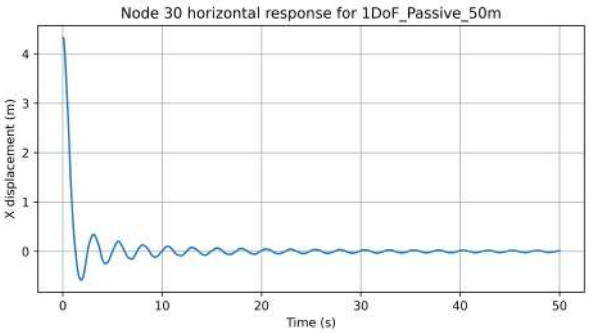

Figure I.4: Time series of the decaying periodic signal for a free vibration of node 30 of the 1DoF Passive concept at 50m water depth.

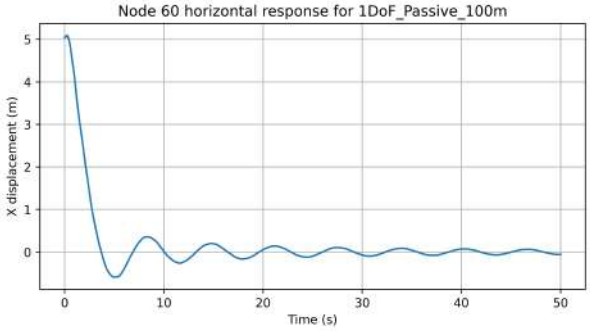

Figure I.5: Time series of the decaying periodic signal for a free vibration of node 60 of the 1DoF Passive concept at 100m water depth.

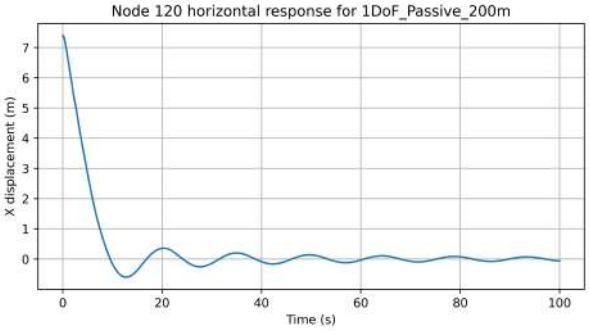

Figure I.6: Time series of the decaying periodic signal for a free vibration of node 120 of the 1DoF Passive concept at 200m water depth.

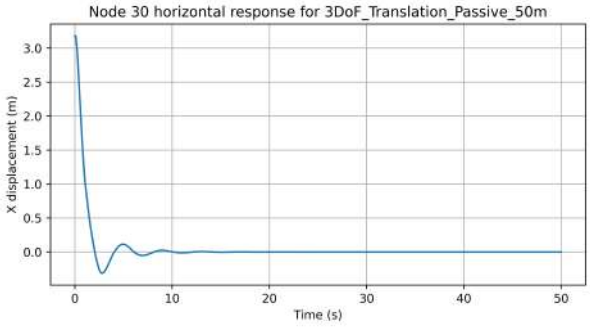

Figure I.7: Time series of the decaying periodic signal for a free vibration of node 30 of the 3DoF Translation Passive concept at 50m water depth.

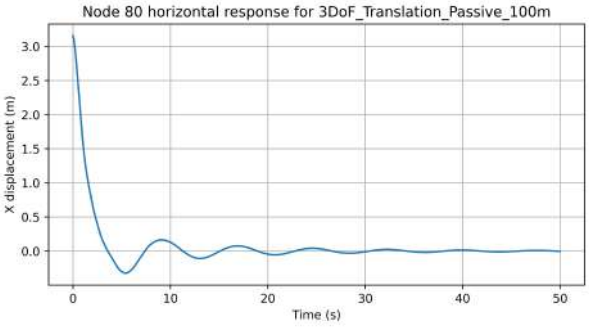

Figure I.8: Time series of the decaying periodic signal for a free vibration of node 80 of the 3DoF Translation Passive concept at 100m water depth.

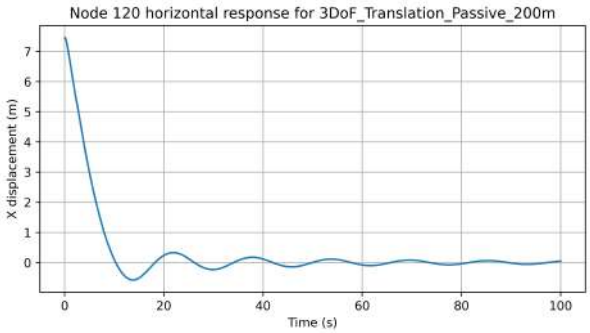

Figure I.9: Time series of the decaying periodic signal for a free vibration of node 120 of the 3DoF Translation Passive concept at 200m water depth.

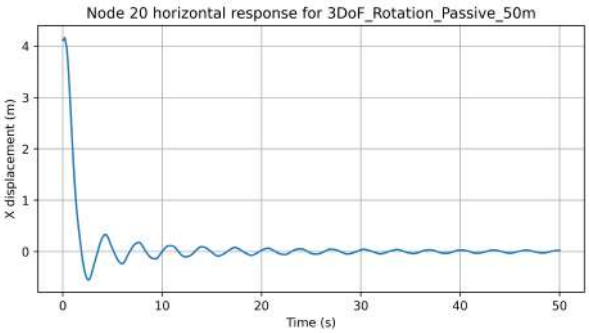

Figure I.10: Time series of the decaying periodic signal for a free vibration of node 20 of the 3DoF Rotation Passive concept at 50m water depth.

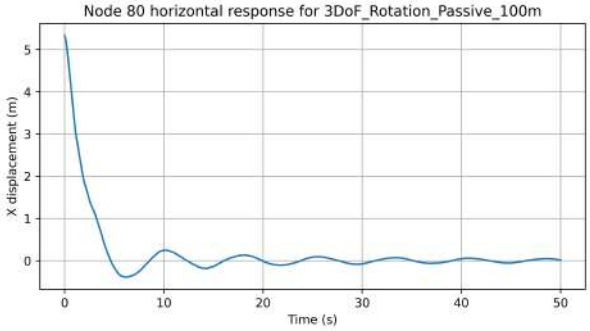

Figure I.11: Time series of the decaying periodic signal for a free vibration of node 80 of the 3DoF Rotation Passive concept at 100m water depth.

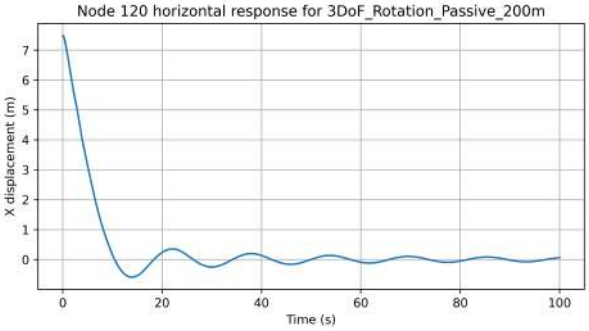

Figure I.12: Time series of the decaying periodic signal for a free vibration of node 120 of the 3DoF Rotation Passive concept at 200m water depth.

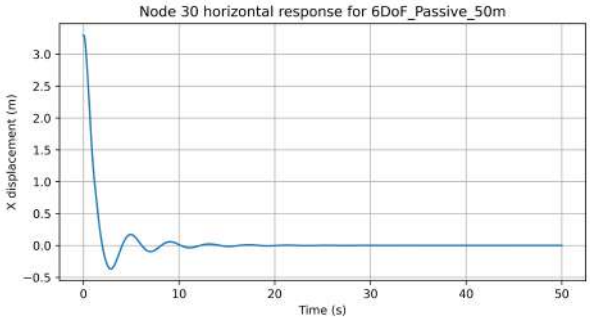

Figure I.13: Time series of the decaying periodic signal for a free vibration of node 30 of the 6DoF Passive concept at 50m water depth.

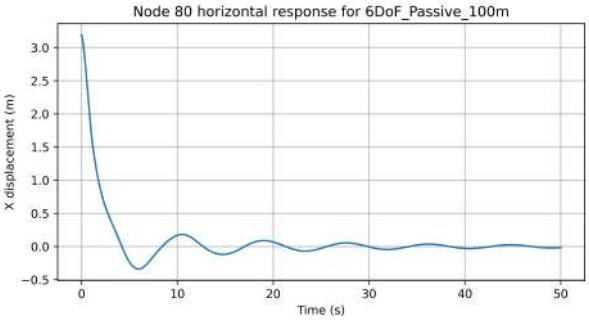

Figure I.14: Time series of the decaying periodic signal for a free vibration of node 80 of the 6DoF Passive concept at 100m water depth.

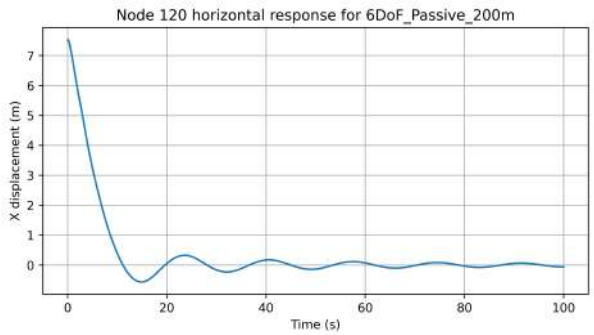

Figure I.15: Time series of the decaying periodic signal for a free vibration of node 120 of the 6DoF Passive concept at 200m water depth.

From the time series it can be seen that for most concepts only one frequency is seen, only on the time series for the 1DoF Active concept an extra frequency is visible. For the other concepts, it can be concluded that all modes but the first mode are almost completely damped out by the damping present in the system. Another observation can be made on the 3DoF Translation Passive concept, here the horizontal motion of the node considered dampens out much faster than other concepts, suggesting that in this system more damping is present than in other. This, of course, is then also true for the 6DoF passive system. The damping ratios calculated via the logarithmic decrement between each peak are given below. Therefore, the damping ratio $r_{d,1-2}$ is calculated taking the logarithmic decrement between the first and second peaks.

Concept	Depth	$r_{d,1-2}$	$r_{d,2-3}$	$r_{d,3-4}$	$r_{d,5-6}$
1DoF Passive	50	0.376	0.105	0.0492	0.0486
	100	0.388	0.0922	0.056	0.045
	200	0.433	0.092	0.0576	0.0416
3DoF Rotation Passive	50	0.388	0.091	0.59	0.045
	100	0.404	0.095	0.056	0.04
	200	0.437	0.0917	0.058	0.042
3DoF Translation Passive	50	0.467	0.234	0.219	0.214
	100	0.377	0.127	0.095	0.083
	200	0.44	0.0996	0.06587	0.0505
6DoF Passive	50	0.425	0.17	0.147	0.138
	100	0.414	0.11	0.0781	0.0636
	200	0.44	0.0981	0.0641	0.0489
Active systems	50	0.26	0.1	0.09	
	100	0.29	0.12	0.07	
	200	0.34	0.11	0.06	0.055

Table I.1: Damping ratios based on the logarithmic decrement for specific nodes for all concepts and water depths.

From the table it can be seen that the damping ratio between the first two peaks is high, and this stabilises when considering it between all other peaks. This indicates that the very first large excitation is dampened out very quickly by the hydrodynamic drag while at lower displacements the lateral drill string velocity is smaller, thus much smaller hydrodynamic drag is visible. At slower drill string motions, the damping in the cylinders becomes more dominant. In the table below are the periods between each of the major peaks observed in the time series.

Concept	Depth	T_{1-2}	T_{other}	$T_{1,undamped}$
1DoF Passive	50	3.1	2.5	2.47
	100	8.4	6.3	6.36
	200	20.3	14.5	14.59
3DoF Rotation Passive	50	4.3	3.4	3.25
	100	10.4	7.8	7.6
	200	22	15.8	15.78
3DoF Translation Passive	50	5	4.1	4.1
	100	9.3	7.7	7.76
	200	22	15.9	15.7
6DoF Passive	50	5	4.1	4.26
	100	10.5	8.5	8.64
	200	23.6	16.9	16.93
Active systems	50	-	1.6	2.39
	100	-	4	6.63
	200	-	11	14.45

Table I.2: Periods of the free-vibration decaying signal of the lateral node position

In this table, it can be observed that for the first period, the time it takes to complete one cycle is longer than for the following cycles. When this is compared to the undamped natural period calculated by OrcaFlex, it can be concluded that there is clearly a higher damping ratio for the first, more intense, excitation. For the rest of the vibrations, the period is relatively similar to the undamped natural period. From this analysis, it is concluded that the system has a high damping ratio, overdamping, for sever excitations that have higher drill string lateral velocity and thus large hydrodynamic damping. The damping included in the cylinders does not cause overdamping and is thus realistic, this is also proved by looking at the power spectral density plots given in Appendix G. Here, the difference between the line with all the damping included and the line with only the hydrodynamic damping is almost the same, indicating that this damping is of small influence and thus not very high. It can also be said that because of this damping characteristic, no destructive behaviour can be seen, as it is quickly dampened out if the vibration has large lateral vibration speeds.
Another way to determine the damping ratio is by deriving the Q factor. The Q factor is a factor that describes the width of the peak and, by this width, the damping ratio can be calculated. The width of the peak is described in figure I.16. With these parameters, the Q factor can be determined as follows.

$$Q = \frac{\omega_n}{\Delta\omega} \tag{I.4}$$

The damping ratio can be calculated then via:

$$\xi = \frac{1}{2Q} \tag{I.5}$$

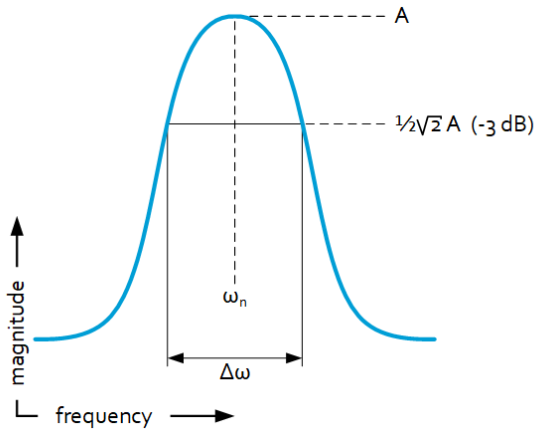

Figure I.16: Definition of the values needed for calculating the Q factor [21].

This has been applied to a response graph of a 200m drill string with the 1DoF Passive motion compensation system. The analysis was done with and without ship motion. The setup is calculated with many different regular waves with different periods, for each period the maximum x-displacement at a specific point along the drill string is recorded. This amplitude is then plotted against the wave period. From this plot, the damping ratio is estimated.

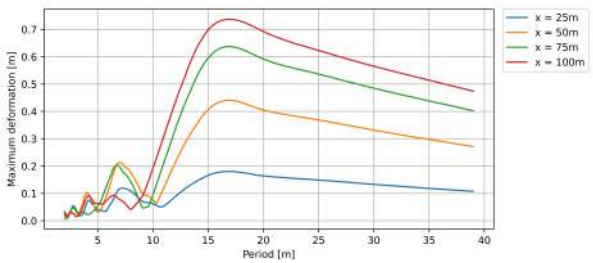

Figure I.17: Maximum x-displacement for different wave periods and at different locations along the drill string, ship motion is excluded.

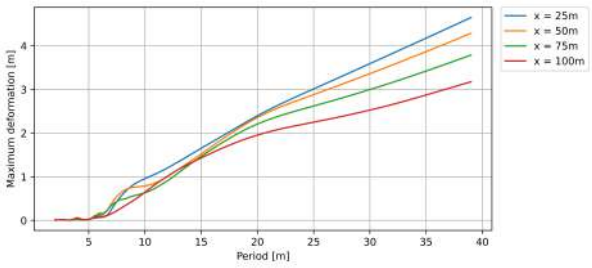

Figure I.18: Maximum x-displacement for different wave periods and at different locations along the drill string, ship motion is included.

It can be directly observed in figure I.18 that when the vessel motion is included, it becomes impossible to distinguish the peaks and the calculation of the Q factor becomes impossible. This is because the RAO values that determine the translational vessel motion increase with the wave period. Therefore, the peaks are less prevalent and the maximum value has an increasing trend with the period. Including vessel motions into this analysis does give the right damping ratio, as the imposed motion of the vessel on the drill string gives more lateral displacements, and thus higher velocities than when the vessel motion is excluded. But when the vessel motion is excluded, as can be seen in figure I.17, the peaks can be distinguished more easily. And from this the Q factor and the damping ratio can be determined, from this graph the damping ratio is calculated to be as the following:

Natural period	Damping ratio
16.9s	0.66
7s	0.15
4.1s	0.12

Table I.3: Calculated damping ratios with the Q-factor method for 1DoF Passive 200m system.

The first natural periods found here do not actually coincide with the natural period reported, but this has to be because OrcaFlex calculates the undamped natural period. Furthermore, combined with this high damping ratio, the natural period could be shifted to higher periods. The damping ratio for the first natural period is computed here as large. It is roughly 1.5 times the damping ratio of what is

calculated as the highest damping ratio via the logarithmic decrement, the 2nd and 3rd natural periods have lower damping ratios. The damping ratios for these modes have not been calculated using the logarithmic decrement method. However, these modes are less important than the first mode.
In general, it is difficult to determine the exact damping ratio when damping is described in a non-linear way. Especially when including vessel motion, which causes greater damping in the upper parts of the drill string. The damping ratio along the drill string is therefore also not consistent. Most analyses in this appendix are done excluding ship motions, the natural periods and damping ratios obtained here are similar, and for the first natural period, damping is high. For other lower natural periods, the damping is also relatively high. Thus, the damping levels in operation when vessel motions are included are higher. The system is excited closely in the first natural period in the regular wave analysis, and no problematic stress levels are observed. This observation leads to the conclusion that if the system is excited in a way that is similar to that in the proposed models, such as induced motion due to ship motion, wave forces, and moonpool, no destructive behaviour can occur. This is specifically true if that excitation is near the natural period of the system, as the stress levels remain below the yield limit. The main argument supporting this conclusion is that the damping ratios are very high for large excitations. These large excitations arise primarily in the form of the first mode of vibration.

J. Platform Optimisation results

Realisation	WoB SD (kN)	$\sigma_{bend,max}$ (MPa)	r_{upper} (m)	r_{lower} (m)	$h_{cylinder}$ (m)	d (m)	V (m^3)	b (Kns/m)
1	2.65	47.712	1.63	7.15	5.93	0.7	4.57	5.02
2	7.31	36.395	1.42	6.66	5.47	0.73	4.55	20.84
3	2.67	45.344	1.63	6.5	5.86	0.59	4.03	5.11
4	2.72	41.409	1.74	6.49	5.68	0.62	4.2	5.04
5	5.65	36.667	1.42	6.66	5.45	0.7	4.09	15.52
6	2.65	46.923	1.63	7.15	5.9	0.7	4.57	5.02
7	5.25	37.063	1.43	6.76	5.45	0.69	3.86	14.32
8	3.83	38.805	1.42	6.66	5.47	0.73	4.55	9.02
9	6.44	36.605	1.42	6.66	5.47	0.71	4.22	18.08
10	3.34	39.077	1.42	6.77	5.47	0.7	3.85	6.75
11	2.81	40.545	2.32	6.49	5.68	0.62	4.73	5.02
12	6.52	36.501	1.42	6.67	5.47	0.73	4.55	18.36
13	7.12	36.499	1.36	6.66	5.47	0.74	4.55	20.47
14	4.27	38.120	1.42	6.66	5.47	0.71	4.31	10.7
15	5.3	36.872	1.43	6.66	5.45	0.7	4.08	14.32
16	4.7	37.535	1.42	6.66	5.47	0.73	4.55	12.25
17	4.02	38.236	1.42	6.66	5.47	0.71	4.21	9.79
18	3.95	38.480	1.35	6.66	5.47	0.71	4.09	9.54
19	3.24	39.338	1.44	6.77	5.47	0.7	3.85	6.14
20	4.57	37.977	1.42	6.67	5.47	0.71	4.08	11.68
21	3.14	39.554	1.42	6.77	5.47	0.7	3.85	5.73
22	2.91	40.211	1.45	6.84	5.52	0.7	4	5.01
23	3.08	39.747	1.31	6.66	5.47	0.7	3.86	5.43
24	2.94	39.769	1.45	6.84	5.51	0.69	4	5.01
25	4.59	37.663	1.42	6.66	5.47	0.71	4.26	11.89
26	4.7	37.535	1.42	6.66	5.47	0.73	4.55	12.25
27	7.18	36.453	1.42	6.65	5.47	0.73	4.69	20.3
28	2.93	40.051	1.39	6.84	5.51	0.7	4	5.01
29	4.67	37.557	1.42	6.66	5.47	0.73	4.55	12.13
30	4.58	37.977	1.42	6.66	5.47	0.71	4.08	11.68